TOWARDS LOW MOLECULAR WEIGHT XANTHENE-BASED DYES WITH ABSORPTION BEYOND 650 NM

A THESIS SUBMITTED TO
THE GRADUATE SCHOOL OF NATURAL AND APPLIED SCIENCES
OF
MIDDLE EAST TECHNICAL UNIVERSITY

BY

ÇAĞLAYAN KIZILENİŞ

IN PARTIAL FULFILLMENT OF THE REQUIREMENTS
FOR
THE DEGREE OF MASTER OF SCIENCE
IN
CHEMISTRY

DECEMBER 2023

Approval of the thesis:

TOWARDS LOW MOLECULAR WEIGHT XANTHENE-BASED DYES WITH ABSORPTION BEYOND 650 NM

submitted by **Çağlayan Kızıleniş** in partial fulfillment of the requirements for the degree of **Master of Science** i**n Chemistry, Middle East Technical University** by,

Prof. Dr. Halil Kalıpçılar
Dean, Graduate School of **Natural and Applied Sciences** _____

Prof. Dr. Özdemir Doğan
Head of the Department, **Chemistry** _____

Assoc. Prof. Dr. Emrullah Görkem Günbaş
Supervisor, **Chemistry, METU** _____

Examining Committee Members:

Assoc. Prof. Dr. Salih Özçubukçu
Chemistry, METU _____

Assoc. Prof. Dr. Emrullah Görkem Günbaş
Chemistry, METU _____

Assoc. Prof. Dr. Emre Büküşoğlu
Chemical Engineering, METU _____

Assoc. Prof. Dr. Özgül Persil Çetinkol
Chemistry, METU _____

Assist. Prof. Dr. Safacan Kölemen
Chemistry, Koç University _____

Date: 11.12.2023

I hereby declare that all information in this document has been obtained and presented in accordance with academic rules and ethical conduct. I also declare that, as required by these rules and conduct, I have fully cited and referenced all material and results that are not original to this work.

Name Last name : Çağlayan Kızıleniş

Signature :

ABSTRACT

TOWARDS LOW MOLECULAR WEIGHT XANTHENE-BASED DYES WITH ABSORPTION BEYOND 650 NM

Kızıleniş, Çağlayan
Master of Science, Chemistry
Supervisor : Assoc. Prof. Dr. Emrullah Görkem Günbaş

December 2023, 96 pages

9H-xanthene (10H-9-oxaanthracene or Xanthene) core based Photodynamic Therapy (PDT) agents became highly sought after since they demonstrated numerous advantages including a high molar extinction coefficient, high photostability, high light-dark toxicity ratio, and availability for both lipophilic and aqueous media. The tunability of the xanthene core makes it a great candidate for imaging and therapeutic purposes. For PDT action, the agent should have a high singlet oxygen generation yield, absorb at the therapeutic window, localize at the subcells, and have a desired hydrophilicity among other factors. In this study, novel low molecular weight, red absorbing, and water-soluble silicon (S**iNO-OMe**, **SiNO-OMe2**) and phosphine oxide (**PNN**, **Morp**) containing xanthene dyes were designed and significant effort has been dedicated to their synthesis. Synthesis of one of the desired silicon containing xanthene dyes was confirmed in High Resolution Mass Spectrometry (HRMS), however isolation of the target has not been fruitful so far. For the synthesis of silicon containing derivatives, several trials were performed for a key demethylation reaction and a nitrosonium based approach for forming a nitrogen bridge on the xanthene core as a new concise synthetic approach was detailly pursued. Aminopeptidase N targeting handle (APN) was synthesized for modifying novel cores pursued in this study to achieve selective accumulation on brain cancer (glioblastoma cells). In the second chapter, a Two Photon Absorption

dye, TPA, was designed, and the donor and acceptor components of this dye (compounds 3.5 and 3.7) were successfully synthesized. As a future work synthesis of SiNO-OMe, PNN-Morp, and TPA will be finalized and their photophysical properties will be investigated. Their aminopeptidase N caged derivatives will also be realized and their performance in *in vitro* studies will be investigated.

Keywords: Photodynamic Therapy, Xanthene, Dye, Cancer Treatment, Therapeutic Window, 2 Photon Absorption, Aminopeptidase N

ÖZ

650 NM ÖTESİNDE SOĞURMA YAPAN DÜŞÜK MOLEKÜLER AĞIRLIKLI KSANTEN BOYALARI

Kızıleniş, Çağlayan
Yüksek Lisans, Kimya
Tez Yöneticisi: Doç. Dr. Emrullah Görkem Günbaş

Aralık 2023, 96 sayfa

9H-Ksanten (10H-9-oxaantren veya Ksanten olarak da bilinir) çekirdek tabanlı Fotodinamik Tedavi (PDT) ajanları, yüksek molar soğurma katsayısı, yüksek fotostabilite, yüksek ışık-karanlık toksisite oranı ve lipofilik ve sulu ortamlar için mevcudiyet gibi birçok avantajı sergiledikleri için son derece aranan hale gelmiştir. Ksanten çekirdeğinin ayarlanabilir olması, görüntüleme ve terapötik amaçlar için harika bir aday yapar. PDT etkisi için ajanın yüksek bir singlet oksijen üretim verimine, terapötik pencerede emilime, hücre altında lokalizasyona ve diğer faktörlere sahip olması gerekmektedir. Bu çalışmada, düşük molekül ağırlıklı, kırmızı emen ve suda çözünen silikon (SiNO-OMe, SiNO-OMe2) ve fosfin oksit (PNN, Morp) içeren Ksanten boyar maddeler tasarlandı ve sentezleri için önemli çaba harcandı. İstenen silikon içeren Ksanten boyar maddelerden birinin sentezi Yüksek Çözünürlüklü Kütle Spektrometrisi (HRMS) ile doğrulandı, ancak hedefin izolasyonu şu ana kadar başarılı olmadı. Silikon içeren türevlerin sentezi için bir ana demetilasyon reaksiyonu ve yeni bir kısa sentetik yaklaşım olarak Ksanten çekirdeğinde bir azot köprüsü oluşturmak için nitrosonyum tabanlı bir yaklaşım için birkaç deneme yapıldı. Bu çalışmada takip edilen yeni çekirdekleri modifiye etmek için Aminopeptidaz N hedefleme kolu (APN) sentezlendi ve bu, beyin kanseri (glioblastoma hücreleri) üzerinde seçici bir birikim elde etmek için bu çalışmada

takip edilen çekirdekleri modifiye etmek için kullanılacaktır. İkinci bölümde, İki Foton Soğurma boyası, TPA, tasarlandı ve bu boyanın (bileşikler 3.5 ve 3.7) donör ve alıcı bileşenleri başarıyla sentezlendi. Gelecekteki çalışmada SiNO-OMe, PNN-Morp ve TPA'nın sentezi tamamlanacak ve fotofiziksel özellikleri araştırılacaktır. Ayrıca bunların Aminopeptidaz N kapalı türevleri gerçekleştirilecek ve *in vitro* çalışmalardaki performansları araştırılacaktır.

Anahtar Kelimeler: Photodinamik Terapi, Ksanten, Boya, Kanser Tedavisi, Terapötik pencere, 2 Foton Absorpsiyon, Aminopeptidaz N

In memory of my beloved father…

ACKNOWLEDGMENTS

I want to express my deepest gratitude to my supervisor Assoc. Prof. Dr. Emrullah Görkem Günbaş for his friendship attitude, guidance, advice, criticism, encouragement, and insight throughout the research. He always motivated me so hard that made me explain all the findings in my journey to him to make a mutual connection. He always enlarged my perspectives from the scientific point of view. He always believed in me and stayed by my side to help me to go through hard times. His presence in my life is invaluable to me as a mentor, as a friend, and as a brother to me.

I would also like to thank Assist. Prof. Dr. Antoine Marion for their computational calculations, innumerable responses to my long conceptual questions, and his friendship attitude toward me.

I would also like to thank Prof. Dr. Saim Ozkar for his knowledge and patience during our deep conversation, and for always having time for me to arrange a meeting even though he was in his hometown with his family.

I would also like to extend my thanks to Assist. Prof. Dr. Safacan Kölemen for his suggestions and comments on my synthetic challenges and his knowledge of the concept of my work.

I would also thank my examining committee members, Assoc. Prof. Dr. Salih Özçubukçu, Assoc. Prof. Dr. Özgül Persil Çetinkol, Assoc. Prof. Dr. Emre Büküşoğlu and Assist. Prof. Dr. Safacan Kölemen for accepting to evaluate my thesis and their valuable suggestions.

I would also like to thank the aforementioned individuals one more time for giving me the lantern to shine the light on my future which makes me feel I’m not alone in this journey and desire to keep in touch with them wherever I live.

I am grateful to all the technicians in our department for their help.

Special thanks to Osman Karaman for being such a good mentor and good friend during my undergraduate year. Without his guidance, I couldn't have reached there. He was always by my side not only in academia but also in real life, he was like a father to me, although he is 2 years older. I would also thank Gizem Atakan Alkan for their positive vibe and for making me energetic in the lab, as well as for their support and knowledge. I am very grateful to Doğuşcan Dönmez, Görkem Aydın, and Emre Özgan for their brotherhood and for always motivating me during this journey.

I want to thank Ceren Akgül, Mustafa Yaşa, Figen Varlıoğlu Yaylalı, Aliekber Karabağ, Zübeyir Elmazoğlu, Dilay Kepil, Zeynep Nas, Sena Tarım, Melike Erkilet, Ezgi Çakmak, Ecem Aydan, Sude Çelebi, Deniz Yılmaz, Sena Nur Aykut for their support and friendship during the Master years.

I feel very fortunate to have found such a diverse environment and opportunities at Flair Group which allowed me to start my journey in academia. Hence, I would like to thank the Group members for their help, friendship, and positive working environment.

I am very grateful to have such insightful friends; Berçin Verda Asya, Bahar Atik, Serhat Çetin Koç, Sercan Han, Murat Yüksel, and Yunus Emre Pekcici.

Last but not the least, I would like to thank my beloved family, my mom for their endless love and both financial and mental support, my sister for their guidance and support throughout my life as my hero, my nieces; Mavi and Deniz for their love and friendship and for making me motivated for keep going, and my brother in law, Ulushan for his support and friendship, he is always like a brother to me, and my beloved father for their endless mental and financial support and for making me motivated throughout all my life and staying behind me for every decision I took, he was an embodiment of pure love, and still will be…

This work is partially funded by the European Research Council. I would like to thank for the financial support. (ERC Starting Grant 2019)

TABLE OF CONTENTS

LIST OF FIGURES

FIGURES

LIST OF ABBREVIATIONS

ABBREVIATIONS	
AcOH	Acetic Acid
Ar	Argon
DCM	Dichloromethane
DMF	Dimethylformamide
DMSO	Dimethyl Sulfoxide
HpD	Hematoporphyrin Derivative
ICT	Intramolecular Charge Transfer
ISC	Intersystem Crossing
LED	Light-Emitting Diode
MeOH	Methanol
n-BuLi	n-Butyllithium
NIR	Near Infrared
NBS	n-Bromosuccinimide
NMR	Nuclear Magnetic Resonance
PDT	Photodynamic Therapy
PS	Photosensitizer
ROS	Reactive Oxygen Species
rt	Room Temperature
THF	Tetrahydrofuran
TLC	Thin Layer Chromatography

CHAPTER 1

INTRODUCTION

1.1 Photodynamic Therapy

Sunray was used for the treatment of human diseases, including psoriasis, skin cancer, vitiligo, and rickers in ancient times, and its healing properties were subjected to ancient religions of Europe, Asia, and America.(Daniell & Hill, 1991) At the end of the nineteenth century, phototherapy came into the light and was made popular by Danish Physician Nielson Finsen, who treated cutaneous tuberculosis with ultraviolet from the sun.(Dolmans et al., 2003) Then, he led the carbon arc phototherapy for this chronic infection of skin tuberculosis and won the Nobel Prize for his discovery in 1903. In this way, the structure of modern light therapy was constructed. Later, Tappainer's student Oscar Raab found out that "infusoria", a species of paramecia, could be sensitized in the presence of acridine. This finding led to further studies by Tappainer and Jodlbauer, following the first "photodynamic" term, which was described by Tappainer.(Lipson & Baldes, 1960) External developments and experiments around the chemical reagents and light components built modern photodynamic therapy (PDT).

PDT is a cancer treatment method that focuses on the elimination of malignant tumor cells efficiently with fewer side effects compared to the current cancer treatment methods. This therapy has become popular in the last two decades and is getting approval among the USA and some European countries for some particular uses like skin, breast, and prostate cancer.(Shafirstein, 2023) PDT has three components: photosensitizer (PS), external light source, and oxygen.

1.1.1 Components of Photodynamic Therapy

PSs are conjugated, light-sensitive dyes that are accumulated selectively on malignant tumor cells according to their structural modification. They produce highly toxic reactive oxygen species like singlet oxygen and free radicals to create cytotoxicity at the subcellular level at tumor cells. So, this decreases the side effects of the therapy(Dabrowski et al., 2011) and makes PDT an almost non-invasive cancer treatment method.

Modifying PS with heavy atoms (-Br, -I, selenophene) enhances the spin-orbit coupling. Thus, intersystem crossing (ISC) becomes more probable during the transition change from singlet excited state to triplet excited state. These increase the singlet oxygen quantum yield.(Hu et al., 2018; Lan et al., 2019; Y. Liu et al., 2018; Monro et al., 2019)

Promising PS should show below properties.(Detty et al., 2004; Juarranz et al., 2008; O'Connor et al., 2009)

- Water-solubility, Fast clearance from the body
- High photostability under illumination
- Amphiphilicity depends on the interested tissue
- Low dark toxicity, high phototoxicity
- High singlet oxygen quantum yield (φΔ)
- Strong absorption band (high molar extinction coefficient "ε")
- Absorption within the therapeutic window

Absorption wavelength is very crucial. Because tissues are bulk medium, light penetration is very restricted due to the strong light absorbers including water, oxyhemoglobin, deoxyhemoglobin, and melanin. There is an optical window for PDT

around 650-1200 nm which absorption wavelength does not interfere with any of these molecules.(Angelier, 1990; Niemz, 2007; Plaetzer et al., 2009) But, the energy of photons decreases as the wavelength increases. So, there should be a limitation for triplet-state photosensitizers that exceed the minimum energy for forming the singlet oxygen. This minimum energy corresponds to the upper level of the absorption wavelength, which is 850 nm.(Anderson & Parrish, 1981) To achieve the deep penetration of light through tissue, excitation wavelength should be greater than 600 nm.(Plaetzer et al., 2009) Thus, these conditions determine the therapeutic window, which PSs are designed to absorb at the wavelength range between 600-800 for optimal efficiency.(Juzeniene et al., 2006)

With the improvement in the light source, PDT became popular. In the early stage, KTP:YAG lasers (Nd:yttrium-aluminum-garnet solid-state lasers, 532 nm) and argon gas laser (488 and 514.5 nm) were predominant due to monochromaticity and intensity. Then, they were coupled with dyes to obtain the desired illumination wavelength. But, they have a high cost and large size. Portable diode lasers then became popular around the PDT community. 690 and 785 nm diode laser are available. Furthermore, some non-coherent light sources, including LED, serves some advantages to a certain extent including low cost, a compact-sized, wide range of the spectrum. Also, fluorescence lamps are available (BLU-U1®, 400–450 nm) and Lumacare® with a specific filter up to near-IR region.(Awuah & You, 2012; Kessel, 1990)

The PDT involves administering a PS, a light-sensitive drug, either orally or topically to the targeted area. PS is Subsequently distributed around the body if it is given orally. Then, PS accumulates on the target of interest depending on the targeting strategies. Once the photosensitizer is absorbed by the targeted cells, a specific wavelength of light is applied to the area, activating the drug. This activation leads to the production of reactive oxygen species, which initiate a cascade of reactions that ultimately destroy the

targeted cells while minimizing damage to surrounding healthy tissue.(X. Li et al., 2020) (Figure 1.1)

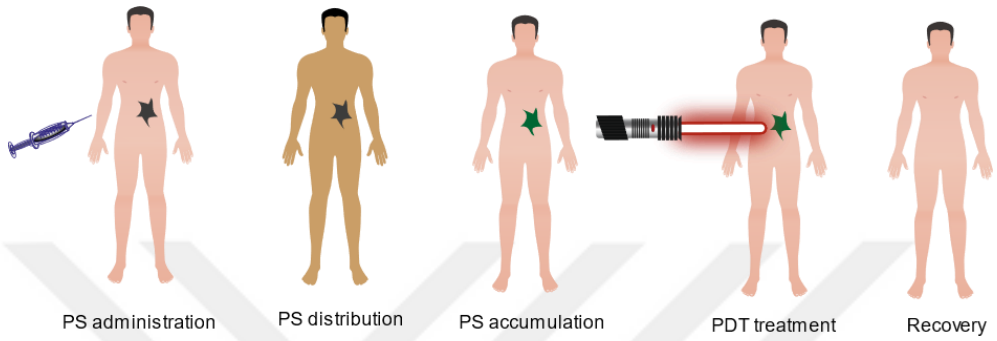

Figure 1.1. Schematic illustration of PDT mechanism in human cell.

Oxygen is the third component of the PDT. PS and light interaction lead to excitation from the triplet-state oxygen to highly reactive singlet oxygen or oxygenated radicals. All of the reactive oxygen species result in the elimination of tumor cells. Tumor cells are known to have poor oxygen concentration, which is defined as a hypoxia condition.(Zhu & Finlay, 2008) This decreases the PDT efficiency toward tumor cells. But, subcellular targeting, such as mitochondria or lysosomes, which have higher oxygen concentration compared to other subcellular locations, is a promising approach.

1.1.2 Working Principle of Photodynamic Therapy

PSs have zero total spin in its ground state called singlet ground state (S0). Illuminating the PS within its singlet ground state excites to the singlet excited state (S1). Singlet excited state is a highly unstable transition state. At this point, excited PS can make fluorescence to emit its energy via radiative decay. PSs, which are used for cancer imaging purposes, make fluorescence. For therapeutic application, PS should undergo intersystem crossing and go triplet excited state (T1) from S1 due to modifications such as the presence of heavy atoms in the structure. Phosphorescence is a forbidden energy

transition state by the quantum selection rule. So, PS with its triplet-state is more stable than in its singlet excited state and allows for a longer lifetime. These situations give triplet-state PS enough time to collide nearby molecules to start electron-transfer reaction (Type I) or transfer its energy (Type II).(Wilson & Hay, 2011) At this point, there are two types of reaction mechanisms.

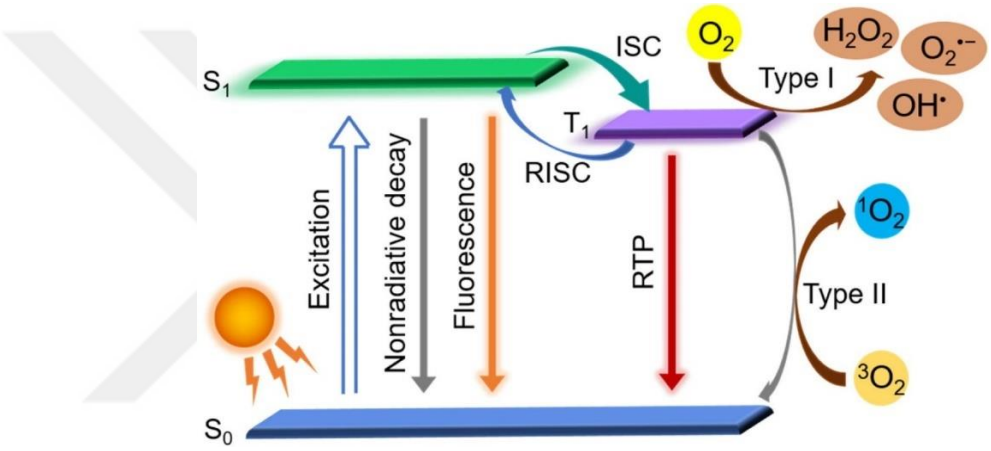

Figure 1.2 Schematic illustration of the Jablonski diagram (W. Li et al., 2022)

(S0: ground state, S1: singlet excited state, T1: triplet excited state, ISC: intersystem crossing, RISC: reversible intersystem crossing, RTP: room temperature phosphorescence.)

In Type I mechanism, excited PS starts electron-transfer reaction with oxygen molecules, organic substrates, or solvent to donate electron or proton. But, most excited PS's are known as oxidants and lead to radical or radical ion which their further reaction with O_2 gives oxygenated radicals including peroxides, superoxide, and hydroxyl radicals. In Type II mechanism, excited PS emits its energy to the ground state triplet oxygen and results in highly reactive singlet oxygen and PS in its ground state.(Abrahamse & Hamblin, 2016)

All of these reactive oxygen species (ROS), which are oxygenated radicals and singlet oxygen, cause oxidation of DNA, proteins as well as lipids.(Foote, 1991) So, this leads

to significant cytotoxicity, disrupt the organization of the membranes, proteins, enzyme structures, and trigger the upregulation of hypoxia-inducible transcription factors' (HIFs) pathways, which enable the survival of tumor cells and stem cells under hypoxia conditions.

1.1.3 Subcellular Localization of Photodynamic Therapy

Cell death mechanisms arise from not only the photodynamic stress but also the subcellular localization of PS, which results in the production of highly reactive singlet oxygen and ROS and corresponding cell signaling pathways.(Bacellar et al., 2015) Due to the low oxygen concentration of tumor cells, PDT activity is restricted to certain subcellular parts of the tumor. Targeting proper organelles is crucial, whereas limited oxygen content leads to lower singlet oxygen or ROS generation.

The inner mitochondrial membrane has around negative 150-170 mV membrane potential(Rubio et al., 2009) which makes positively charged PSs accumulate selectively in mitochondria.(Ormond & Freeman, 2013) Mitochondria is a well-known oxygen-rich organelle compared to other subcellular parts, and also many proteases and proteins, which trigger the apoptosis cell signaling.

Singlet oxygen has a maximum action radius around 20 nm and a short lifetime of around 40 ns.(Moan & Berg, 1991; Pavani et al., 2009) These create selective cytotoxicity at the site of action within the subcellular level.

Solubility of the PS is another factor that affects its selectivity. Hydrophobic PSs can easily accumulate in the membrane, but they lack proper delivery methods in aqueous media. Hydrophilic PSs have several advantages over hydrophobic ones. Removing hydrophilic PS from the body is faster which results in fewer side effects.(Dysart & Patterson, 2005)

1.1.4 Cell Death Mechanisms in Photodynamic Therapy

PDT causes both vascular and cellular phototoxicity. Vascular phototoxicity is achieved by disruption of endothelium and vascular walls through PS activation by the external light source. (Sakamoto et al., 2002) Vasculature damage results in blood-flow status via blood vessel constriction. Thus, oxygen and nutrient transportation is restricted, and tumor regression occurs.(Calzavara-Pinton et al., 2001) Cellular phototoxicity is achieved by direct tumor cell damage via PS activation, and results in disruption of intra-cellular medium. Both phototoxicity mechanisms are coexist and vary depending on PS, drug-light interval, wavelength, tissue, and clinical approach.(Sakamoto et al., 2002)

PDT results in three types of cell death mechanisms, which are apoptotic (apoptosis) cell death mechanism, and non-apoptotic ones which are necrosis and autophagy. Key elements that dominate one of these mechanisms is subcellular localization include endoplasmic reticulum, lysosomes, plasma membrane and mitochondria. Also, PDT concentration, light intensity, and PDT-light interval are the other factors.(Wilson & Hay, 2011)

Apoptosis is a controlled cell death pathway by mediating caspases. The disruption of endoplasmic reticulum and mitochondria are the well-known apoptotic pathway.(W. Wang et al., 2012) Also, Danial and coworkers' studies indicated that there is an integration between glucose metabolism and the apoptotic pathway.(Danial & Korsmeyer, 2004) Second, autophagy is mainly initiated by disruption of lysosomes and endosomes due to the PDT localization on them.(Danial et al., 2003) They can be thought of as "eating itself" cell death mechanisms. The third type is necrosis, which is an unprogrammable and violent cell death mechanism and responsible for the destruction, swelling of organelles, and loss of cytoplasm contents(Mroz et al., 2011). They arise from the loss of the plasma membrane integrity due to the localized PDT action on the plasma membrane.(Tsujimoto, 2012) In contrast to in vitro studies, in vivo

situations led to unequal light distribution to tissues, and inhomogeneous PS localization on targeting organelles can result in not a single death mechanism but a mixture of them.(Danial et al., 2003)

Recently, Jung et al. reported that targeting and inhibition of carbonic anhydrase 9 which is located on the mitochondria membrane, through acetazolamide (AZ)-conjugated BODIPY photosensitizer triggers the HIF pathway resulting in the dysfunction of mitochondria and cell signaling for apoptosis.(Kessel & Poretz, 2000)

Also, Kawai and coworkers indicate that detachment of cytochrome c from mitochondria is attributed to the apoptosis through lipid oxidation and changing of the inner mitochondrial membrane.(Jung et al., 2017) These studies show that targeting and disrupting the mitochondria membrane regulates apoptosis and overcomes the hypoxia condition for PDT.

1.2 Photosensitizers

1.2.1 Photosensitizers Based on Porphyrin Structure

Most of the clinically approved PDT agents are porphyrin derivatives which are cyclic tetrapyrrole-based structures that include porphyrin, chlorin, and bacteriochlorin (Figure 1.3)(Kawai et al., 2014; Mroz et al., 2011)

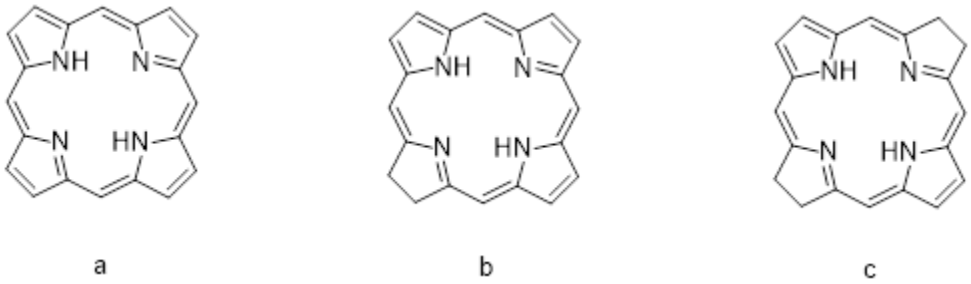

a b c

Figure 1.3. Structures of (a) porphyrin, (b) chlorin, and (c) bacteriochlorin.

5-Aminolaevulinic acid (ALA) has been a commonly used topical photodynamic therapy agent since 1999. It has a porphyrin ring structure when it is converted to protoporphyrin IX in cells. Then, illuminating the areas with radiation makes protoporphyrin IX start PDT action.(Sternberg et al., 1998) Typically, ALA is used in skin cancer treatment. (Figure 1.4)

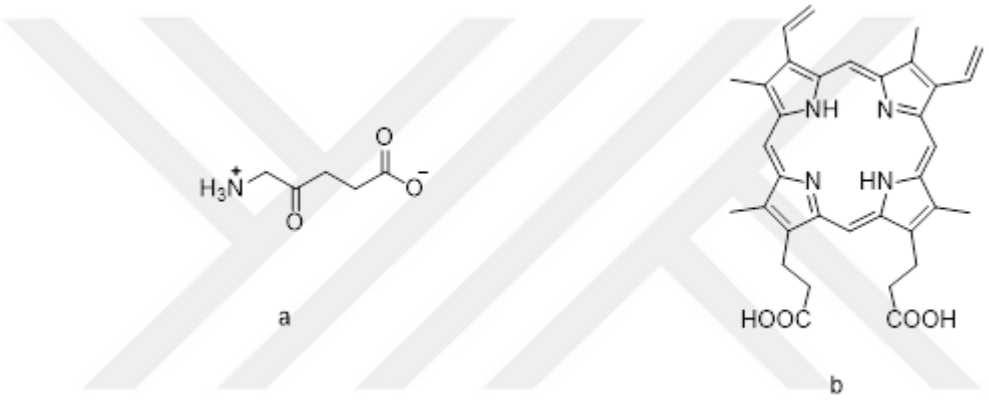

Figure 1.4. (a) structure of ALA, (b) structure of protoporphyrin IX

Porphyrin based PDT agents have some drawbacks including lack of solubility in water, dark toxicity, photosensitivity which lasts several weeks, limited depth of irradiation, severe pain during illumination and not being modifiable for further analogous (Morton et al., 2002)

Hematoporphyrin is the first-generation PDT agent whereas m-THPP and m-THPC are the second-generation PDT agents which are chemically pure and have greater tumor selectivity than the first generations. Saturation of one double bond in m-THPP yields chlorin based porphyrin derivative, m-THPC (Foscan®) which results in a bathochromic shift.(Nyman & Hynninen, 2004) (Figure 1.5)

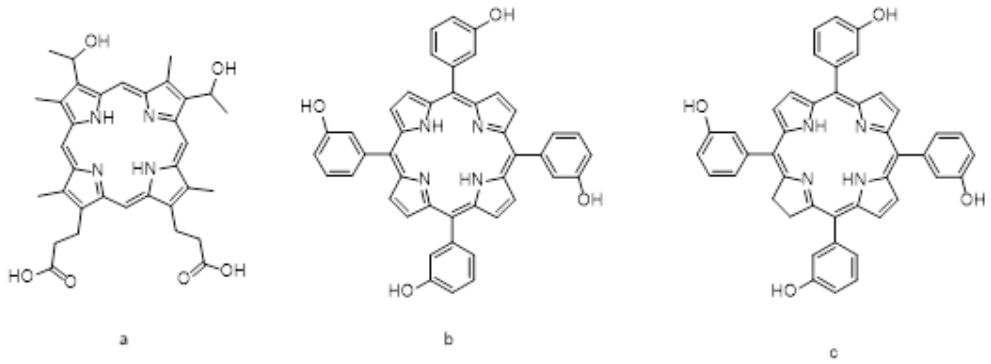

Figure 1.5. Structure of (a) hematoporphyrin (b) m-THPP, (b) m-THPC.

1.2.2 Photosensitizers Based on Non-Porphyrin Structure

Although Porphyrin-based PDT agents dominate through industry and research interest, non-porphyrin-based PDT agents are also found. Several non-porphyrin-based PS candidates (Figure 1.6), which are second generation, show high-level PDT activity and better cellular targeting properties than porphyrin-based PSs.(Senge & Brandt, 2011)

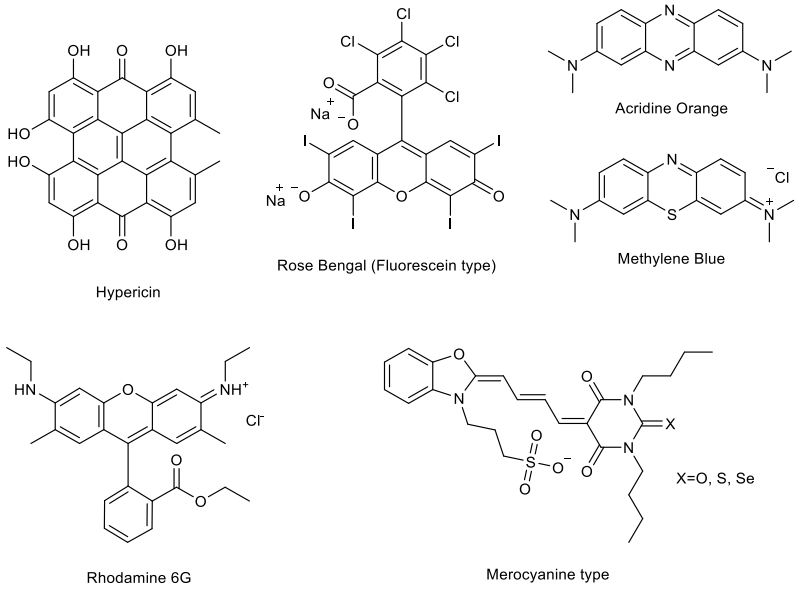

Figure 1.6. Examples of non-porphyrin based PS.

1.2.3 Photosensitizers Based on Xanthene Dyes

The promising properties of xanthene-based dyes, such as water solubility, photostability, and ease of modification, motivated researchers to investigate the modification of classical dyes such as fluorescein and rhodamine B (Figure 1.7) towards realizing NIR absorbing/emitting dyes with highly cancer-selective activation for imaging and treatment opportunities(Xiao & Qian, 2020). These efforts proved fruitful, and several novel xanthene-based dyes were developed with remarkable properties.

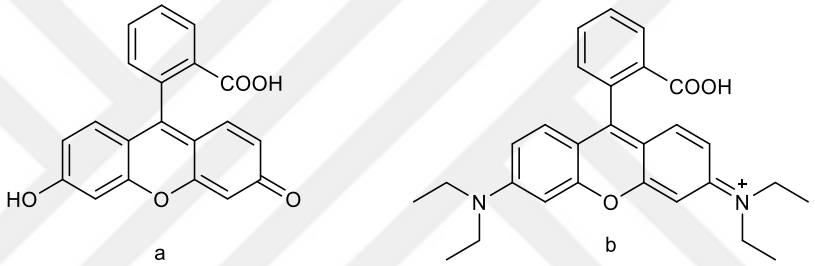

Figure 1.7. Structures of (a) Fluorescein (b) Rhodamine B.

In classical xanthene dyes, oxygen occupies the 10th position, replacing oxygen with any other elements, such as the pnictogens (group 4), the chalcogens (group 5), or boron have seen significant interest due to several orbital interactions leading to a decrease in the band gap. This bathochromic shift is crucial for imaging and treating deep tumors. Up to the present, carbon, silicon, germanium, tin, sulfur, and boron substituted pyronine scaffolds (Figure 1.8) have been proposed with red-shifted emission, and a wide range of biological applications was reported where classical pyronines were not effective.

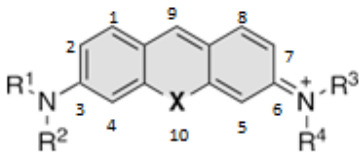

Figure 1.8. Structure of classical xanthene core (pyronine scaffold)

Silicon substituted pyronine (Si-Pyronine, SiP), is one of the classes of pyronine, and the Fu group reported the first silicon incorporation into the commercial xanthene core.(Fu et al., 2008) They showed that single silicon atom substitution resulted in a simultaneous decrease in LUMO energy level and increased HOMO energy level due to r* (silicon atom) p* (adjacent carbon atom) interaction that resulted in a 90 nm bathochromic shift. Besides the red-shift, narrow absorption with a 2-fold increase in molar absorption coefficient was observed compared to classical pyronine, which bears oxygen atom at the 10th position. It is crucial to mention that polar protic solvents resulted in lower quantum fluorescence yield. This observation was attributed to the electron-deficient character of the carbon atom at position 9. Thus, increasing the bulkiness at this position became one of the endeavors in the community for reaching higher quantum yields.

Hybrid xanthene dyes, particularly ones bearing silicon or phosphine oxide as the bridging unit of xanthene moiety, gained significant interest not only due to their excellent photochemical properties in aqueous media, high fluorescence quantum yield, photostability but also their proper absorption and emission maxima that allow for deep tissue imaging and therapy.

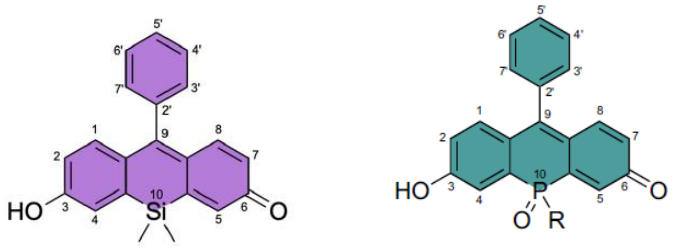

Figure 1.9. Structures of (a) Si fluorescein (b) Phosphine oxide fluorescein

In addition to group 4 elements Si and Ge and group 6 elements S, Se, and Te, Phosphorus (group 5) was used for the electronic modifications of p-conjugated systems due to the orbital interaction between p-skeleton and significant perturbation of the

electronic structure. The oxidation of the phosphorus atom enhanced the electron-accepting ability and chemical stability of the p- skeleton. Wang's group demonstrated the first introduction of phosphorus into xanthene dyes in 2015.(Chai et al., 2015) Replacement of bridging oxygen atom in the classic rhodamine framework with phosphine oxide yielded a series of phosphorous substituted tetraethyl rhodamines (PRs). Replacement of the bridging oxygen atom with silicon yielded near-infrared (NIR) Si-rhodamine with an emission maximum of around 650 nm. When phosphorus was integrated into conjugated ring systems, r*- p* orbital interactions increased, and the energy level of the LUMO decreased, resulting in greater shift towards the NIR region. (Figure 1.9, Figure 1.10)

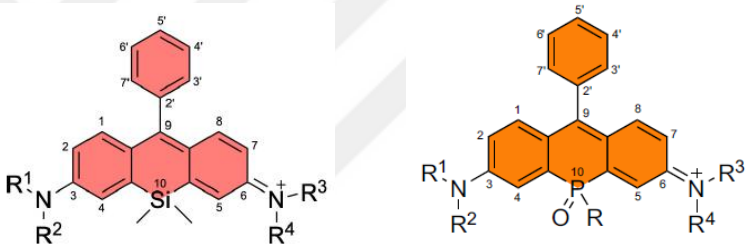

Figure 1.10. Structures of (a) Si rhodamine (b) Phosphine oxide rhodamine

The review written by O. Karaman, G.A. Alkan, C. Kizilenis et al.(Karaman et al., 2023) aims to highlight these exciting advancements towards searching for ‘‘the core”, focusing on xanthene dyes bearing heteroatoms other than oxygen at the 10-position due to their significantly red-shifted absorption and emission maxima with preserved optimal features of their ancestors.

1.2.4 Two-photon absorption dyes

Two-photon absorption (2PA) is the simultaneous absorption of two photons by an atom, molecule, or semiconductor that results in a transition to a higher energy state. This phenomenon is distinct from the more common single-photon absorption, which was originally shown experimentally in 1961 and involves the excitation of an electron by a single photon. (Kaiser & Garrett, 1961)

Since two photons with energy lower than the difference between the starting and end states are absorbed simultaneously in a typical 2PA process, there shouldn't be an intermediate excited state. (Fig. 1.11) The combined energy of the two photons, which is highly dependent on the intensity of the incoming light, is sufficient to excite one electron to a higher energy state. The probability of 2PA increases by the square of intensity of the light, in contrast to single-photon absorption, which depends linearly on intensity.(Pawlicki et al., 2009)

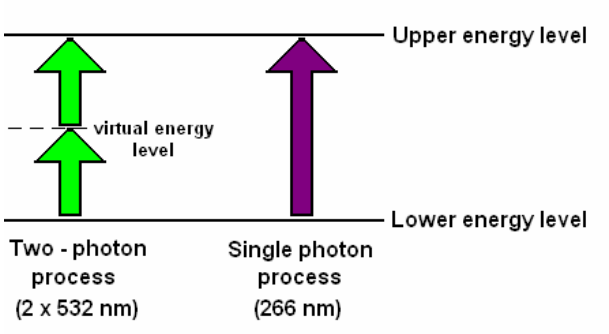

Figure 1.11. Demonstration of simultaneous absorption of 2 photons (Moagar-Poladian, 2008)

TPA is frequently used in two-photon microscopy, a method for high-resolution imaging of biological material. Compared to conventional one-photon excitation, 2PA has the benefit of deeper penetration into biological tissues with less photodamage. (Tkachenko, 2006) In the context of cellular and biological imaging, greater TPA cross-sections allow

deeper penetration in more scattering tissue samples and lower laser intensities to excite more molecules. This reduces the risk of tissue heat damage.

TPA is more prominent in materials with particular features, such as a high two-photon absorption cross-section (GM), specified by Maria Göppert-Mayer, who created the theory of two-photon absorption in the 1930s. (Göppert-Mayer, 1931)

2PA dyes should exhibit a relatively high two-photon absorption cross-section. This parameter quantifies the probability of the dye undergoing 2PA and is crucial for efficient excitation with low-power laser sources. Branched planar chromophores which are linear dipolar, quadrupolar (Figure 1.12) as well as octupolar systems are widely investigated due to tunability of their charge transfer ability. (Pawlicki et al., 2009)

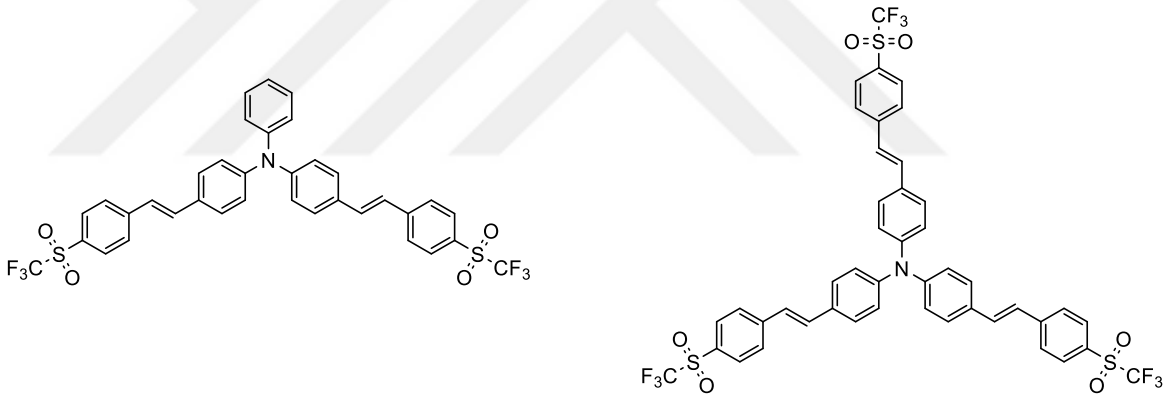

Figure 1.12. Structure of a) quadrupolar and b) octupolar systems

Quadrupolar and octupolar systems consist of two donor or two acceptor unit at the end, and one conjugated core which show sensible charge polarization at the center and bond with conjugated linker contains ethynylene and vinyl units are represented as A-π-D-π-A and D-π-A-π-D (Figure 1.13)

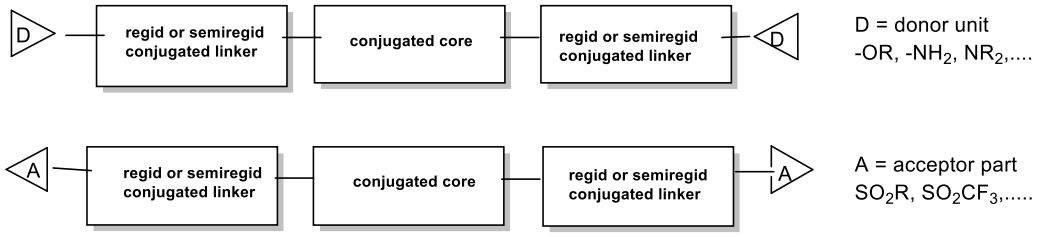

Figure 1.13. A-π-D-π-A and D-π-A-π-D systems in quadrupolar and octupolar systems.

Variation of each of these groups change its 2PA characteristics like 2PA cross-section and its absorption band. For example, ethynylene-linked systems have less conjugation compared to vinylene-linked (*trans*) due to π–π and π*–π* energy mismatches at C(sp1)-C(sp2) connections (Drobizhev et al., 2006), and result in slightly lower two photon cross-section (GM), and so lead lower fluorescence quantum yield.

But in sterically hindered systems, having twisted out (where vinylene bridge makes the bonded units twist out the conjugation) properties can make the conjugation in more planer surface(Pawlicki et al., 2009), and result in better 2PA cross-section. Rebane, Spangler, and co-workers showed (Drobizhev et al., 2006) that the vinylene-linked porphyrin has a lower cross-section than the ethynylene-linked ones. (Figure 1.14)

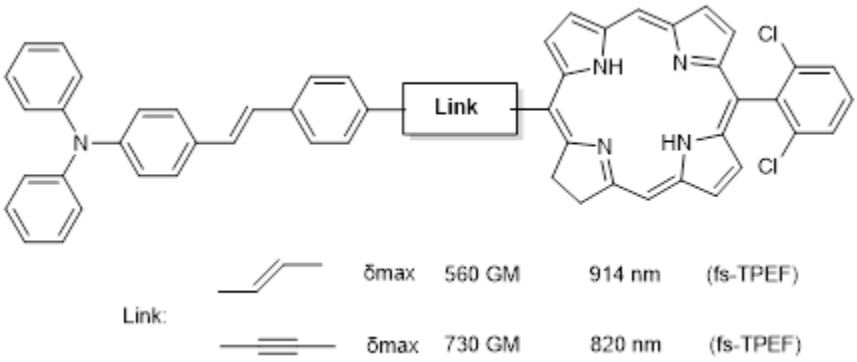

Figure 1.14. Demonstration of Spangler and coworkers‘ work

Other widely investigated systems are dipolar linear chromophores which are conjugated strong push-pull olefins like diphenylacetylenes and found out that they can show great 2PA properties for used both imaging and therapeutic purposes.(Chisholm et al., 2019; Gala De Pablo et al., 2020)

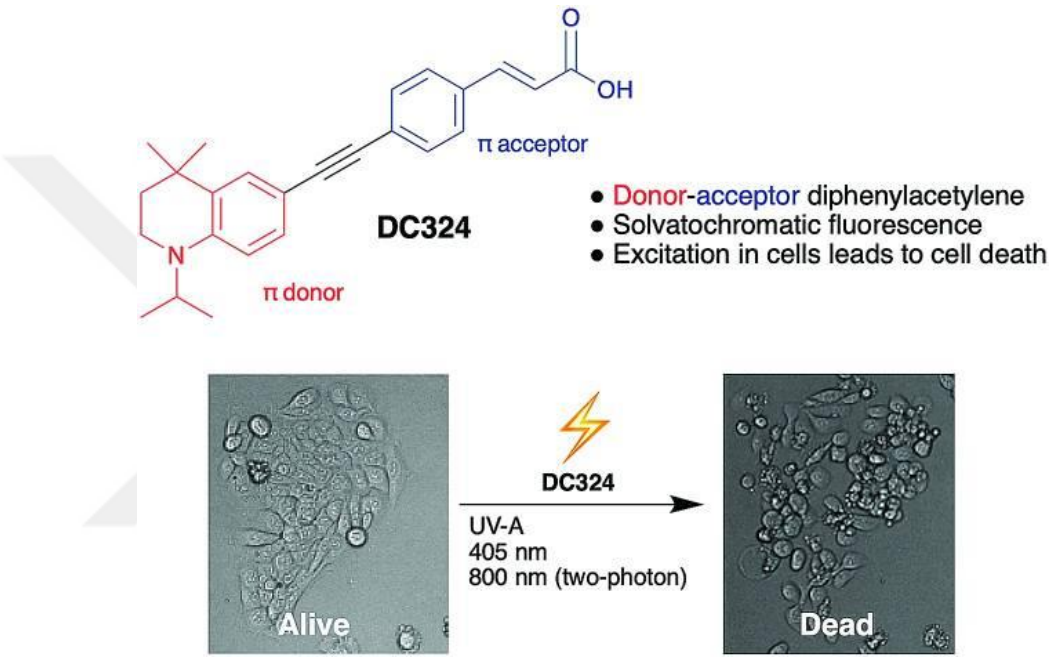

Figure 1.15. Structure of Diphenylacetylene type dipolar chromophore (DCM324)

1.3 Aim

1.3.1 Silicon and Phosphine Oxide Bearing Xanthene Dyes

In this study, the aim is to introduce novel activable silicon and phosphine oxide bearing xanthene dyes that exceed 600 nm absorption when they are in ON state at the target site, and their brominated product on the main core to use in PDT action.

In 2018 Miller's group (Choi & Miller, 2018) foreseen that in addition to the modification of classical xanthene core by replacing the bridging oxygen moiety with heteroatom, they replaced the carbon atom at the 9-position with nitrogen, could yield a further NIR shift in the absorption maximum. (Figure 1.16)

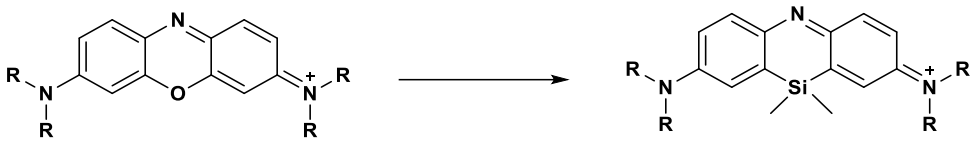

Figure 1.16. Demonstration of structural modification done by Miller Group

Difluoro and dimethyl derivatives of the azetidine- bearing azasilane dyes were synthesized. (Figure 1.17) The difluoro derivative ASiFluor710 and dimethyl derivative AsiFluor730 showed red-shifted absorption maxima beyond 700 nm. The fluorescence quantum yield of ASiFluor730 was low in aqueous medium however showed good photostability, where irradiation at its peak absorption wavelength for 1 h did not result in any decomposition, where its difluoro derivative decomposes in aqueous medium. This work also shows that introduction of electronically different substituents on the azasiline core determine the xanthene core stability.

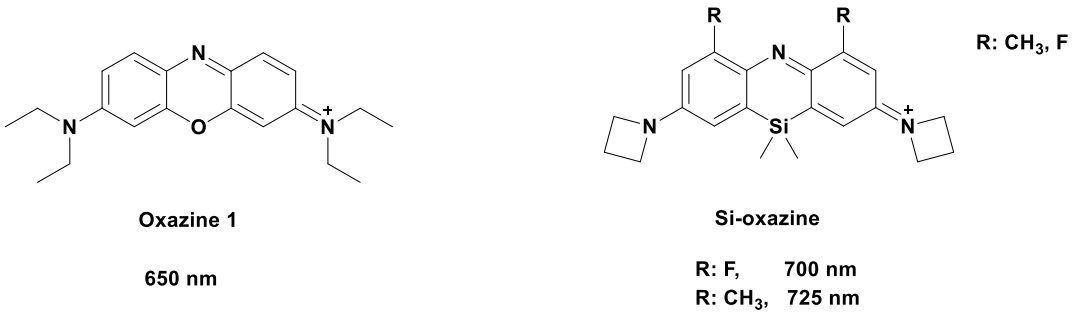

Figure 1.17. Structure of (a) Oxazine 1, (b) Si-oxazine derivatives

With the findings of heteroatom substitution on xanthene core of fluoresceins and rhodamines on 10-position and nitrogen replacement with carbon on 9-position, we

designed silicon and phosphine oxide bearing xanthene dyes which can be used in both imaging and for therapeutic purposes at NIR region upon heavy atom modification.

We designed the synthetic pathway of our candidates in the light of Wang's work which they did amine cyclization through producing nitrosonium cation in acidic reaction medium in ethanol with $NaNO_2$. (L. Wang et al., 2020). Although reaction yield of both amine derivatives are below 10%, these reaction decrease 3 or 4 reaction steps for achieving desired xanthene core and also readily available starting materials in the market which are 3-bromo-N,N,5-trialkylaniline derivatives, makes for a practical synthetic route. (Figure 1.18)

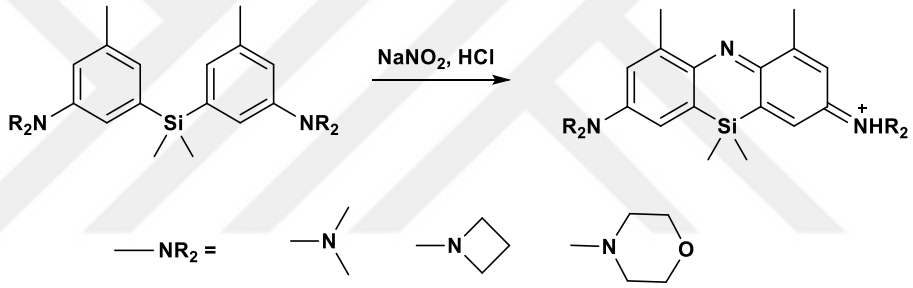

Figure 1.18. Amine cyclization of silyl alanine with $NaNO_2$ in acidic condition

This pathway has been utilized in our labs for the silicon-fluorescein derivatives without any success. We speculated the difference in reactivity occurred due to difference in donating ability of oxygen versus nitrogen. Hence, we designed new silicon-fluorescein derivatives with additional oxygen at 1- and 8-position that can enhance donation significantly. Additional phospha-analogue was pursued as a novel red shifted-dye utilizing the similar synthetic approach. (Figure 1.19)

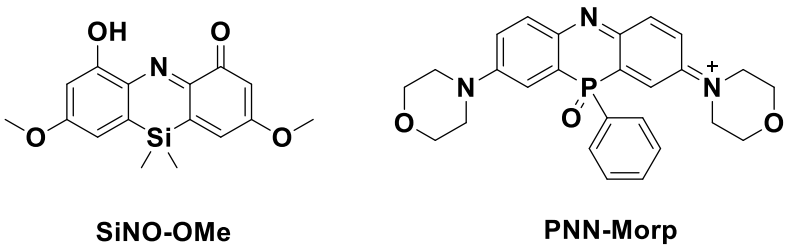

Figure 1.19. Structure of (a) **SiNO-OMe**, (b) **PNN-Morp**

Introduction of appropriate handles for effective targeting

The "handle" is one of the most crucial components of a PDT drug. PSs are often made so that they switch from an OFF to an ON state when the handle is cleaved. The singlet oxygen generation occurs only when a PS in an ON state is illuminated. These handles are engineered to be cleaved at the tumor site while leaving healthy tissue unharmed by a small biomolecule or enzyme that is specifically expressed by cancer cells. A well-known illustration of these handles is boronic esters. H_2O_2, an oxidant that some cancer cells produce excessively, cleaves these handles, causing the PS to go into the ON state.(H. W. Liu et al., 2017) Unfortunately, even though there are several handles known for a variety of cancers, brain tumor-specific handles to be used for realizing targeted activatable PDT on brain cancer is unknown. In fact, specific targeting of brain tumors has proven to be a difficult task. Here, a progressive approach is going to be followed.

First, PS will be modified with a handle which targets an enzyme that is known to be upregulated in human glioblastoma: aminopeptidase N **(APN)**. Recent studies have shown that APN is upregulated in several human malignancies (mostly in solid tumors) including brain tumors, and acts by regulating a variety of processes such as cell−cell contact, proliferation, tumor invasion and metastasis, angiogenesis, and tumor progression. (J. Li et al., 2014) There is presently no research on targeting these enzymes for brain cancer treatment, even though they are potential candidates that are employed

in selective fluorescence imaging for the investigations of brain cancer cells. Hence, **SiNO-OMe-X** or **SiNO-OMe2-X** will be modified by APN-specific handle towards a first-ever targeted and effective PDT-based brain cancer treatment. (Figure 1.20)

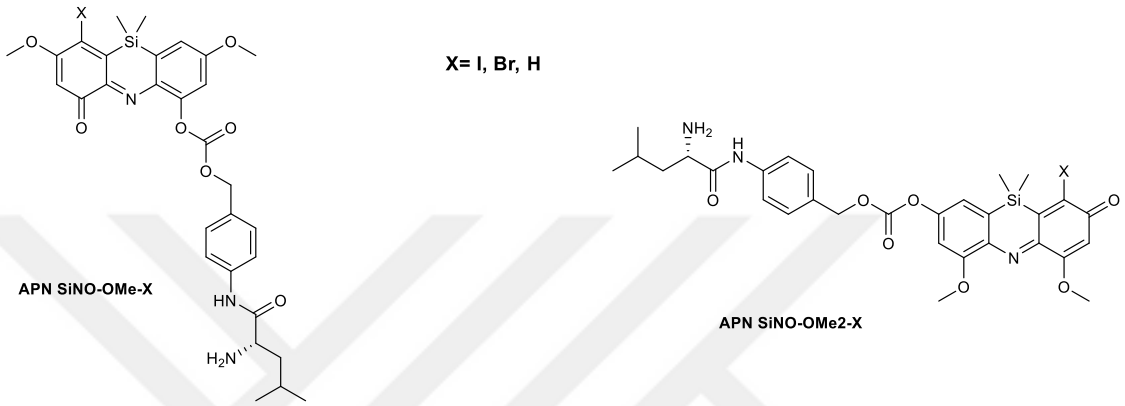

Figure 1.20. Structure of (a) **APN SiNO-OMe-X**, (b) **APN SiNO-OMe2-X**

1.3.2 Two Photon Absorption Dyes

Chisholm and coworkers' found out that diphenylacetylene type retinoid derivative (Figure 1.15) showed 2PA PDT action.(Chisholm et al., 2019) Thus in the light of this work, another aim of this study is to introduce novel 2PA dye based on low molecular diphenylacetylene type linear dipolar chromophore towards realizing a more straightforward and higher yielding synthetic approach with strong acceptor characteristics of chromone (Z. Wang et al., 2017) and donor characteristics of trialkyl amine moieties. (Figure 1.21) The dye expected to show non-linear optic properties and have near strong absorption in the NIR region to fit in the therapeutic window.

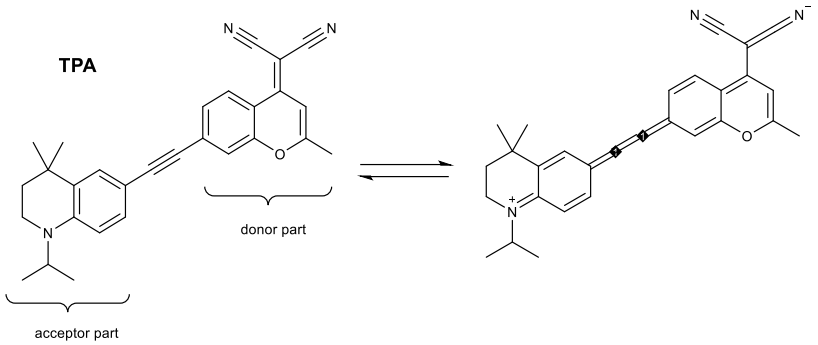

Figure 1.21. Structure of TPA

CHAPTER 2

RESULTS AND DISCUSSION

2.1 Design of the Target Photosensitizers

In previous studies from our group (Figure 2.1) which I also contributed, two fluorophores were successfully synthesized. Slicon substituted xanthene core with N bridge (**SiNO**) showed absorption at around 650 nm where the phosphine oxide substituted one (**PNO**) gave an absorption maxima at around 600 nm. Unfortunately, silicon based derivative showed no significant fluorescence which hinders its utilization as for both imaging and treatment. Even though several fluorescence quenching mechanisms are known in the literature, the specific mechanism in our case is, as of now, unknown. On the other hand, phosphine oxide substituted dye PNO showed strong fluorescence.

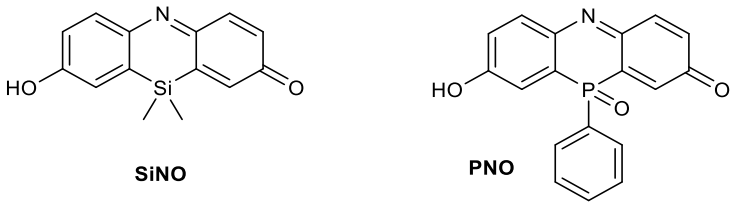

Figure 2.1. Structure of **SiNO** and **PNO**

We ended up with the tagret **SiNO-OMe 2** which was designed for ease of synthesis and to make steric hindarence around the nitrogen to avoid any interaction of water with nitrogen bridge and see the effect of donating units methoxy instead of methyl in the outcome of the absorption characteristics.

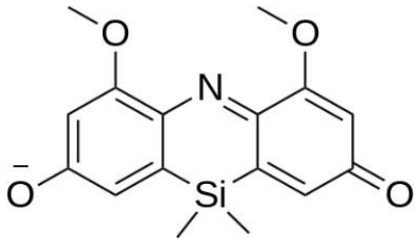

Excited State 1: Singlet*Sym 1.9416 eV **638.55 nm** f=1.2580
<S**2>=0.000 83 -> 84 0.70710
HOMO (83): -5.232477024
LUMO (84): -2.872161578

Figure 2.2. Theoretical outcome of absorption characteristics of **SiNO-OMe 2**

Density functional theory used in theoretical calculations confirms that proposed dye (**SiNO-OMe 2**) will absorb beyond 600 nm. But, main challinging issue will be the position of the methoxy unit with respect to bridging nitrogen on the core structure. Our proposed straightforward synthetic path has no favored selectivity on methoxy unit compared to hydroxyl during cylazation reaction thus two possible structures are expected. We investigated both possible outcome theoretically, in which hydroxyl unit are on the 1 and 8 position.

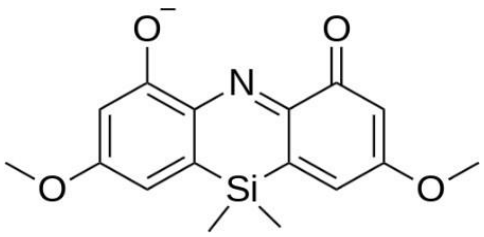

Excited State 1: Singlet*Sym 1.8816 eV **658.92 nm** f=0.7963
<S**2>=0.000 83 -> 84 0.70741
HOMO (83): -5.214789624
LUMO (84): -2.8261743393

Figure 2.3. Theoretical outcome of absorption characteristics of **SiNO-OMe**

Density functional theory used in theoretical calculations confirms that second dye (**SiNO-OMe**) will absorb beyond 600 nm as well, even 20 nm higher than **SiNO-OMe 2**. Suprisingly position of the hydroxy unit on the xanthene core which contributes to resonance structure through their p orbital mesomerically, change their absortion maxima, means deacreases the energy difference between HUMO and LUMO gap of the target molecule. This findings is one of the rare examples where the position of the resonance contributer unit on the main core changes the absorption charecteristics.

With the promising results on the phosphine oxide substituted xanthene core studied in the our lab (**PNO**), an alky amine substituted on 3- and 6-position instead of hydroxy units was targeted to realize hybrid xanthene core (**PNN-Morp**) as a rhodamine analog towards comparing their photophysical properties and *in vitro* behaviors like subcellular localization. (Figure 1.19)

Computational Calculations

Time Dependent Density Functional Theory is very well known tool for determination of electronic excited states of small molecules (up to 100 atom systems).(Bauernschmitt & Ahlrichs, 1996; Casida et al., 1998; Marques & Gross, 2004; Runge & Gross, 1984; Stratmann et al., 1998). Tuttle group's work show that inclusion of the solvent is needed to predict excitation energy calculations of several oxazine dyes and found out that SMD description of solvent method was show greater accuracy compare to CPCM in that sytstems. (Fleming et al., 2011) So, parameters and methods used in **SiNO-OMe** and **SiNO-OMe 2** are taken from Tuttle group's work. But, equilibriam solvation method was applied for consistency of the results with the decreasing the band gap of ground state and excitated state which is not mentioned in that work.

2.2 Approach for the Synthesis of Target Photosensitizers

2.2.1 Approach for the Synthesis of SiNO-OMe.

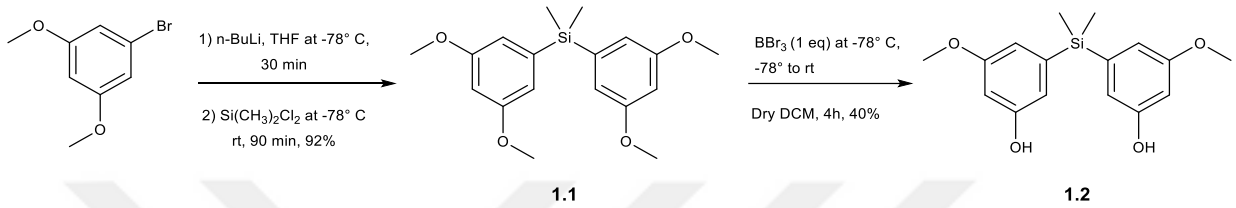

Figure 2.4. Early synthetic route of compound **1.2**

In the early stages, 1-bromo-3,5-dimethoxybenzene was subjected to lithium-halogen exchange reaction, and subsequently, the silicon unit was coupled with a 92%. (Compound **1.1**, Appx. **A.1**, **A.2**) After that 2 methoxy parts of the molecule were subjected to the demethylation with BBr_3. But due to having a total of 4 methoxy on the main structure and not achieving selectivity, 5 different demethylated products were obtained. Temperature screening showed that reaction did not undergo through kinetic product, all products started to occur at -40 °C simultaneously and their yields were similar. Even though the major product was the desired product on the crude NMR data, their separation was quite impractical by silica column chromatography. (Figure 2.4)

Reagent	Equivalency	Temperature (°C)	Yield of desired product	Observation
Ethanethiol	2	reflux	8%	Si-C bond broken
Ethanethiol	2	80	8%	Si-C bond broken
Dodecanethiol	2	reflux	8%	Si-C bond broken
Hydroiodic acid	6	0	ND	Si-C bond broken
BBr3	2	-78	28%	5 different demethylated product
BBr3	1	-78	40%	5 different demethylated product

Table 1. Demethylation trials of compound 1.5 with various reagent and conditions

Hence, we started with the demethylation of 1-bromo-3,5-dimethoxybenzene first achieving the reaction with 72% yield. (Compound **1.3**, Appx. **A.5**, **A.6**) Then,

protection of hydroxyl unit with benzyl bromide was performed with 98% yield. (Compound **1.4**, Appx. **A.7**, **A.8**) (Figure 2.5)

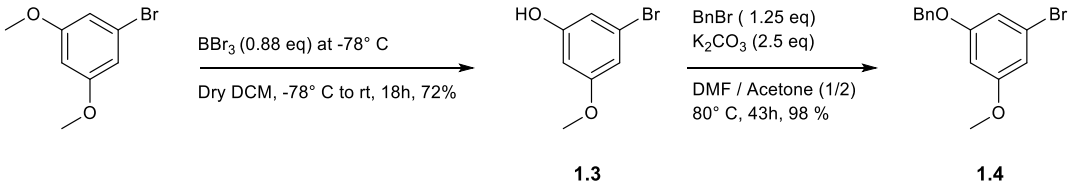

Figure 2.5. Synthetic route of compound **1.4**

Then the product was subjected to lithium halogen exchange reaction with *n*-BuLi. However, lithium halogen exchange reaction followed by introduction of the silicon based electrophile did not give the expected product either in THF or Et_2O. (Figure 2.6)

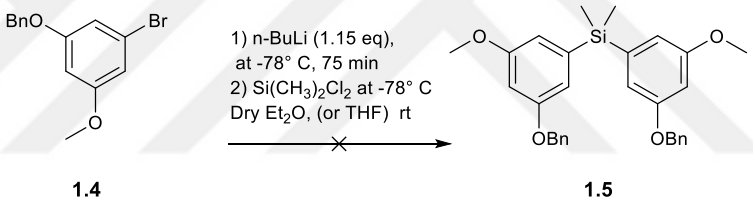

Figure 2.6. Lithium-halogen exchange attempts on **1.4**

Other lithium sources such as *sec*-BuLi and *tert*-BuLi gave similar results. Hence, grignard-halogen exchange was attempted. However, the reaction did not proceed as well and starting material was recovered. (Figure 2.6)

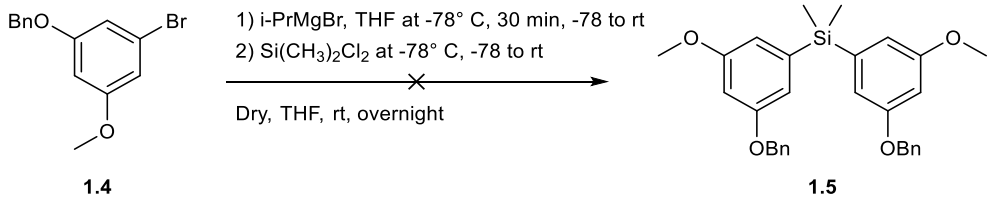

Figure 2.7. Magnesium-halogen exchange attempts on **1.4**

Butyllithium reagents exist as tetramer or dimer coordinated structures in solvents.(Tai et al., 2017) So, tetramethyl ethylenediamine (TMEDA) was added as a ligand to break

this coordinated form and increase the basicity of the *n*-butyl lithium reagent, and lithium halogen exchange reaction proceeded. Subsequent quenching with the silicon electrophile unit gave 89% yield (Compound **1.5**, Appx. **A.9**, **A.10**) without any impurities and any column chromatography. (Figure 2.8)

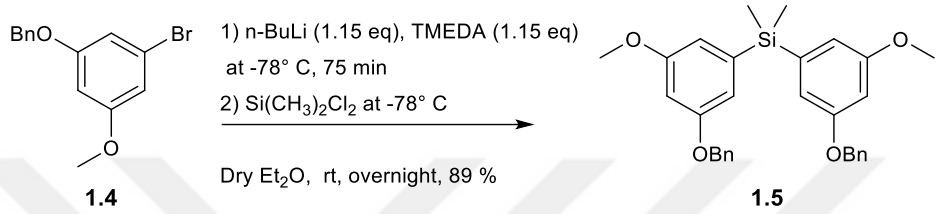

Figure 2.8. Lithium halogen exchange attempts on **1.4** with TMEDA

Then, the debenzylation reaction on the palladium/carbon catalyst gave the target compound in 92% yield. (Compound **1.2**, Appx. **A.3**, **A.4**) Overall, these 4 steps gave a much higher total yield (58%) compared to the earlier attempts (36%). Their separation and isolation processes were much easier and time and solvent-saving.

Next, several amine cyclization reactions were attempted to obtain the xanthene core structure. As a first nitration attempt, $NaNO_2$ was used in acidic ethanol according to the work of Wang group (L. Wang et al., 2020), however complex mixture formation was observed. HRMS data indicated the desired product was in the mixture however, isolation efforts were not fruitful. (Appx. **A.27**) (Figure 2.9)

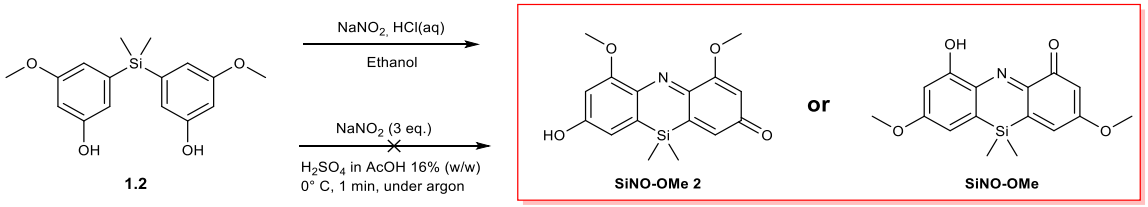

Figure 2.9. Amine cyclization attempts with $NaNO_2$.

Hence, other, milder amine cyclization reactions were attempted with isoamyl nitrite and nitrosonium tetrafluoroborate respectively. In the isoamyl nitrite reaction, NMR

data showed that one of the rings was nitrosylated. Further modification of the reaction condition like increasing the acidity of the medium and increasing the temperature did not give the desired cyclized product. (Figure 2.10)

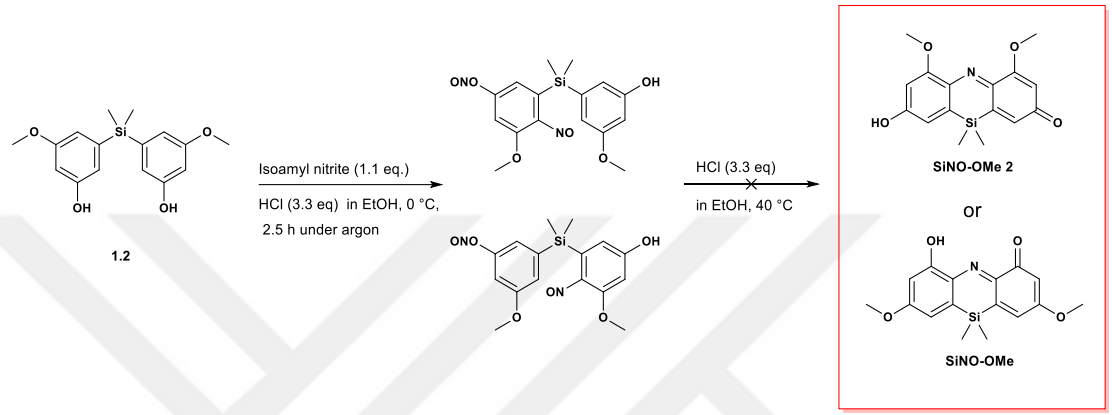

Figure 2.10. Amine cyclization attempt with isoamyl nitrite

Then, we concentrated on nitrosonium tetrafluoroborate and the nitrosylating agent. After the addition $NOBF_4$, the reaction medium turns blue from colorless. A dark red color spot arises above the starting. But this spot could not be isolated as it turned back to starting material during purification processes. In the second trial, TLC was heated with a heat gun to test if the dark red spot was an intermediate and needed energy to overcome another transition state to complete the cyclization processes. The dark red spot turned to a red fluorescent material which is consistent with the desired product. So, the reaction medium refluxed overnight after all starting turned to intermediate. However, this fluorescent spot also turned to starting material when we tried to extract it from the medium. (Data not shown) (Figure 2.11)

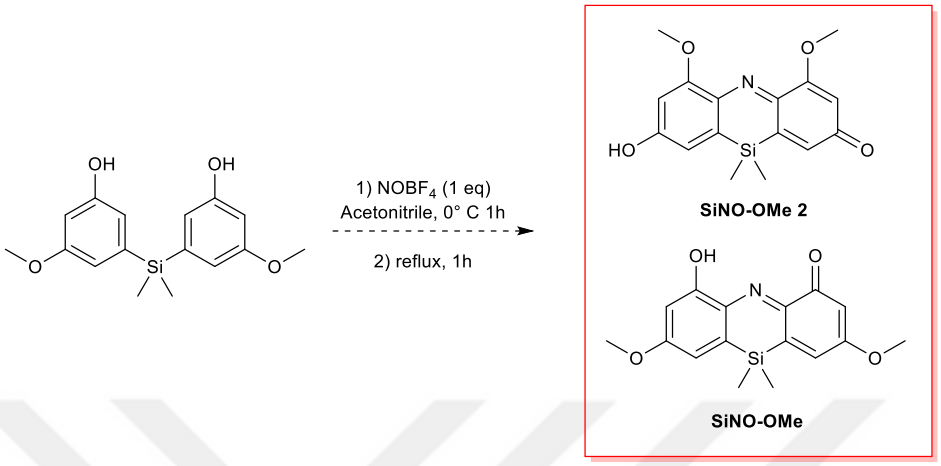

Figure 2.11. Amine cyclization attempt on **1.2** with nitrosonium tetrafluoroborate

As the next attempt, we envisioned to iodinate the compound followed by utilization of C-N cross-coupling reaction to realize the nitrogen bridge.

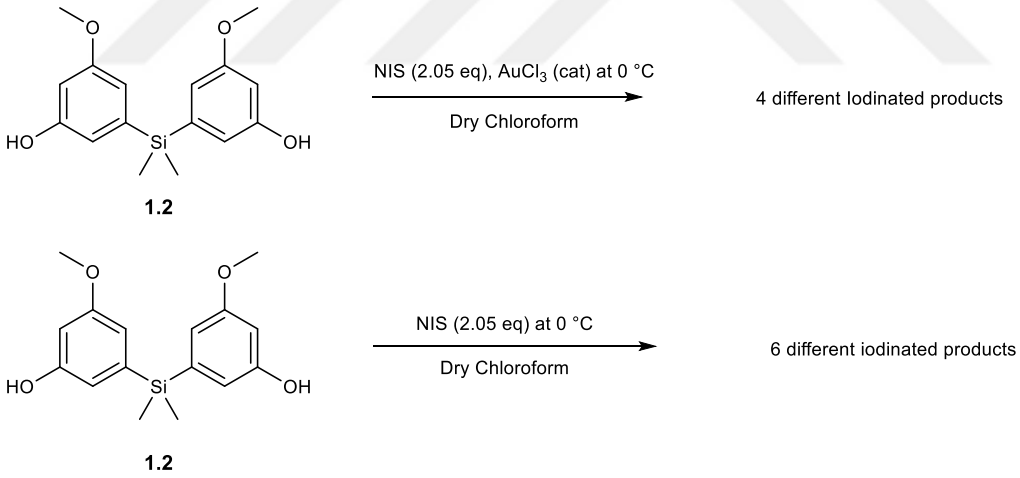

Figure 2.12. Iodination attempts on **1.2**

Although using $AuCl_3$ as a catalyst made the reaction cleaner and with less side products, four different iodinated products occurred. (Figure 2.12) Tetra-iodinated product, which can be used for further C-N cross-coupling reaction for achieving desired PDT reagent. (Figure 2.13)

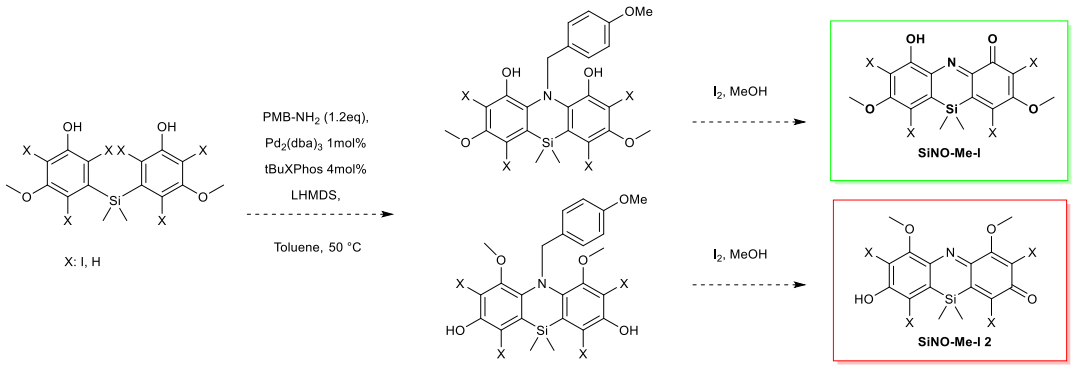

Figure 2.13. Proposed synthetic route for iodinated **SiNO-OMe**, and **SiNO-OMe2**

We decided that the difficult isolation process and poor selectivity makes this reaction impractical. So, we planned to focus on selective bromination with NBS at -60 °C (Schmalzbauer et al., 2013), followed by Buchwald-Hartwig coupling as a promising approach to achieve the synthesis of SiNO-OMe in the future.

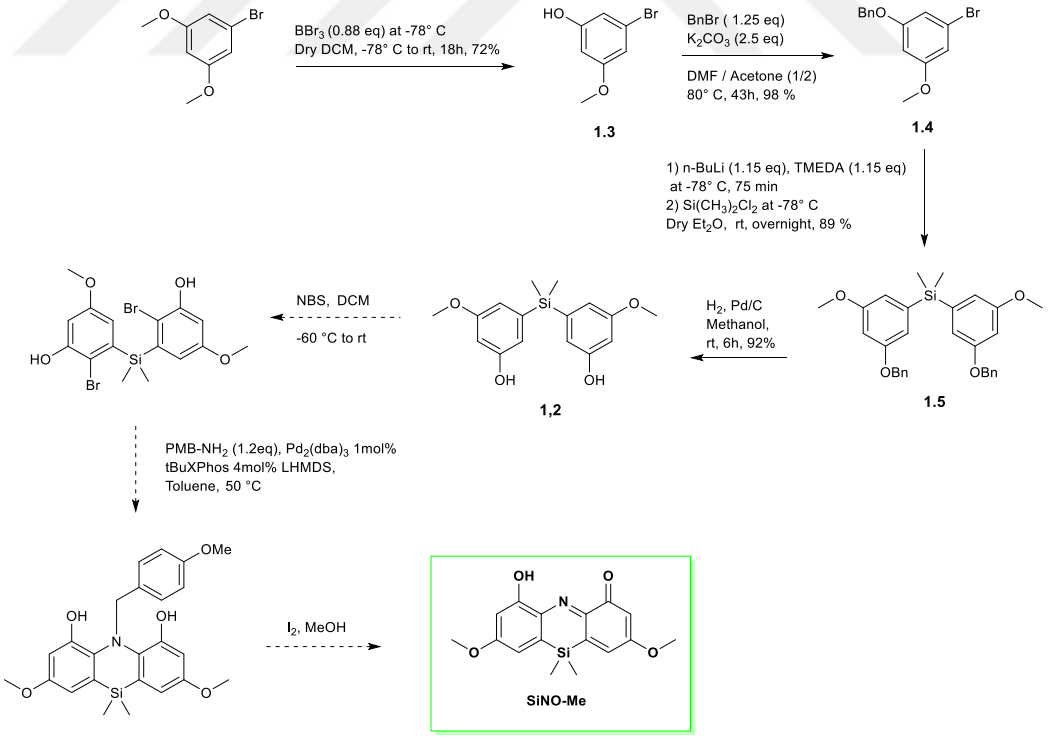

Scheme 1. Synthetic pathway of compound **SiNO-OMe**.

Studies for the Synthesis of APN Handle for SiNO-Me

Most of the active substrates for APN are L-leucine and L-alanine (Schreiber & Smith, 2018) where cleavage of the N- terminal of neutral amino acids from peptides are conducted by APN. (Mina-Osorio, 2008)

Cleaving the N- terminus of the amino acid releases the dye which will be available to sensitize, defined as ON state. Where our proposed tracing agent or PS has hydroxyl unit on the leaving site, additional traceless linker will need to get N- terminal on the substrate (Y. Wang et al., 2016). This traceless linker has entropically favored cleaved further release the drug as ON state. (Scheme 2)

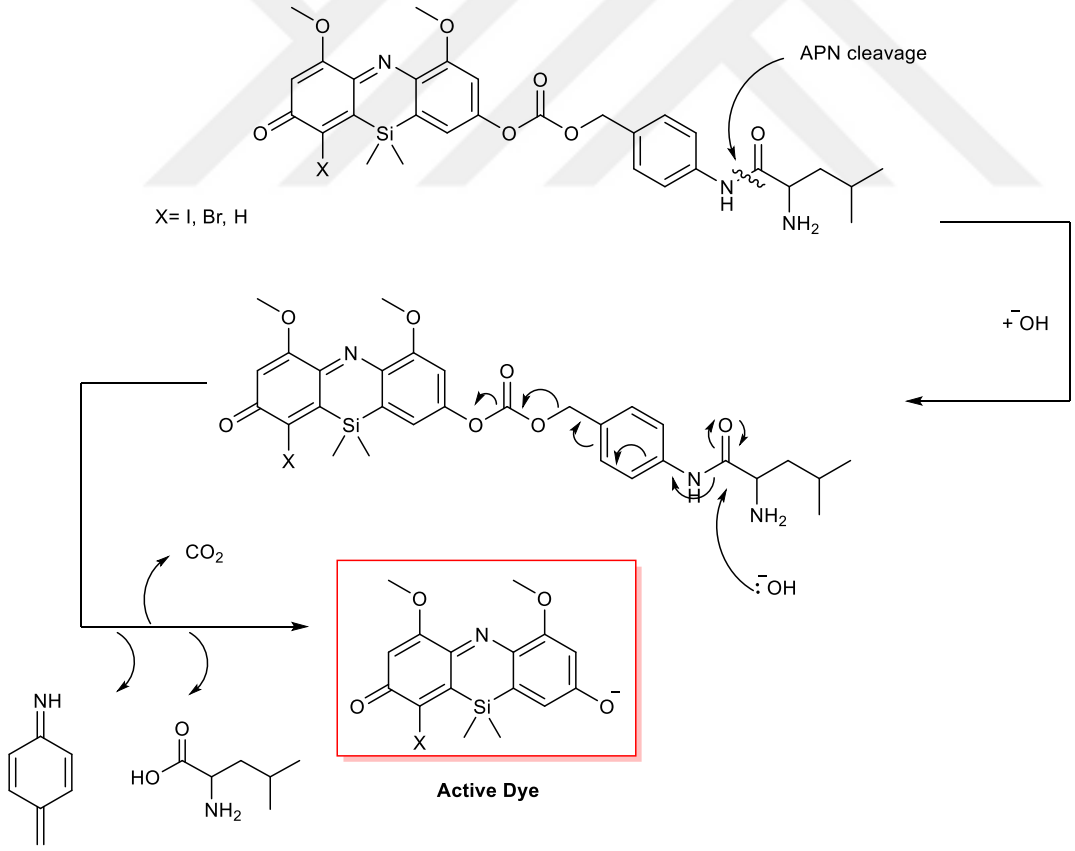

Scheme 2. APN cleavage mechanism of **APN SiNO-OMe 2**

Boc-protected leucine was coupled with 4-Aminobenzyl alcohol with EEDQ at room temperature, and the reaction was straightforward. Crude NMR confirmed the product, although there is some citric acid in it because of the work-up process. (Appx. **A.17**)

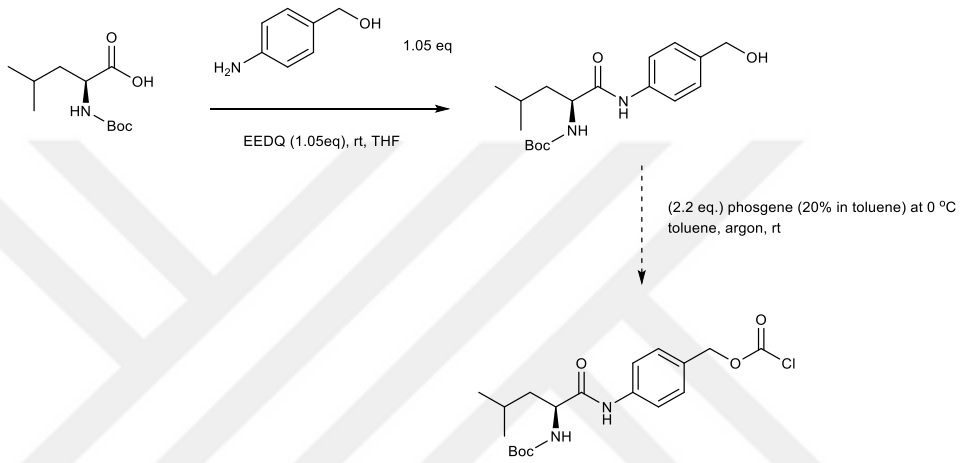

Scheme 3. Synthetic pathway of APN handle

Where the acyl chloride unit is quite reactive and has short shelf life, acylation reaction will be conducted right before coupling with the **SiNO-OMe** or **SiNO-OMe2** upon their successful synthesis. (Scheme 3)

2.2.2 Approach for the Synthesis PNN-Morp.

Buchwald–Hartwig C-N cross-coupling reaction of 1,3-dibromobenzene with morpholine was achieved by 69%. After that, the lithium-halogen exchange reaction on the aminated product was not accomplished and NMR spectra showed that there was 1 proton instead of 2 on the morpholine unit which underlines that the acidic α proton of the morpholine unit reacted with the *n*-butyllithium. (Figure 2.14)

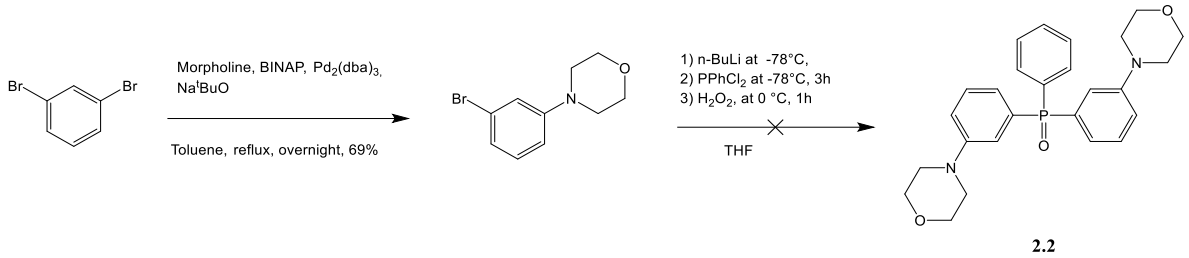

Figure 2.14. Early synthetic attempt of compound 2.2

So, I attempted to lithium-halogen exchange reaction before the amination of the core. Lithium-halogen Exchange on 1,3-dibromobenzene was quite straightforward and 2 units of 1,3-dibromobenzenes were coupled to 1 unit of phosphine followed by oxidation. (Compound **2.1**, Appx. **A.11**, **A.12**) In an earlier stage of the work, THF was utilized as the reaction solvent but then it was realized that diethyl ether increases the reaction yield to 96% from 72%. Then, other bromine units on each side were further coupled with morpholine with Buchwald–Hartwig C-N cross-coupling. (Compound **2.2**, Appx. **A.13**, **A.14**) (Scheme 4)

After the coupling process, a nitrosylation/cyclization reaction was with $NaNO_2$ in ethanol according to Wang group (L. Wang et al., 2020) but the reaction didn't run although the reaction temperature was increased gradually to reflux, and the starting material was recovered. (Figure 2.15)

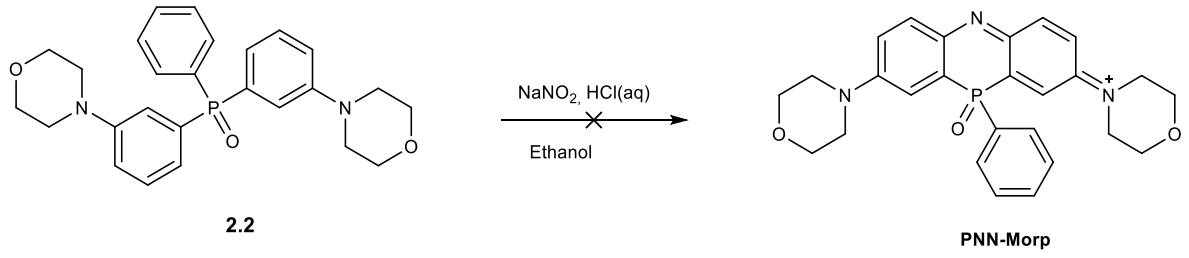

Figure 2.15. Amine cyclization attempt on compound **2.2** with $NaNO_2$

As a second nitrosylation/cyclization attempt, nitrosonium tetrafluoroborate was used. But the reaction didn't proceed even though the reaction temperature was increased up to the reflux condition. (Figure 2.16)

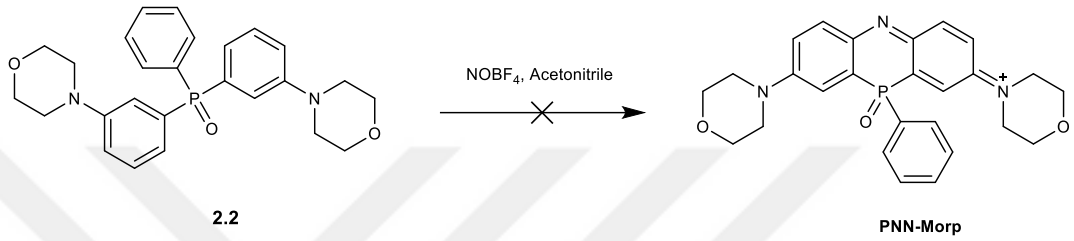

Figure 2.16. Amine cyclization attempt with nitrosonium tetrafluoroborate

Next, iodination of compound 2.2 was attempted for utilization in C-N cross-coupling reaction for making nitrogen bridge, but neither NIS or $AuCl_3$/NIS didn't yield the desired product. NMR data showed that one of the major isolated is probably related to the cleavage of the morpholine unit and iodinated from single side. (Figure 2.17)

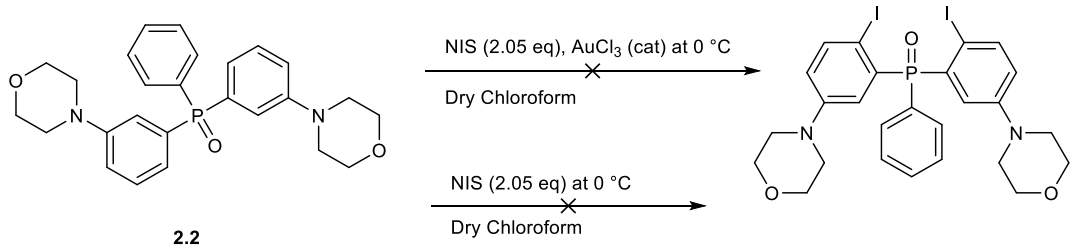

Figure 2.17. Iodination attempts of compound **2.2** with NIS

Bromination with NBS in acetonitrile on the other hand was fruitful and gave the desired product in 82% yield. (Compound **2.3**, Appx. **A.15**, **A.16**) (Figure 2.18)

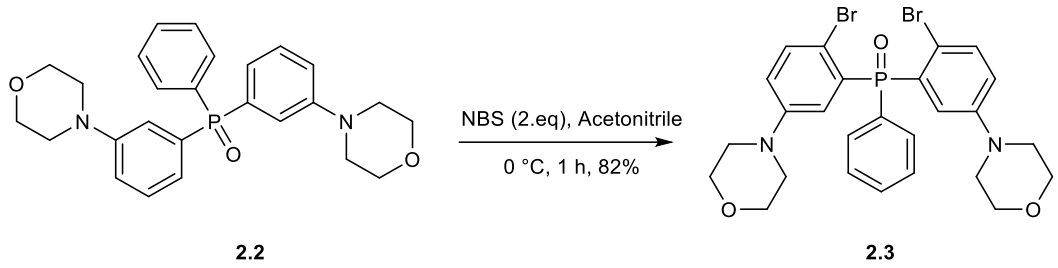

Figure 2.18. Bromination of compound 2.2 with NBS

Future work will be concentrated on effective Ullman type couplings for the installing of the nitrogen bridge (Scheme 4).

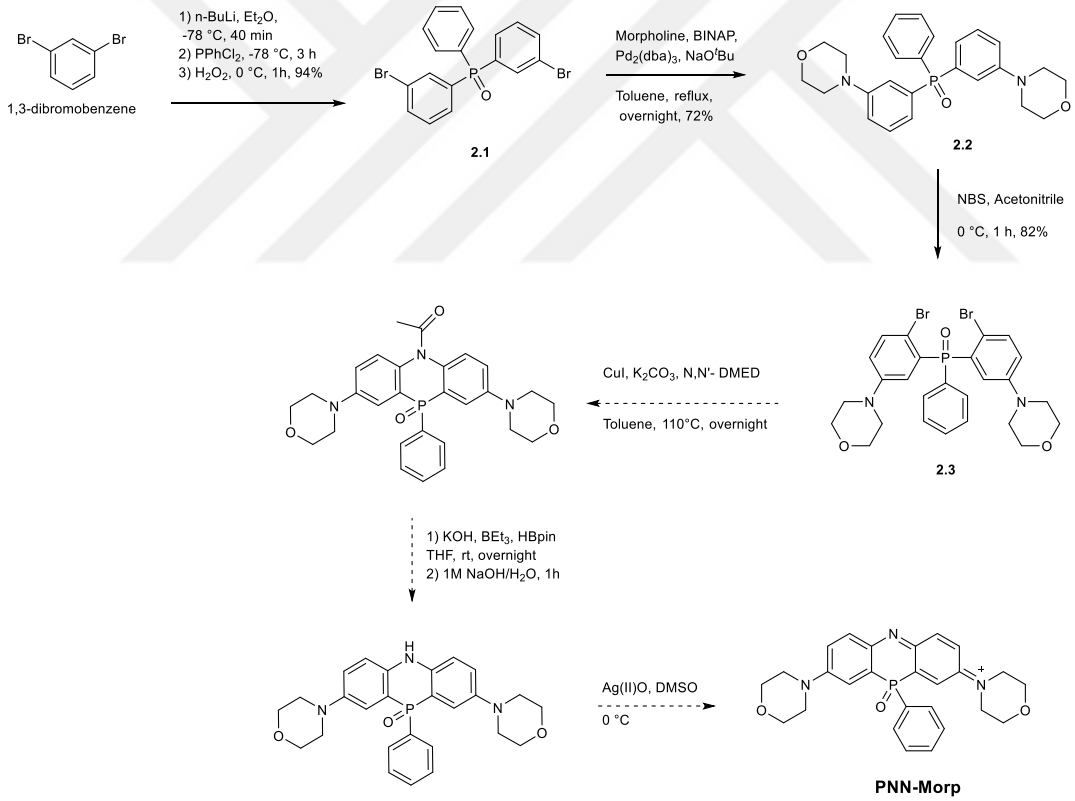

Scheme 4. Synthetic pathway of compound **PNN-Morp**

2.2.3 Approach for the Synthesis of TPA

Donor part

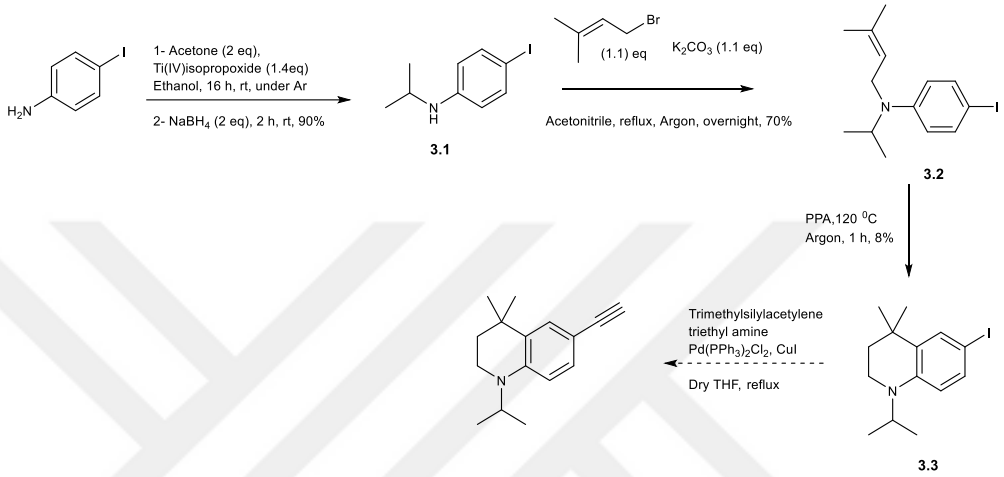

Figure 2.19. Early synthetic route for the donor part

4-iodoaniline was subjected to the reductive amination with acetone in the absence of titanium isopropoxide as a catalyst. After 16 h, $NaBH_4$ was added to reduce the imine to the desired secondary amine in 90% yield. (Compound **3.1**, Appx. **A.18**) Then, **3.1** was subjected to the nucleophilic substitution reaction with 1-bromo-3-methylbut-2-ene in the presence of a potassium carbonate to give desired tertiary amine in 70%. (Compound **3.2**, Appx. **A.19**) (Figure 2.20)

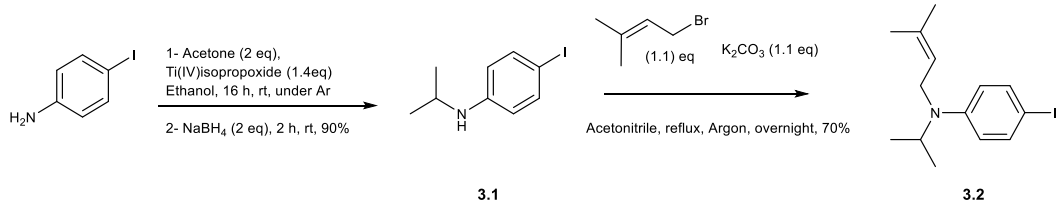

Figure 2.20. Early synthetic route for **3.2**

Then cyclization reaction was tried with polyphosphoric acid which is a polymeric acid commonly used in these types of cyclization reactions. But due to its syrup like form, it

is impractical to stir the reaction medium. So, reaction medium was mixed time to time with a sonicator, after 1 hour later reaction was quenched and subjected to the first silica column and then preparative HPLC to isolate the desired product in 8%. (Compound **3.3**, Appx. **A.20**) (Figure 2.21)

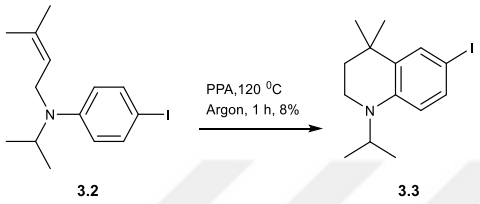

Figure 2.21. Acid catalyzed ring cyclization of **3.2**

The major product of the reaction was **3.1**. We propose that the reason behind the cleavage of the alkyl unit on the structure could be the ring strain on nitrogen atom when its protonated form under acidic conditions.

So, the synthetic path was modified in a way that, alkylation of 4-iodoaniline with 1-bromo-3-methylbut-2-ene was performed to yield a secondary amine. (Compound **3.4**, Appx. **A.21**) Then, cyclization with PPA gave the desired cyclic secondary amine with better yield (according to crude NMR) (Compound **3.5**, Appx. **A.22**), and easier isolation. (Figure 2.22)

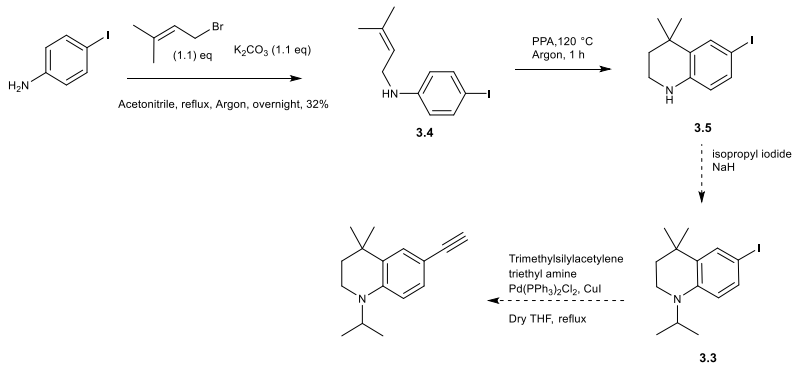

Figure 2.22. New synthetic route for donor part

Acceptor Part

7-amino-2-methyl-4H-chromen-4-one was subjected to the Sandmeyer reaction to yield the iodinated product in 35% yield. (Compound **3.6**, Appx. **A.23**, **A.24**) It is important to note that the reaction solidified at around 5 °C and the reaction started to run if $NaNO_2$ is 3 M in the reaction medium. Then, malononitrile based condensation took place in glacial acetic anhydride in 21% yield (Compound **3.7**, Appx. **A.25**, **A.26**) which can be further optimized. (Figure 2.23)

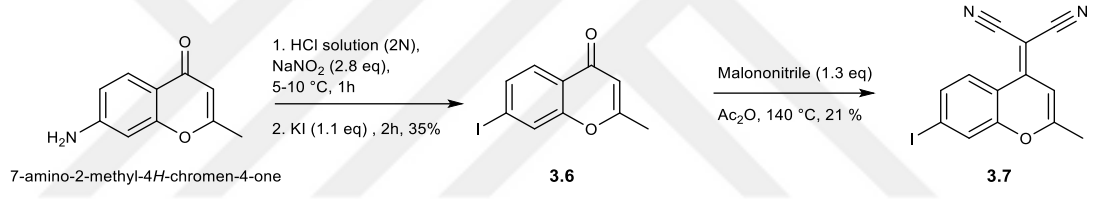

Figure 2.23. Synthetic route for acceptor part

CHAPTER 3

EXPERIMENTAL

3.1 Materials

All solvents and reagents used in the experiments were purchased from Sigma Aldrich without further purification. Thin layer chromatography (TLC) was performed using 0.25 mm silica gel plates. Visualization with UV lamp with short wavelength was achieved. All reactions were carried out in glassware washed with base and flame dried. The inert atmosphere was maintained by a slight positive pressure of Argon.

3.2 Synthesis of compound SiNO-OMe

3.2.1 Synthesis of compound 1.1

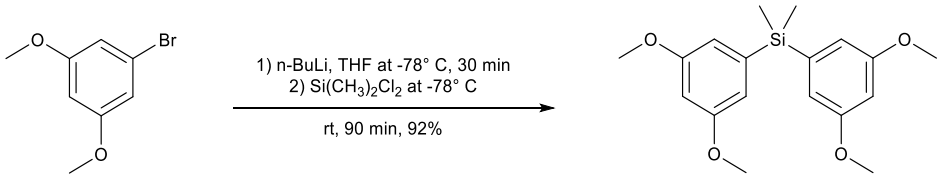

Figure 3.1 Synthetic route of compound **1.1**.

1-bromo-3,5-dimethoxybenzene (3 g, 13.8 mmol) was dissolved with dry THF (30 ml) and the reaction medium was cooled to -78 °C under argon. Subsequently, n-BuLi (1.6 M in Hexane) (1.05 eq, 8.64 ml) was added dropwise. After 30 min, $Si(CH_3)_2Cl_2$ (0.42 eq, 5.75 mmol, 0.7 mL) was added at -78°C dropwise and the mixture was stirred at this temperature for 90 min. Reaction was quenched with saturated NH_4Cl solution, diluted

with water and extracted with EtOAc. Then the combined extracts were washed with brine, dried over $MgSO_4$, filtered and the solvent was evaporated. Silica column chromatography was performed using DCM: Hexane (1:3) to (1:1) gradient to give the title compound as a colorless viscous liquid (2.1 g, 90%). ^{1}H NMR (400 MHz, $CDCl_3$) δ 6.66 (d, *J* = 2.3 Hz, 4H), 6.46 (t, *J* = 2.3 Hz, 2H), 3.78 (s, 12H), 0.52 (s, 6H). ^{13}C NMR (101 MHz, $CDCl_3$) δ 160.6, 140.5, 112.0, 101.1, 55.4, -2.3.

3.2.2 Synthesis of compound 1.2

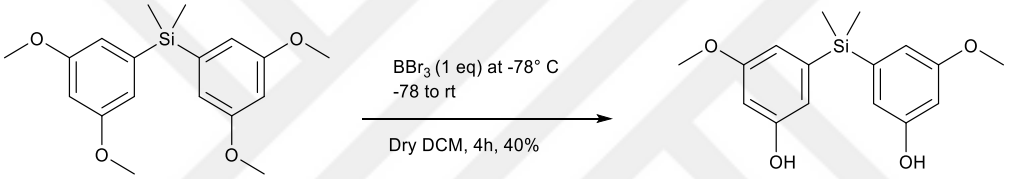

Figure 3.2 Early Synthetic route of compound **1.2**.

Compound **1.1** (2.6 g, 7.67 mmol) was dissolved in dry DCM (200 mL), and BBr_3 (1M in DCM) (1 eq, 7.7 mL) was added dropwise at -78 °C under an inert atmosphere. The reaction was allowed to warm up to rt and stirred for 4 h. The reaction medium was quenched with $NaHCO_3$/Methanol at 0 °C. All volatiles were evaporated under reduced pressure. Then, washed with saturated $NaHCO_3$ solution and extracted with EtOAc, and dried over Na_2SO_4, filtered and the solvent was evaporated. Silica column chromatography was performed using EtOAc: Hexane (1:1) as eluent and then flash column chromatography was performed and gave the title compound as a colorless solid (0.9 g, 40%).

3.2.3 Synthesis of compound 1.3

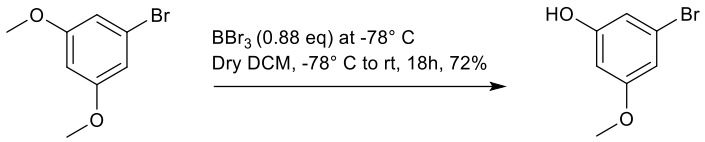

Figure 3.3 Synthetic route of compound **1.3**.

1-bromo-3,5-dimethoxybenzene (4.23g, 19.4 mmol) was dissolved in 30 ml dry DCM. Then, 17 mL BBr_3 (1M in DCM) was added dropwise at -78 °C. Then the reaction mixture was warmed to room temperature and stirred for 18 h. The reaction medium was quenched with $NaHCO_3$/Methanol at 0 °C. All volatiles were evaporated under reduced pressure. The mixture was then washed with saturated $NaHCO_3$ solution and dried over Na_2SO_4, filtered and the solvent was evaporated under reduced pressure. Silica column chromatography was performed using EtOAc: Hexane (1:3) as the eluent to give the title compound as a colorless solid (2.85 g, 72%). ^{1}H NMR (400 MHz, $CDCl_3$) δ 6.65 (s, 1H), 6.61 (s, 1H), 6.33 (t, *J* = 2.1 Hz, 1H), 4.95 (s, 1H), 3.76 (s, 3H). ^{13}C NMR (101 MHz, $CDCl_3$) δ 161.5, 157.3, 123.1, 111.7, 110.1, 55.7.

3.2.4 Synthesis of compound 1.4

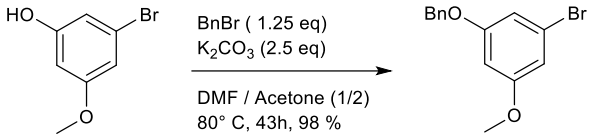

Figure 3.4 Synthetic route of compound **1.4**.

Compound **1.3** (1.61 g, 7.89 mmol) and K_2CO_3 (2.70 g, 19.7 mmol) were dissolved with DMF: Acetone (1:2) (60 ml) in a Schlenk-tube. Then the reaction was stirred for 43 h at 80 °C. After the reaction reached completion, the volatiles were evaporated under

reduced pressure. Then, 100 ml water was added and medium of the pH was set to 8 with 1M HCl. Then, the organic compound was extracted with EtOAc. The combined extracts were washed with brine, and dried over Na_2SO_4, filtered and the solvent was evaporated. Silica column chromatography was performed using EtOAc: Hexane (1:2) as eluent to give the title compound as a colorless viscous liquid (2.6 g, 98%). ^{1}H NMR (400 MHz, $CDCl_3$) δ 7.43 – 7.32 (m, 5H), 6.77 – 6.74 (m, 1H), 6.71 – 6.66 (m, 1H), 6.46 (t, *J* = 2.1 Hz, 1H), 5.01 (s, 2H), 3.76 (s, 3H). ^{13C}NMR (101 MHz, $CDCl_3$) δ 161.3, 160.5, 136.4, 128.8, 128.3, 127.7, 123.1, 110.8, 110.3, 100.7, 70.4, 55.7.

3.2.5 Synthesis of compound 1.5

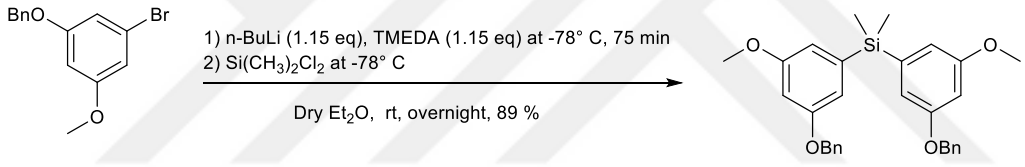

Figure 3.5 Synthetic route of compound **1.5**.

Compound **1.4** (934 mg, 3.19mmol) was dissolved with dry diethyl ether (11 ml) and N,N,N′,N′-Tetramethyl ethylenediamine (1.05 eq, 0.5 ml) was added to the reaction medium under inert atmosphere and medium was cooled to -78 °C. Subsequently, n-BuLi (2.5M in Hexane) (1.05 eq, 1.47 ml) was added dropwise. After 75 min, $Si(CH_3)_2Cl_2$ (0.42 eq, 1.36 mmol) was added at -78 °C dropwise and reaction mixture was stirred overnight at room temperature under an inert atmosphere. Reaction was quenched with saturated NH_4Cl solution, diluted with water and extracted with EtOAC. Then, the combined extracts were washed with brine, dried over $MgSO_4$, filtered and solvent was evaporated. Crude compound was the pure title compound which was yellow oil (685 mg, 89%). ^{1}H NMR (400 MHz, $CDCl_3$) δ 7.36 – 7.28 (m, 8H), 7.27 – 7.22 (m, 2H), 6.65 (d, *J* = 2.1 Hz, 2H), 6.59 (d, *J* = 2.2 Hz, 2H), 6.47 (t, J = 2.3 Hz, 2H),

4.94 (s, 4H), 3.69 (s, 6H), 0.43 (s, 7H). ^{13}C NMR (101 MHz, $CDCl_3$) δ 160.5, 159.7, 140.5, 137.0, 128.7, 128.1, 127.8, 112.7, 112.3, 70.2, 55.4, -2.3.

3.2.6 Synthesis of compound 1.2 with new path

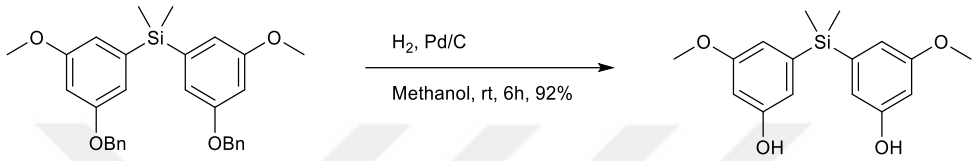

Figure 3.6 Synthetic route of compound **1.2**.

Compound **1.5** (1.36 g, 2.8 mmol) and 10% palladium on carbon (71 mg) were added to ethanol (30 mL). Then the reaction flask was filled with H_2 (2.6 bar) and stirred for 6h. The reaction was filtered from celite and washed with methanol. The solvent was evaporated to give the title compound as a greenish solid (940 mg, 92%). ^{1}H NMR (400 MHz, $CDCl_3$) δ 6.64 (s, 2H), 6.52 (s, 2H), 6.41 (s, 2H), 4.99 (s, 2H), 3.76 (s, 6H), 0.48 (s, 6H). ^{13}C NMR (101 MHz, $CDCl_3$) δ 160.6, 156.5, 140.9, 113.3, 112.4, 102.3, 55.4, -2.5.

Footnote: Green color of the title compound came from an inorganic impurity during cellite filtration, or something related with its deprotonated form. After a time, it was turning its original colorless solid form as mentioned **3.2.2**

3.3 Synthesis of compound PNN-Morp

3.3.1 Synthesis of compound 2.1

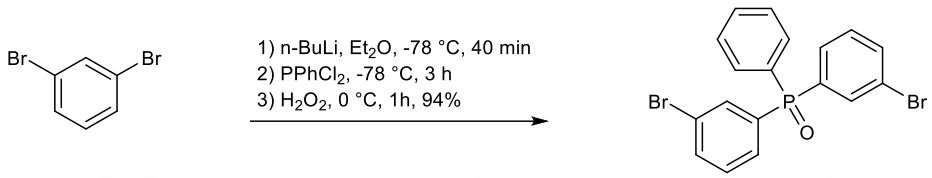

Figure 3.7 Synthetic route of compound **2.1**.

1,3-Dibromobenzene (2.356 g, 10 mmol,1 eq.) was dissolved in 20 ml dry Et_2O and reaction mixture was cooled to -78 °C. Then, n-BuLi (10.5 mmol, 1.05 eq) was added dropwise and mixture was stirred for 40 min at that temperature. After that, $PPhCl_2$ (5 mmol, 0.678 ml, 0.5 eq.) was added dropwise and reaction mixture stirred for 3 hours at that temperature. Then, the reaction mixture was heated to 0 °C and H_2O_2 (30 % (w/w) in H_2O, 2.4 ml) was added to the reaction mixture and stirred at that temperature. Then residual H_2O_2 was quenched using saturated solution of Na_2SO_3. Reaction mixture was extracted with EtOAc, washed with brine and then dried over $MgSO_4$, filtered and volatiles were removed under reduced pressure. Silica column chromatography was performed using EtOAc: Hexane (3:1) as eluent to give title compound as a colorless viscous oil (2.05 g, 94%). ^{1}H NMR (400 MHz, $CDCl_3$) δ 7.81 (d, *J* = 12.1 Hz, 2H), 7.71 – 7.68 (m, 2H), 7.68 – 7.61 (m, 2H), 7.60 – 7.54 (m, 2H), 7.51 (ddd, *J* = 10.3, 4.6, 2.0 Hz, 3H), 7.35 (td, *J* = 7.8, 3.4 Hz, 2H). ^{13}C NMR (100 MHz, $CDCl_3$) δ 135.2, 135.2, 134.9, 134.5, 134.4, 133.9, 132.5, 131.8, 131.7, 131.3, 130.3, 130.2, 130.1, 128.8, 128.7, 123.3, 123.1.

3.3.2 Synthesis of compound 2.2

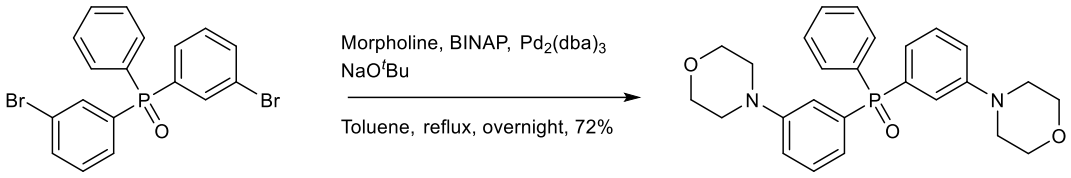

Figure 3.8 Synthetic route of compound **2.2**.

Compound **2.1** (1.29 g, 2.97 mmol, 1eq.), Morpholine (543 mg, 6.23 mmol, 2.1 eq.), BINAP (185 mg, 0.297 mmol, 0.1 eq.), $Pd_2(dba)_3$ (272 mg, 0.297 mmol, 0.1 eq.), Sodium *tert*-butoxide (684 mg, 7.12 mmol, 2.4 eq.) was dissolved in 6 ml dry Toluene. Then, the reaction mixture was allowed to be stirred overnight under reflux. After that, the reaction was filtered through cellite, and then volatiles were removed under reduced pressure. Then silica column chromatography was performed using 5% MeOH in EtOAc as eluent to give title compound as a pale brown solid (0.96 g, 72%). ^{1}H NMR (400 MHz, $CDCl_3$) δ 7.64 (dd, *J* = 11.4, 7.8 Hz, 2H), 7.52 (t, *J* = 7.3 Hz, 1H), 7.42 (dd, *J* = 22.0, 10.5 Hz, 4H), 7.30 (td, *J* = 7.9, 3.3 Hz, 2H), 7.05 (d, *J* = 8.1 Hz, 2H), 6.93 (dd, J = 11.1, 7.6 Hz, 2H), 3.81 (t, 8H), 3.16 (t, 8H). ^{13}C NMR (101 MHz, $CDCl_3$) δ 151.3, 151.1, 133.8, 133.3, 132.7, 132.2, 132.2, 132.1, 132.0, 132.0, 129.3, 129.2, 128.6, 128.5, 123.3, 123.1, 118.7, 118.6, 66.8, 48.9.

3.3.3 Synthesis of Compound 2.3

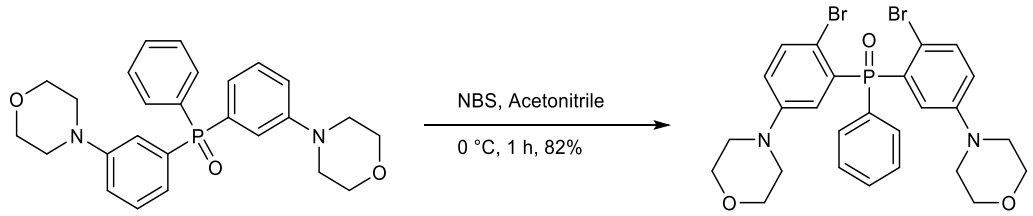

Figure 3.9 Synthetic route of compound **2.3**.

Bis(3-morpholinophenyl)(phenyl)phosphine oxide (224 mg, 0.5 mmol) was dissolved in 5 ml Acetonitrile and N-Bromosuccinimide (182 mg, 1.03 mmol, 2.05 eq.) was added portion wise at 0 °C and stirred for 1 hour at that temperature. The reaction mixture was washed with saturated $NaHCO_3$ solution and extracted with ethyl acetate. Then, all the combined extracts were washed with brine, dried over Na_2SO_4, filtrated, and volatiles were removed under reduced pressure. Silica column chromatography was performed using 4% MeOH in EtOAc as eluent to give title compound as a white solid (250 mg, 82%). ^{1}H NMR (400 MHz, $CDCl_3$) δ 7.84 (dd, *J* = 12.5, 7.2 Hz, 2H), 7.60 – 7.54 (m, 1H), 7.49 (ddd, *J* = 11.9, 8.1, 4.1 Hz, 4H), 7.29 (dd, *J* = 15.1, 3.0 Hz, 2H), 6.91 (dd, *J* = 8.7, 2.7 Hz, 2H), 3.79 (t, 8H), 3.06 (t, 8H). ^{13C}NMR (101 MHz, $CDCl_3$) δ 150.1, 150.0, 135.2, 135.1, 133.1, 132.8, 132.7, 132.3, 132.1, 131.4, 130.3, 128.6, 128.4, 123.3, 123.2, 120.2, 115.0, 66.6, 48.6.

3.4 Synthesis of APN Handle

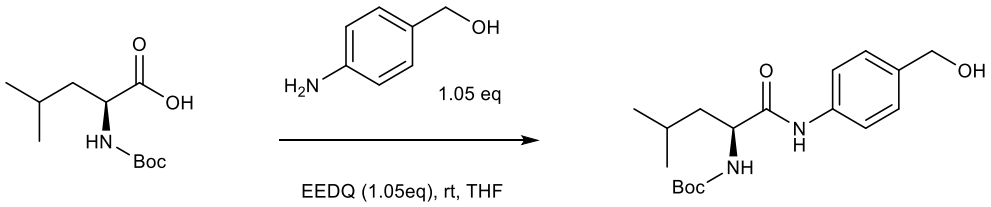

Figure 3.10 Synthetic route of APN handle.

Boc-L-Leucine monohydrate (230 mg, 0.92 mmol) and 4-iodobenzyl alcohol (120 mg, 0.98 mmol) were dissolved with 6 ml dry THF, and then N-Ethoxycarbonyl-2-ethoxy-1,2-dihydroquinoline (242.3 mg, 0.98 mmol) was added to the reaction mixture and stirred overnight at room temperature. Then reaction mixture was washed with saturated $NaHCO_3$ solution, extracted with EtOAc and then all the combined extracts were washed with 10% aqueous Citric acid solution and brine respectively, dried over Na_2SO_4, filtrated, and volatiles were removed under reduced pressure. 200 mg yellow

solid crude product was obtained. ^{1}H NMR (400 MHz, Methanol-d4) δ 7.54 (d, *J* = 8.1 Hz, 2H), 7.31 (d, *J* = 8.1 Hz, 2H), 4.56 (s, 2H), 4.24 – 4.18 (m, 1H), 1.78 – 1.70 (m, 1H), 1.63 – 1.55 (m, 2H), 1.45 (s, 9H), 1.00 – 0.95 (m, 6H).

3.5 Synthesis of TPA

3.5.1 Donor Part

3.5.1.1 Synthesis of Compound 3.1

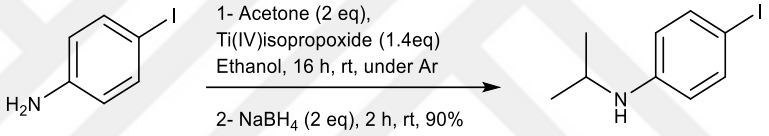

Figure 3.11. Synthetic route of Compound **3.1.**

4-Iodoaniline (1.27 g, 5.81 mmol) was dissolved with 4 ml Ethanol and Acetone (2.0 eq, 670 mg). Then, titanium (IV) isopropoxide (1.4 eq, 2.3 g) was carefully added to the mixture under inert atmosphere and reaction mixture was stirred 16 hours at room temperature. After that, $NaBH_4$ (2.0 eq) was added portion wise over 10 min and stirred for 2 hours. Reaction mixture was cooled to 0 °C and quenched with aqueous ammonia (2N, 10 mL). The Occurred precipitates were filtered and washed with Et_2O, and filtrate was concentrated until water left under reduced pressure. Then, organic compound was extracted with Et_2O and washed with brine, dried over $MgSO_4$, filtrated and volatiles were removed under reduced pressure. Silica column chromatography was performed using Hexane: EtOAc (4:1) as eluent to give title compound as a yellow liquid (1.36 g, 90 %) ^{1}H NMR (400 MHz, $CDCl_3$) δ 7.40 (d, *J* = 8.8 Hz, 2H), 6.38 (d, *J* = 8.8 Hz, 2H), 3.57 (p, *J* = 6.3 Hz, 1H), 1.19 (d, *J* = 6.3 Hz, 6H).

3.5.1.2 Synthesis of Compound 3.2

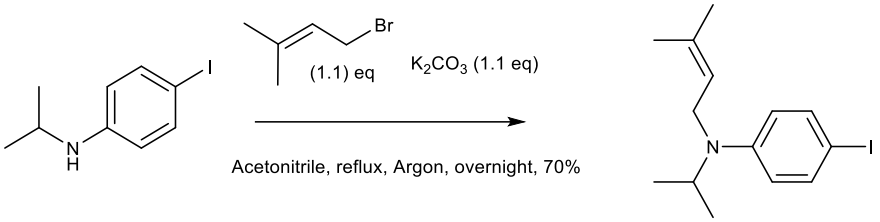

Figure 3.12. Synthetic route of Compound **3.2**.

Compound **3.1** (254 mg, 0.97 mmol), K_2CO_3 (148 mg, 1.1 mmol), and 1-bromo-3-methylbut-2-ene (159 mg, 1.1 mmol) were dissolved with 3 ml Acetonitrile and reaction mixture was stirred overnight at reflux. After the reaction reached completion, reaction mixture was washed with water and extracted with EtOAc. Combined extracts were dried over Na_2SO_4, filtrated, and volatiles were removed under reduced pressure. Silica column chromatography was performed using Hexane: EtOAc (19:1) as eluent to give title compound as a colorless liquid (228 mg, 70%) ^{1}H NMR (400 MHz, $CDCl_3$) δ 7.41 (d, *J* = 9.0 Hz, 2H), 6.48 (d, *J* = 9.0 Hz, 2H), 5.05 (t, *J* = 5.5 Hz, 1H), 4.02 (sept, *J* = 13.2, 6.6 Hz, 1H), 3.73 (d, *J* = 5.2 Hz, 2H), 1.71 (s, 3H), 1.69 (s, 3H), 1.16 (d, *J* = 6.6 Hz, 6H).

3.5.1.3 Synthesis of Compound 3.3

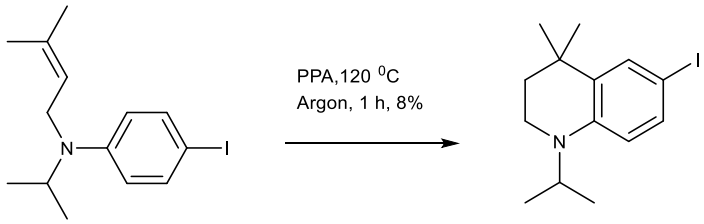

Figure 3.13. Synthetic route of Compound **3.3**.

Compound **3.2** (134 mg, 0.41 mmol) and PPA (498 mg) were added to the Schlenk tube and mixture was heated for 1 hour at 120 °C under inert atmosphere. Then, the reaction was washed with saturated $NaHCO_3$ solution and extracted with EtOAc. Combined extracts were dried over Na_2SO_4, filtrated and volatiles were removed under reduced pressure. Silica column chromatography was performed using Hexane: Et_2O (19:1) as eluent and then HPLC was performed to isolate the title compound as a pink liquid. (8 mg, 8%) ^{1}H NMR (400 MHz, $CDCl_3$) δ 7.39 (d, *J* = 2.2 Hz, 1H), 7.29 (dd, *J* = 8.8, 2.2 Hz, 1H), 6.49 (d, *J* = 8.8 Hz, 1H), 4.05 (dt, *J* = 13.2, 6.6 Hz, 1H), 3.19 – 3.13 (m, 2H), 1.70 – 1.63 (m, 2H), 1.25 (d, *J* = 5.3 Hz, 7H), 1.19 (d, *J* = 6.6 Hz, 6H).

3.5.1.4 Synthesis of Compound 3.4

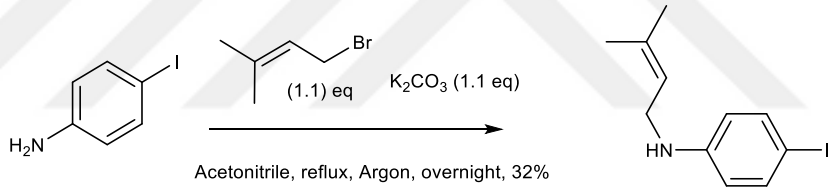

Figure 3.14. Synthetic route of Compound **3.4**.

Compound **3.3** (210 mg, 0.97 mmol), K_2CO_3 (148 mg, 1.1 mmol), and 1-bromo-3-methylbut-2-ene (159 mg, 1.1 mmol) were dissolved with 3 ml Acetonitrile and reaction mixture was stirred overnight at reflux. After the reaction reached completion, the reaction mixture was washed with water and extracted with EtOAc. Combined extracts were dried over Na_2SO_4, filtrated, and volatiles were removed under reduced pressure. Silica column chromatography was performed using Hexane: EtOAc (19:1) as eluent to give title compound as a colorless liquid (92 mg, 32 %) ^{1}H NMR (400 MHz, $CDCl_3$) δ 7.41 (d, *J* = 8.9 Hz, 2H), 6.39 (d, *J* = 8.8 Hz, 2H), 5.29 (t, *J* = 6.7 Hz, 1H), 3.64 (d, *J* = 6.7 Hz, 2H), 1.75 (s, 3H), 1.70 (s, 3H).

3.5.1.5 Synthesis of compound 3.5

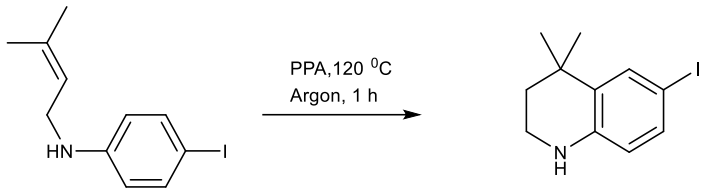

Figure 3.15. Synthetic route of Compound **3.5**.

Same procedure described as for the synthesis of compound **3.3** except HPLC. ^{1}H NMR (400 MHz, $CDCl_3$) δ 7.40 (d, *J* = 2.0 Hz, 1H), 7.19 (dd, *J* = 8.4, 2.0 Hz, 1H), 6.26 (d, *J* = 8.4 Hz, 1H), 3.33 – 3.27 (m, 2H), 1.71 – 1.68 (m, 2H), 1.26 (s, 6H).

3.5.2 Acceptor Part

3.5.2.1 Synthesis of compound 3.6

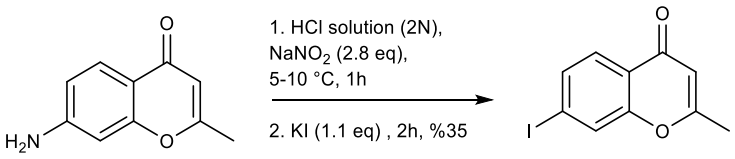

Figure 3.16. Synthetic route of Compound **3.6**.

7-amino-2-methyl-4H-chromen-4-one (450 mg, 2.6 mmol) was dissolved with 4.5 ml water. Then, 1.5 ml of 8M HCl and $NaNO_2$ (1.2 g,18 mmol) were added respectively to the mixture portion wise and stirred for 1 hour at 10 °C. Then, saturated KI solution (1.1 eq) was added dropwise to the reaction mixture and mixture was stirred for 2 hours. The reaction mixture was washed with saturated $NaHCO_3$ solution and extracted with EtOAc, dried over Na_2SO_4, filtrated, and volatiles were removed under reduced pressure. Silica column chromatography was performed using Hexane: EtOAc (1:1) as eluent to give title compound as a colorless solid (260 mg, 35%). ^{1}H NMR (400 MHz,

$CDCl_3$) δ 7.88 – 7.83 (m, 2H), 7.70 (dd, *J* = 8.3, 1.4 Hz, 1H), 6.17 (s, 1H), 2.37 (s, 3H). ^{13C}NMR (101 MHz, $CDCl_3$) δ 177.7, 166.2, 156.2, 134.3, 127.1, 126.9, 123.0, 110.9, 99.8, 20.7.

3.5.2.2 Synthesis of compound 3.7

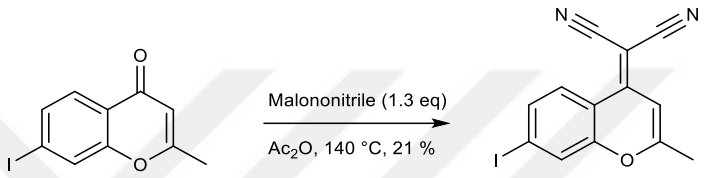

Figure 3.17. Synthetic route of Compound **3.7**.

Compound **3.6** (80 mg, 0.28 mmol), malononitrile (24 mg, 0.36 mmol) and 0.3 ml acetic anhydride were added to the Schlenk tube and mixture was stirred overnight at reflux. Then, the reaction was cooled to 55 °C and 2.4 ml Methanol was added to the mixture and mixture was stirred for 2 hours. After that, volatiles were evaporated under reduced pressure. The remaining part was washed with saturated $NaHCO_3$ solution and extracted with EtOAc. Combined extracts were dried over Na_2SO_4, filtrated, and volatiles were removed under reduced pressure. Silica column chromatography was performed using Hexane: EtOAc (3:1) to (1:1) gradient to give title compound as a red solid (20 mg, 21%). ^{1}H NMR (400 MHz, $CDCl_3$) δ 8.59 (d, *J* = 8.8 Hz, 1H), 7.86 (d, *J* = 1.6 Hz, 1H), 7.75 (dd, *J* = 8.8, 1.6 Hz, 1H), 6.70 (s, 1H), 2.41 (s, 3H). ^{13C}NMR (101 MHz, $CDCl_3$) δ 161.5, 152.6, 135.3, 127.9, 126.5, 117.0, 116.3, 115.2, 105.6, 101.1, 63.1, 20.5.

Material and methods (Computational)

Geometric pre-optimization was done with the IqMol software which uses the force field for the geometrical optimization.

Then, B3LYP functional and 6-31+G* basis set were used for the geometric conformational optimization using the Gaussian09 software.

For the excited state calculations, Time Dependent Density Functional Theory was used with the B3LYP functional and 6-31+G* basis set, again using the Gaussian09 software. In addition, for the excited state calculations the excited state solvation method was performed. Implicit solvation method was used for vertical excitation. (Frank-Condon principle) (Koç, 2018; Yang, 2003)

CHAPTER 4

CONCLUSION

Several demethylation attempts performed on bis-aryl silicon derivative (**1.1**) and found that uses of soft bases like hydroiodic acid and thiols as demethylation agent break the carbon-silicon bond where their demethylation mechanism same which first nucleophile make nucleophilic attack on methoxy carbon then, cleavage of carbon and oxygen bond. On the other hand, BBr_3 is quite a strong Lewis base and commonly used for demethylation of methoxy unit on aromatic compounds and their mechanisms involve forming boron oxygen covalent bond and then, breaking carbon oxygen bond by nucleophilic attack of a nucleophile (free bromine in the solution) to the methoxy carbon. For our case, demethylation reaction worked well, and no C-Si bond cleavage observed in crude NMR.

Several nitrosation/cyclization attempts were done for **1.2** and **2.2**. None of them were fruitful for bis-aryl silicone and phosphine derivatives. When this work was ongoing, Romieu et al. published their work (Jenni et al., 2022) which involve nitrosation/cyclization reaction on bis-aryl ether and silicon analogue. Where nitrosation/cyclization reaction with $NOBF_4$ worked for Bis-aryl ether derivative, silicon analogue did not yield desired results. (Scheme 5)

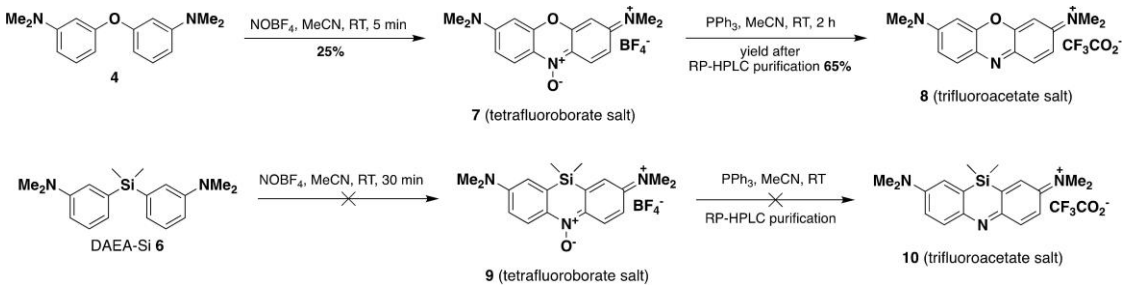

Scheme 5. Schematic demonstration of nitrosation/cyclization reaction on bis-aryl ether and silicon analogue (Jenni et al., 2022)

This can be attributed to the size of the silicon atom and C-Si bond length such a way that carbons on the adjacent aryl units are too far away to form nitrogen bridge compared to bis-aryl ether. Thus, forming nitrogen bridge between two aryl units can be quite energy demanding. Although Wang group (L. Wang et al., 2020) achieved success in forming nitrogen bride with nitrosation/cyclization reaction for a bis-aryl silicone derivative in low yields (Figure 1.18), their structure had tertiary amine units on the para positions which is better ring activating group compared to methoxy or hydroxy unit. To install the nitrogen bridge and exceed the energy barrier of its transition state, future work will be concentrated on Ullmann and Buchwald-Hartwig cross couplings for the synthesis of both **SiNO-OMe** and **PNN-Morp**. (Scheme 6) (Scheme 8)

Another challenge in front of the success in the synthesis of **SiNO-OMe** is the control for the final position hydroxy units. To overcome this problem, selective bromination will be involved before the coupling reaction in the future work. If selectivity is achieved, the position of the resonance contributors on the xanthene core structures can be arranged for the desired applications which will be milestone for the facile synthesis of new type of near IR absorbing dyes.

For the substitution of heavy atom on the **SiNO-OMe**, easily cleavable alkyl halide unit will be substituted to the hydroxy unit. In this way, electron delocalization will be hindered, and heavy atom will be installed to the structure.(Almammadov et al., 2020,

2022) After that, the cleavable unit will be cleaved with a mild acid, SiNO-OMe-X (X: I or Br) will be obtained as PDT agent.

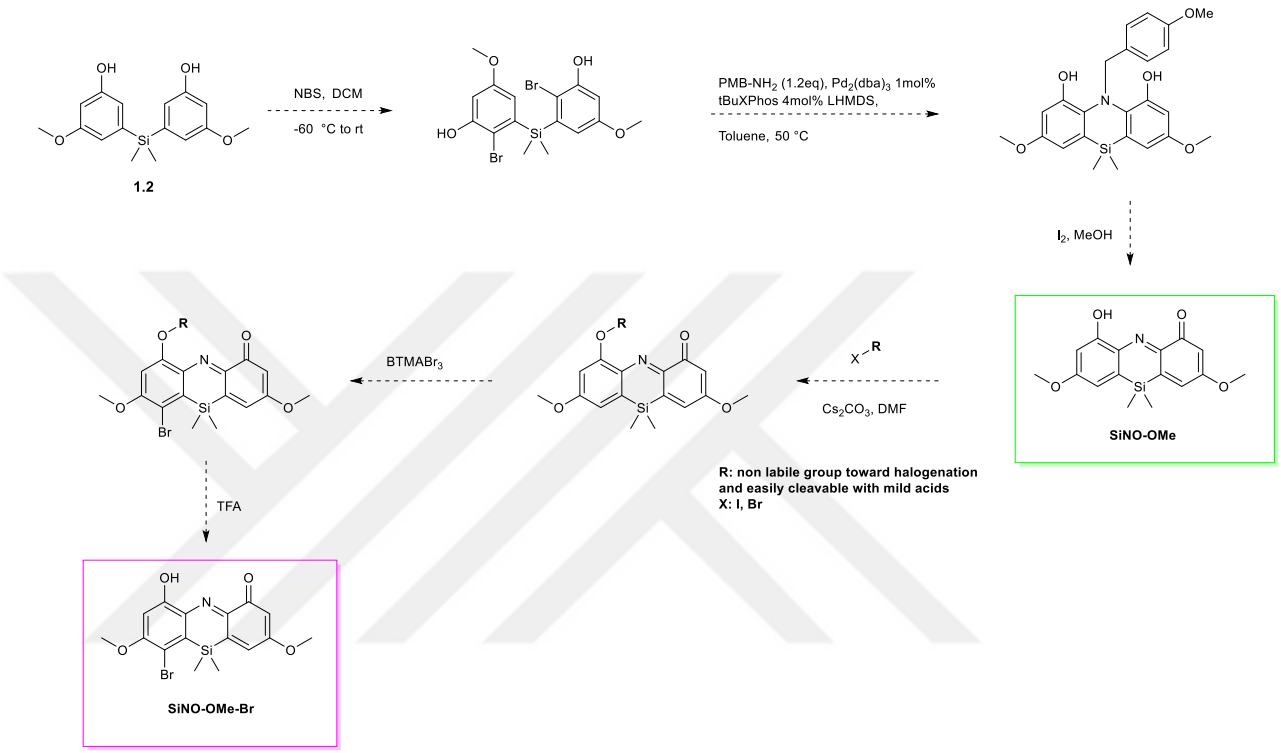

Scheme 6. Proposed synthetic pathway of **SiNO-OMe** and **SiNO-OMe-Br**.

To obtain ON-OFF PS, APN handle will be substituted in the presence of a Cs_2CO_3 and then boc group will be cleaved with TFA. (Scheme 7)

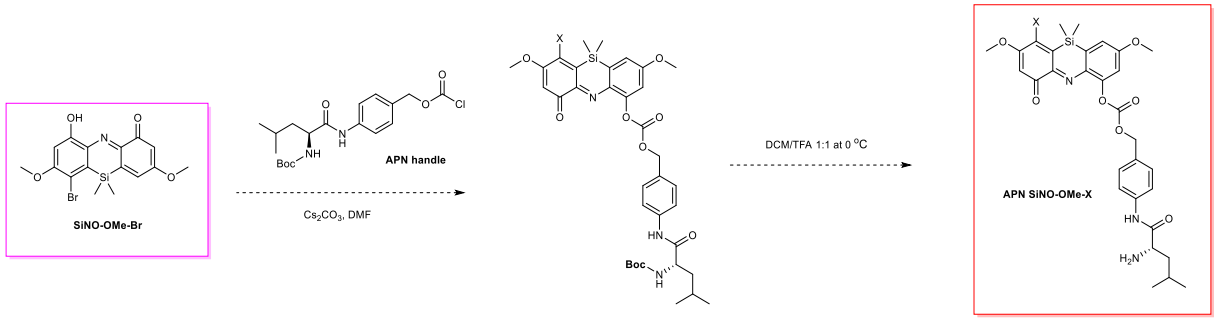

Scheme 7. Proposed synthetic pathway of **APN SiNO-OMe-X**

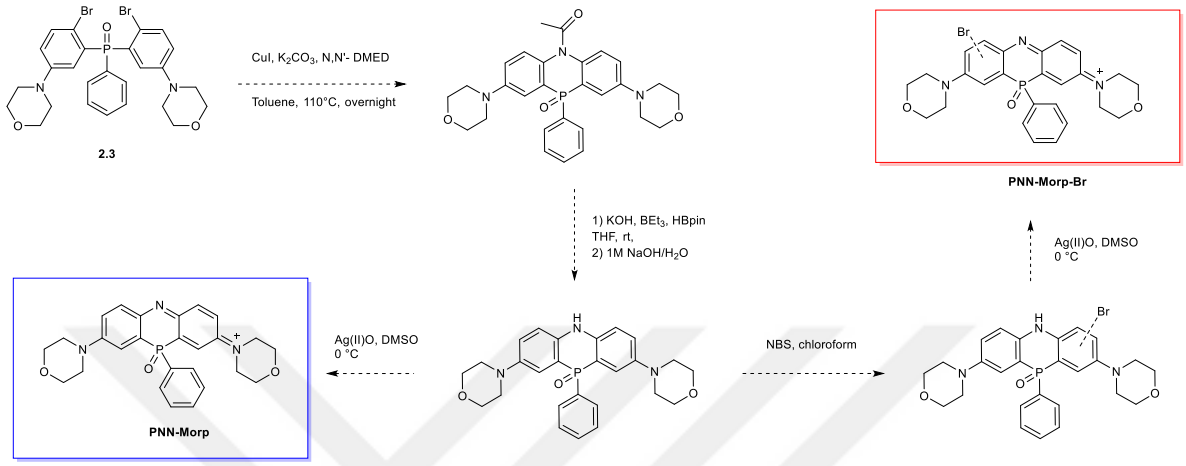

Scheme 8. Proposed synthetic pathway of **PNN-Morp** and **PNN-Morp-Br**.

After all the synthesis of mentioned dyes, their optical properties and performance in *in vitro* studies will be evaluated as well.

We found out that tertiary amine on the retinoid structure (donor part of the **TPA**) made a ring strain during the cyclization reaction under acidic condition and decomposed to its earlier precursor. The new synthetic route developed in this thesis made cyclization reaction straightforward and rendered isolation easier. In the future work, reaction condition will be optimized, and compound **3.5** will be alkylated. Hence, the donor part will be ready for Sonogashira coupling with acceptor part to yield TPA (Scheme 9), then its photophysical properties and in vitro studies will be evaluated.

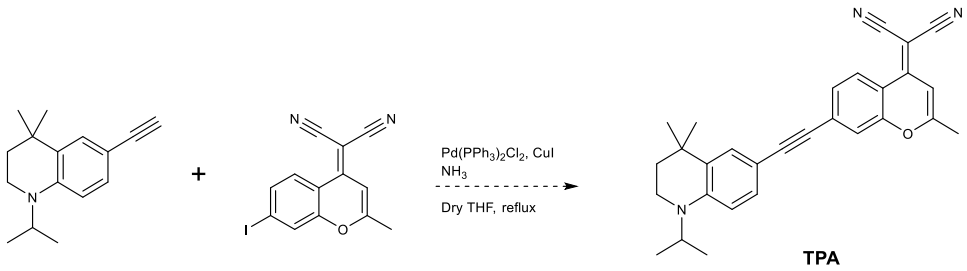

Scheme 9. Proposed synthetic route of **TPA**.

REFERENCES

Abrahamse, H., & Hamblin, M. R. (2016). New photosensitizers for photodynamic therapy. *Biochemical Journal*, *473*(4), 347–364. https://doi.org/10.1042/BJ20150942

Almammadov, T., Atakan, G., Leylek, O., Ozcan, G., Gunbas, G., & Kolemen, S. (2020). Resorufin Enters the Photodynamic Therapy Arena: A Monoamine Oxidase Activatable Agent for Selective Cytotoxicity. *ACS Medicinal Chemistry Letters*, *11*(12), 2491–2496. https://doi.org/10.1021/ACSMEDCHEMLETT.0C00484/ASSET/IMAGES/LARGE/ML0C00484_0006.JPEG

Almammadov, T., Elmazoglu, Z., Atakan, G., Kepil, D., Aykent, G., Kolemen, S., & Gunbas, G. (2022). Locked and Loaded: β-Galactosidase Activated Photodynamic Therapy Agent Enables Selective Imaging and Targeted Treatment of Glioblastoma Multiforme Cancer Cells. *ACS Applied Bio Materials*, *2022*, 4293. https://doi.org/10.1021/ACSABM.2C00484/ASSET/IMAGES/MEDIUM/MT2C00484_M001.GIF

Anderson, R. R., & Parrish, J. A. (1981). The Optics of Human Skin. *Journal of Investigative Dermatology*, *77*(1), 13–19. https://doi.org/10.1111/1523-1747.EP12479191

Angelier, J. (1990). Inversion of field data in fault tectonics to obtain the regional stress—III. A new rapid direct inversion method by analytical means. *Geophysical Journal International*, *103*(2), 363–376. https://doi.org/10.1111/J.1365-246X.1990.TB01777.X

Awuah, S. G., & You, Y. (2012). Boron Dipyrromethene (BODIPY)-Based Photosensitizers For Photodynamic Therapy. *RSC Advances*, *2*(30), 11169–11183. https://doi.org/10.1039/C2RA21404K

Bacellar, I. O. L., Tsubone, T. M., Pavani, C., & Baptista, M. S. (2015). Photodynamic Efficiency: From Molecular Photochemistry to Cell Death. *International Journal of Molecular Sciences 2015, Vol. 16, Pages 20523-20559*, *16*(9), 20523–20559. https://doi.org/10.3390/IJMS160920523

Bauernschmitt, R., & Ahlrichs, R. (1996). Treatment of electronic excitations within the adiabatic approximation of time dependent density functional theory. *Chemical Physics Letters*, *256*(4–5), 454–464. https://doi.org/10.1016/0009-2614(96)00440-X

Calzavara-Pinton, P., Szeimies, R.-M., & Ortel, B. (2001). *Photodynamic Therapy and Fluorescence Diagnosis in Dermatology* (Vol. 2). Elsevier.

Casida, M. E., Jamorski, C., Casida, K. C., & Salahub, D. R. (1998). Molecular excitation energies to high-lying bound states from time-dependent density-functional response theory: Characterization and correction of the time-dependent local density approximation ionization threshold. *The Journal of Chemical Physics*, *108*(11), 4439–4449. https://doi.org/10.1063/1.475855

Chai, X., Cui, X., Wang, B., Yang, F., Cai, Y., Wu, Q., & Wang, T. (2015). Near-Infrared Phosphorus-Substituted Rhodamine with Emission Wavelength above 700 nm for Bioimaging. *Chemistry – A European Journal*, *21*(47), 16754–16758. https://doi.org/10.1002/CHEM.201502921

Chisholm, D. R., Lamb, R., Pallett, T., Affleck, V., Holden, C., Marrison, J., O'toole, P., Ashton, P. D., Newling, K., Steffen, A., Nelson, A. K., Mahler, C., Valentine, R., Blacker, T. S., Bain, A. J., Girkin, J., Marder, T. B., Whiting, A., & Ambler, C. A. (2019). *Photoactivated cell-killing involving a*

low molecular weight, donor-acceptor diphenylacetylene †. https://doi.org/10.1039/c9sc00199a

Choi, A., & Miller, S. C. (2018). Silicon Substitution in Oxazine Dyes Yields Near-Infrared Azasiline Fluorophores That Absorb and Emit beyond 700 nm. *Organic Letters*, *20*(15), 4482–4485. https://doi.org/10.1021/ACS.ORGLETT.8B01786/ASSET/IMAGES/LARGE/OL-2018-017866_0002.JPEG

Dabrowski, J. M., Urbanska, K., Arnaut, L. G., Pereira, M. M., Abreu, A. R., Simões, S., & Stochel, G. (2011). Biodistribution and Photodynamic Efficacy of a Water-Soluble, Stable, Halogenated Bacteriochlorin against Melanoma. *ChemMedChem*, *6*(3), 465–475. https://doi.org/10.1002/CMDC.201000524

Danial, N. N., Gramm, C. F., Scorrano, L., Zhang, C. Y., Krauss, S., Ranger, A. M., Datta, S. R., Greenberg, M. E., Licklider, L. J., Lowell, B. B., Gygi, S. P., & Korsmeyer, S. J. (2003). BAD and glucokinase reside in a mitochondrial complex that integrates glycolysis and apoptosis. *Nature 2003 424:6951*, *424*(6951), 952–956. https://doi.org/10.1038/nature01825

Danial, N. N., & Korsmeyer, S. J. (2004). Cell Death: Critical Control Points. *Cell*, *116*(2), 205–219. https://doi.org/10.1016/S0092-8674(04)00046-7

Daniell, M. D., & Hill, J. S. (1991). A history of photodynamic therapy. *Australian and New Zealand Journal of Surgery*, *61*(5), 340–348.

Detty, M. R., Gibson, S. L., & Wagner, S. J. (2004). Current clinical and preclinical photosensitizers for use in photodynamic therapy. *Journal of Medicinal Chemistry*, *47*(16), 3897–3915. https://doi.org/10.1021/JM040074B/ASSET/IMAGES/LARGE/JM040074BC00019.JPEG

Dolmans, D. E. J. G. J., Fukumura, D., & Jain, R. K. (2003). Photodynamic therapy for cancer. *Nature Reviews Cancer 2003 3:5*, *3*(5), 380–387. https://doi.org/10.1038/nrc1071

Drobizhev, M., Meng, F., Rebane, A., Stepanenko, Y., Nickel, E., & Spangler, C. W. (2006a). Strong two-photon absorption in new asymmetrically substituted porphyrins: Interference between charge-transfer and intermediate-resonance pathways. *Journal of Physical Chemistry B*, *110*(20), 9802–9814. https://doi.org/10.1021/JP0551770

Drobizhev, M., Meng, F., Rebane, A., Stepanenko, Y., Nickel, E., & Spangler, C. W. (2006b). Strong two-photon absorption in new asymmetrically substituted porphyrins: Interference between charge-transfer and intermediate-resonance pathways. *Journal of Physical Chemistry B*, *110*(20), 9802–9814. https://doi.org/10.1021/JP0551770/ASSET/IMAGES/MEDIUM/JP0551770E00019.GIF

Dysart, J. S., & Patterson, M. S. (2005). Characterization of Photofrin photobleaching for singlet oxygen dose estimation during photodynamic therapy of MLL cells in vitro. *Physics in Medicine & Biology*, *50*(11), 2597. https://doi.org/10.1088/0031-9155/50/11/011

Fleming, S., Mills, A., & Tuttle, T. (2011). Predicting the UV–vis spectra of oxazine dyes. *Beilstein Journal of Organic Chemistry 7:56*, *7*(1), 432–441. https://doi.org/10.3762/BJOC.7.56

Foote, C. S. (1991). Definition of Type I And Type II Photosensitized Oxidation. *Photochemistry and Photobiology*, *54*(5), 659–659. https://doi.org/10.1111/J.1751-1097.1991.TB02071.X

Fu, M., Xiao, Y., Qian, X., Zhao, D., & Xu, Y. (2008). A design concept of long-wavelength fluorescent analogs of rhodamine dyes: replacement of oxygen with silicon atom. *Chemical Communications*, *15*, 1780–1782. https://doi.org/10.1039/B718544H

Gala De Pablo, J., Chisholm, D. R., Ambler, C. A., Peyman, S. A., Whiting, A., & Evans, S. D. (2020). Detection and time-tracking activation of a photosensitiser on live single colorectal cancer cells using Raman spectroscopy †. *Cite This: Analyst*, *145*, 5878. https://doi.org/10.1039/d0an01023e

Göppert-Mayer, M. (1931). Über Elementarakte mit zwei Quantensprüngen. *Annalen Der Physik*, *401*(3), 273–294. https://doi.org/10.1002/ANDP.19314010303

Hu, F., Xu, S., Liu, B., Hu, F., Xu, S., & Liu, B. (2018). Photosensitizers with Aggregation-Induced Emission: Materials and Biomedical Applications. *Advanced Materials*, *30*(45), 1801350. https://doi.org/10.1002/ADMA.201801350

Jenni, S., Renault, K., Dejouy, G., Debieu, S., Laly, M., & Romieu, A. (2022). In Situ Synthesis of Phenoxazine Dyes in Water: Application for “Turn-On” Fluorogenic and Chromogenic Detection of Nitric Oxide**. *ChemPhotoChem*, *6*(5), e202100268. https://doi.org/10.1002/CPTC.202100268

Juarranz, Á., Jaén, P., Sanz-Rodríguez, F., Cuevas, J., & González, S. (2008). Photodynamic therapy of cancer. Basic principles and applications. *Clinical and Translational Oncology*, *10*(3), 148–154. https://doi.org/10.1007/S12094-008-0172-2/METRICS

Jung, H. S., Han, J., Shi, H., Koo, S., Singh, H., Kim, H. J., Sessler, J. L., Lee, J. Y., Kim, J. H., & Kim, J. S. (2017). Overcoming the Limits of Hypoxia in Photodynamic Therapy: A Carbonic Anhydrase IX-Targeted Approach. *Journal of the American Chemical Society*, *139*(22), 7595–7602. https://doi.org/10.1021/JACS.7B02396/ASSET/IMAGES/LARGE/JA-2017-02396M_0011.JPEG

Juzeniene, A., Nielsen, K. P., & Moan, J. (2006). Biophysical Aspects of Photodynamic Therapy. *Journal of Environmental Pathology, Toxicology and Oncology*, *25*(1–2), 7–28. https://doi.org/10.1615/JENVIRONPATHOLTOXICOLONCOL.V25.I1-2.20

Kaiser, W., & Garrett, C. G. B. (1961). Two-Photon Excitation in CaF2:Eu2+. *Physical Review Letters*, *7*(6), 229. https://doi.org/10.1103/PhysRevLett.7.229

Karaman, O., Alkan, G. A., Kizilenis, C., Akgul, C. C., & Gunbas, G. (2023). Xanthene dyes for cancer imaging and treatment: A material odyssey. *Coordination Chemistry Reviews*, *475*, 214841. https://doi.org/10.1016/J.CCR.2022.214841

Kawai, C., Ferreira, J. C., Baptista, M. S., & Nantes, I. L. (2014). Not only oxidation of cardiolipin affects the affinity of cytochrome c for lipid bilayers. *Journal of Physical Chemistry B*, *118*(41), 11863–11872. https://doi.org/10.1021/JP504518G/ASSET/IMAGES/LARGE/JP-2014-04518G_0006.JPEG

Kessel, D. (1990). *Photodynamic Therapy of Neoplastic Disease* (Vol. 1). CRC Press.

Kessel, D., & Poretz, R. D. (2000). Sites of Photodamage Induced by Photodynamic Therapy with a Chlorin e6 Triacetoxymethyl Ester (CAME). *Photochemistry and Photobiology*, *71*(1), 94–96. https://doi.org/10.1562/0031-8655(2000)0710094SOPIBP2.0.CO2

Koç, H. (2018). Analytical Evaluation for Calculation of Two-Center Franck-Condon Factor and Matrix Elements. *Journal of Chemistry*, *2018*. https://doi.org/10.1155/2018/3147981

Lan, M., Zhao, S., Liu, W., Lee, C. S., Zhang, W., & Wang, P. (2019). Photosensitizers for Photodynamic Therapy. *Advanced Healthcare Materials*, *8*(13), 1900132. https://doi.org/10.1002/ADHM.201900132

Li, J., Chen, L., Wu, W., Zhang, W., Ma, Z., Cheng, Y., Du, L., & Li, M. (2014). Discovery of bioluminogenic probes for aminopeptidase N imaging. *Analytical Chemistry*, *86*(5), 2747–2751. https://doi.org/10.1021/AC404176X/SUPPL_FILE/AC404176X_SI_001.PDF

Li, W., Zhang, J., Gao, Z., Qi, J., & Ding, D. (2022). *Advancing biomedical applications via manipulating intersystem crossing*. https://doi.org/10.1016/j.ccr.2022.214754

Li, X., Lovell, J. F., Yoon, J., & Chen, X. (2020). Clinical development and potential of photothermal and photodynamic therapies for cancer. *Nature Reviews Clinical Oncology*, *17*. https://doi.org/10.1038/s41571-020-0410-2

Lipson, R. L., & Baldes, E. J. (1960). The Photodynamic Properties of a Particular Hematoporphyrin Derivative. *Archives of Dermatology*, *82*(4), 508–516. https://doi.org/10.1001/ARCHDERM.1960.01580040026005

Liu, H. W., Hu, X. X., Li, K., Liu, Y., Rong, Q., Zhu, L., Yuan, L., Qu, F. L., Zhang, X. B., & Tan, W. (2017). A mitochondrial-targeted prodrug for NIR imaging guided and synergetic NIR photodynamic-chemo cancer therapy. *Chemical Science*, *8*(11), 7689–7695. https://doi.org/10.1039/C7SC03454G

Liu, Y., Jiang, Y., Zhang, M., Tang, Z., He, M., & Bu, W. (2018). Modulating Hypoxia via Nanomaterials Chemistry for Efficient Treatment of Solid Tumors. *Accounts of Chemical Research*, *51*(10), 2502–2511. https://doi.org/10.1021/ACS.ACCOUNTS.8B00214/ASSET/IMAGES/LARGE/AR-2018-00214H_0007.JPEG

Marques, M. A. L., & Gross, E. K. U. (2004). TIME-DEPENDENT DENSITY FUNCTIONAL THEORY. *Https://Doi.Org/10.1146/Annurev.Physchem.55.091602.094449*, *55*, 427–455. https://doi.org/10.1146/ANNUREV.PHYSCHEM.55.091602.094449

Mina-Osorio, P. (2008). The moonlighting enzyme CD13: old and new functions to target. *Trends in Molecular Medicine*, *14*(8), 361–371. https://doi.org/10.1016/J.MOLMED.2008.06.003

Moagar-Poladian, G. (2008). Sub-wavelength resolution laser lithography in the field of MEMS. *Https://Doi.Org/10.1117/12.801971*, *7007*, 158–168. https://doi.org/10.1117/12.801971

Moan, J., & Berg, K. (1991). The Photodegradation of Porphyrins In Cells Can Be Used To Estimate The Lifetime of Singlet Oxygen. *Photochemistry and Photobiology*, *53*(4), 549–553. https://doi.org/10.1111/J.1751-1097.1991.TB03669.X

Monro, S., Colón, K. L., Yin, H., Roque, J., Konda, P., Gujar, S., Thummel, R. P., Lilge, L., Cameron, C. G., & McFarland, S. A. (2019). Transition Metal Complexes and Photodynamic Therapy from a Tumor-Centered Approach:

Challenges, Opportunities, and Highlights from the Development of TLD1433. *Chemical Reviews*, *119*(2), 797–828. https://doi.org/10.1021/ACS.CHEMREV.8B00211/ASSET/IMAGES/LARGE/CR-2018-00211X_0016.JPEG

Morton, C. A., Brown, S. B., Collins, S., Ibbotson, S., Jenkinson, H., Kurwa, H., Langmack, K., Mckenna, K., Moseley, H., Pearse, A. D., Stringer, M., Taylor, D. K., Wong, G., & Rhodes, L. E. (2002). Guidelines for topical photodynamic therapy: report of a workshop of the British Photodermatology Group. *British Journal of Dermatology*, *146*(4), 552–567. https://doi.org/10.1046/J.1365-2133.2002.04719.X

Mroz, P., Yaroslavsky, A., Kharkwal, G. B., & Hamblin, M. R. (2011). Cell Death Pathways in Photodynamic Therapy of Cancer. *Cancers 2011, Vol. 3, Pages 2516-2539*, *3*(2), 2516–2539. https://doi.org/10.3390/CANCERS3022516

Niemz, M. H. (2007). *Laser-tissue interactions fundamentals and applications.* (3rd ed.). Springer.

Nyman, E. S., & Hynninen, P. H. (2004). Research advances in the use of tetrapyrrolic photosensitizers for photodynamic therapy. *Journal of Photochemistry and Photobiology B: Biology*, *73*(1–2), 1–28. https://doi.org/10.1016/J.JPHOTOBIOL.2003.10.002

O'Connor, A. E., Gallagher, W. M., & Byrne, A. T. (2009). Porphyrin and Nonporphyrin Photosensitizers in Oncology: Preclinical and Clinical Advances in Photodynamic Therapy. *Photochemistry and Photobiology*, *85*(5), 1053–1074. https://doi.org/10.1111/J.1751-1097.2009.00585.X

Ormond, A. B., & Freeman, H. S. (2013). Dye Sensitizers for Photodynamic Therapy. *Materials 2013, Vol. 6, Pages 817-840*, *6*(3), 817–840. https://doi.org/10.3390/MA6030817

Pavani, C., Uchoa, A. F., Oliveira, C. S., Iamamoto, Y., & Baptista, M. S. (2009). Effect of zinc insertion and hydrophobicity on the membrane interactions and PDT activity of porphyrin photosensitizers. *Photochemical and Photobiological Sciences*, *8*(2), 233–240. https://doi.org/10.1039/B810313E/METRICS

Pawlicki, M., Collins, H. A., Denning, R. G., & Anderson, H. L. (2009a). Two-Photon Absorption and the Design of Two-Photon Dyes. *Angewandte Chemie International Edition*, *48*(18), 3244–3266. https://doi.org/10.1002/ANIE.200805257

Pawlicki, M., Collins, H. A., Denning, R. G., & Anderson, H. L. (2009b). Two-photon absorption and the design of two-photon dyes. *Angewandte Chemie - International Edition*, *48*(18), 3244–3266. https://doi.org/10.1002/ANIE.200805257

Plaetzer, K., Krammer, B., Berlanda, J., Berr, F., & Kiesslich, T. (2009). Photophysics and photochemistry of photodynamic therapy: Fundamental aspects. *Lasers in Medical Science*, *24*(2), 259–268. https://doi.org/10.1007/S10103-008-0539-1/FIGURES/5

Rubio, N., Fleury, S. P., & Redmond, R. W. (2009). Spatial and temporal dynamics of in vitro photodynamic cell killing: Extracellular hydrogen peroxide mediates neighbouring cell death. *Photochemical and Photobiological Sciences*, *8*(4), 457–464. https://doi.org/10.1039/B815343D/METRICS

Runge, E., & Gross, E. K. U. (1984). Density-Functional Theory for Time-Dependent Systems. *Physical Review Letters*, *52*(12), 997. https://doi.org/10.1103/PhysRevLett.52.997

Sakamoto, K., Kato, T., Kawaguchi, T., Ohno-Okumura, E., Urano, T., Yamaoka, T., Suzuki, S., & Cook, M. J. (2002). Photosensitizer efficacy of non-peripheral substituted alkylbenzopyridoporphyrazines for photodynamic therapy of cancer. *Journal of Photochemistry and Photobiology A: Chemistry*, *153*(1–3), 245–253. https://doi.org/10.1016/S1010-6030(02)00292-7

Schmalzbauer, B., Herrmann, J., Müller, R., & Menche, D. (2013). Total synthesis and antibacterial activity of dysidavarone A. *Organic Letters*, *15*(4), 964–967. https://doi.org/10.1021/OL400156U/SUPPL_FILE/OL400156U_SI_001.PDF

Schreiber, C. L., & Smith, B. D. (2018). Molecular Imaging of Aminopeptidase N in Cancer and Angiogenesis. *Contrast Media and Molecular Imaging*, *2018*. https://doi.org/10.1155/2018/5315172

Senge, M. O., & Brandt, J. C. (2011). Temoporfin (Foscan®, 5,10,15,20-Tetra(m-hydroxyphenyl)chlorin)—A Second-generation Photosensitizer†,‡. *Photochemistry and Photobiology*, *87*(6), 1240–1296. https://doi.org/10.1111/J.1751-1097.2011.00986.X

Shafirstein, G. (2023). Current status of PDT in the United States. *Photodiagnosis and Photodynamic Therapy*, *41*, 103439. https://doi.org/10.1016/J.PDPDT.2023.103439

Sternberg, E. D., Dolphin, D., & Brückner, C. (1998). Porphyrin-based photosensitizers for use in photodynamic therapy. *Tetrahedron*, *54*(17), 4151–4202. https://doi.org/10.1016/S0040-4020(98)00015-5

Stratmann, R. E., Scuseria, G. E., & Frisch, M. J. (1998). An efficient implementation of time-dependent density-functional theory for the calculation of excitation energies of large molecules. *The Journal of Chemical Physics*, *109*(19), 8218–8224. https://doi.org/10.1063/1.477483

Tai, O., Hopson, R., & Williard, P. G. (2017). Aggregation and Solvation of n-Butyllithium. *Organic Letters*, *19*(15), 3966–3969. https://doi.org/10.1021/ACS.ORGLETT.7B01644

Tkachenko, N. V. (2006). Optical Spectroscopy: Methods and Instrumentations. In *Elsevier*. Elsevier.

Tsujimoto, Y. (2012). Multiple ways to die: Non-apoptotic forms of cell death. *Acta Oncologica*, *51*(3), 293–300. https://doi.org/10.3109/0284186X.2011.648340

Wang, L., Liu, J., Zhao, S., Zhang, H., Sun, Y., Wei, A., Guo, W., Li, R., Chemcomm, /, & Communication, C. (2020). Fluorescence imaging of hypochlorous acid and peroxynitrite in vitro and in vivo with emission wavelength beyond 750 nm †. *Chem. Commun*, *7718*, 7718. https://doi.org/10.1039/d0cc02322a

Wang, W., Moriyama, L. T., & Bagnato, V. S. (2012). Photodynamic therapy induced vascular damage: an overview of experimental PDT. *Laser Physics Letters*, *10*(2), 023001. https://doi.org/10.1088/1612-2011/10/2/023001

Wang, Y., Li, J., Feng, L., Yu, J., Zhang, Y., Ye, D., & Chen, H. Y. (2016). Lysosome-targeting fluorogenic probe for cathepsin B imaging in living

cells. *Analytical Chemistry*, *88*(24), 12403–12410. https://doi.org/10.1021/ACS.ANALCHEM.6B03717/ASSET/IMAGES/LARGE/AC-2016-03717M_0006.JPEG

Wang, Z., Wu, H., Liu, P., Zeng, F., & Wu, S. (2017). A self-immolative prodrug nanosystem capable of releasing a drug and a NIR reporter for in vivo imaging and therapy. *Biomaterials*, *139*, 139–150. https://doi.org/10.1016/J.BIOMATERIALS.2017.06.002

Wilson, W. R., & Hay, M. P. (2011). Targeting hypoxia in cancer therapy. *Nature Reviews Cancer 2011 11:6*, *11*(6), 393–410. https://doi.org/10.1038/nrc3064

Xiao, Y., & Qian, X. (2020). Substitution of oxygen with silicon: A big step forward for fluorescent dyes in life science. *Coordination Chemistry Reviews*, *423*, 213513. https://doi.org/10.1016/J.CCR.2020.213513

Yang, D.-S. (2003). *Comprehensive Coordination Chemistry II* (Vol. 2). Elsevier.

Zhu, T. C., & Finlay, J. C. (2008). The role of photodynamic therapy (PDT) physics. *Medical Physics*, *35*(7Part1), 3127–3136. https://doi.org/10.1118/1.2937440

APPENDICES

A. NMR Spectra

Each compound was analyzed by Bruker Spectrospin Avance DPX-400 Spectrometer with $CDCl_3$ or CD_3OD as the solvent and TMS as the internal reference.

A.1 NMR Spectra of SiNO-OMe

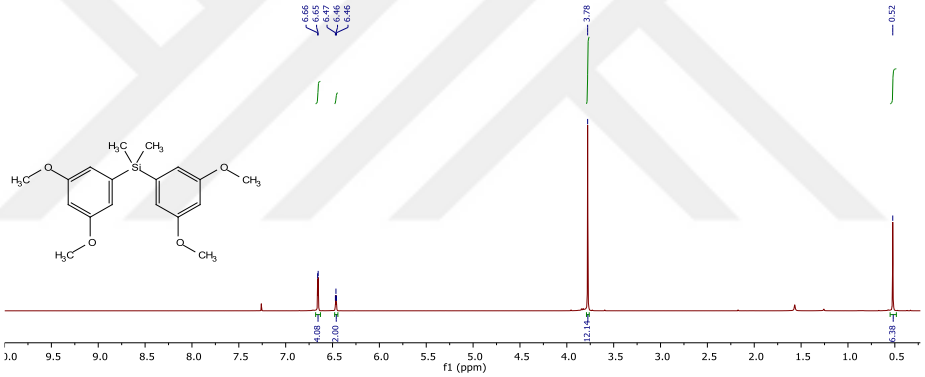

Figure A.1 ^{1H}NMR spectrum of compound **1.1** in $CDCl_3$.

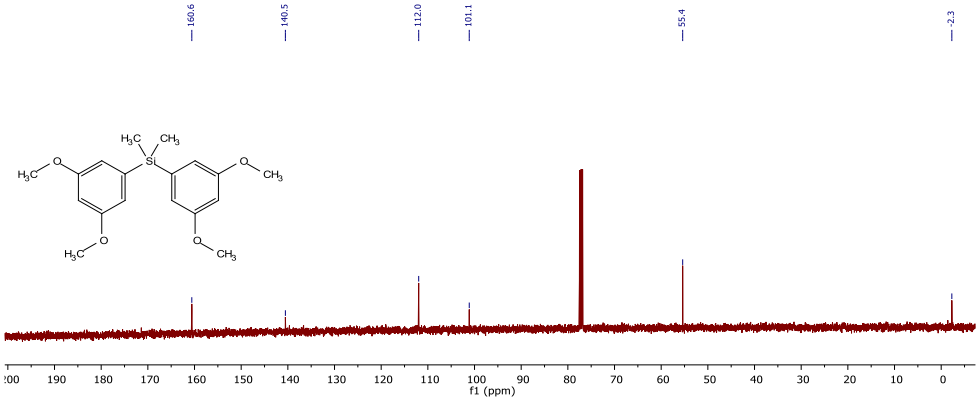

Figure A.2. ^{13C}NMR spectrum of compound **1.1** in $CDCl_3$.

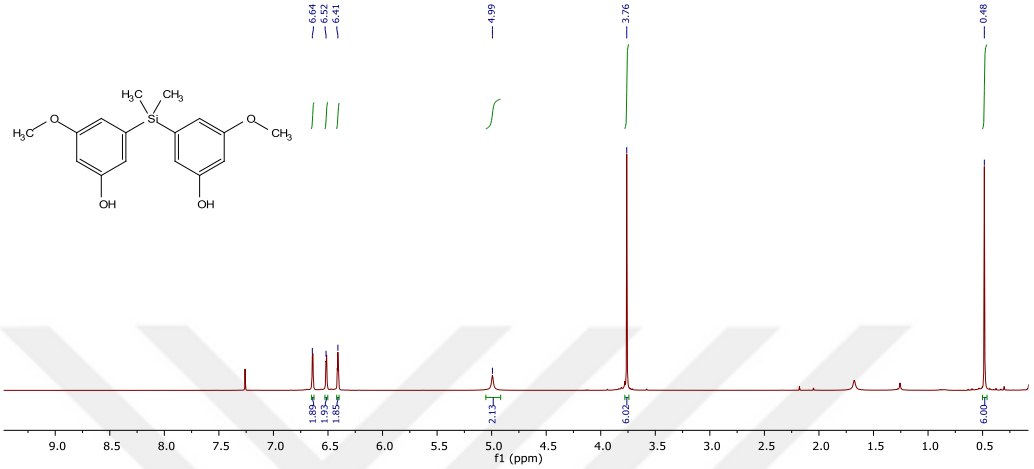

Figure A.3. ^{1H}NMR spectrum of compound **1.2** in $CDCl_3$.

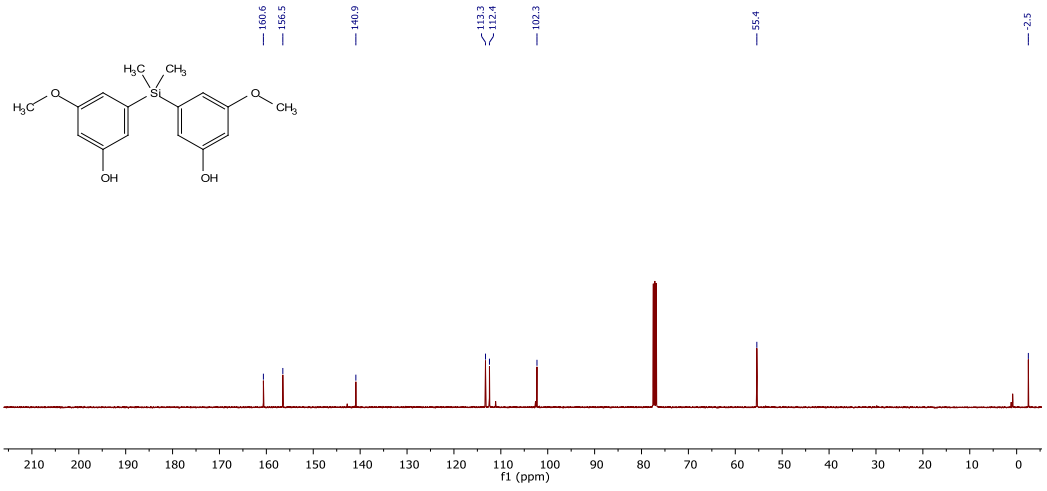

Figure A.4. ^{13C}NMR spectrum of compound **1.2** in $CDCl_3$.

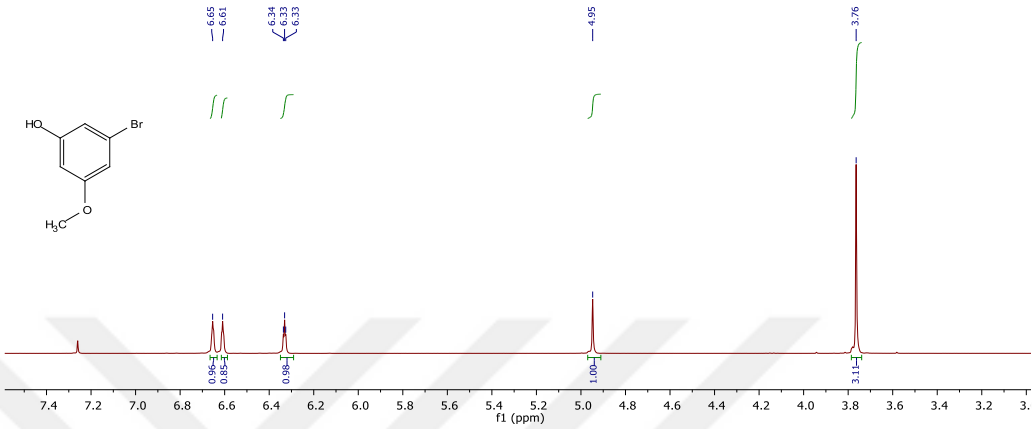

Figure A.5. ^{1H}NMR spectrum of compound **1.3** in $CDCl_3$.

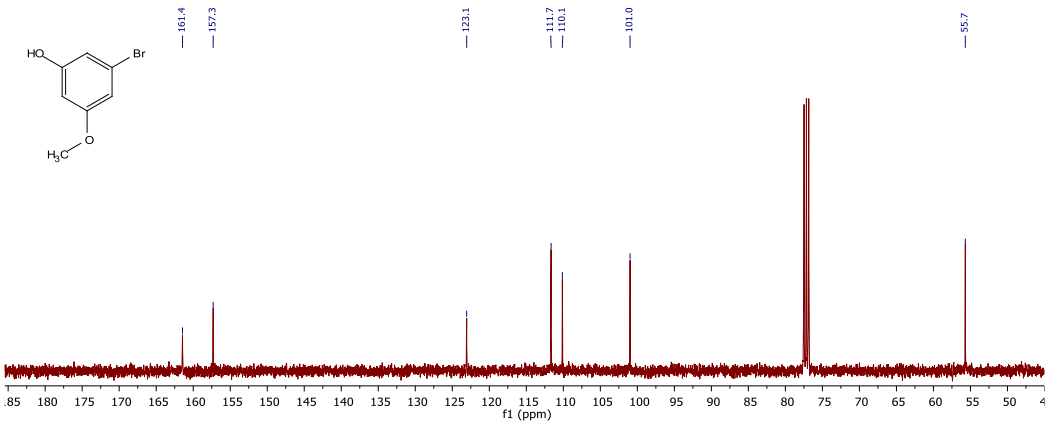

Figure A.6. ^{13C}NMR spectrum of compound **1.3** in $CDCl_3$.

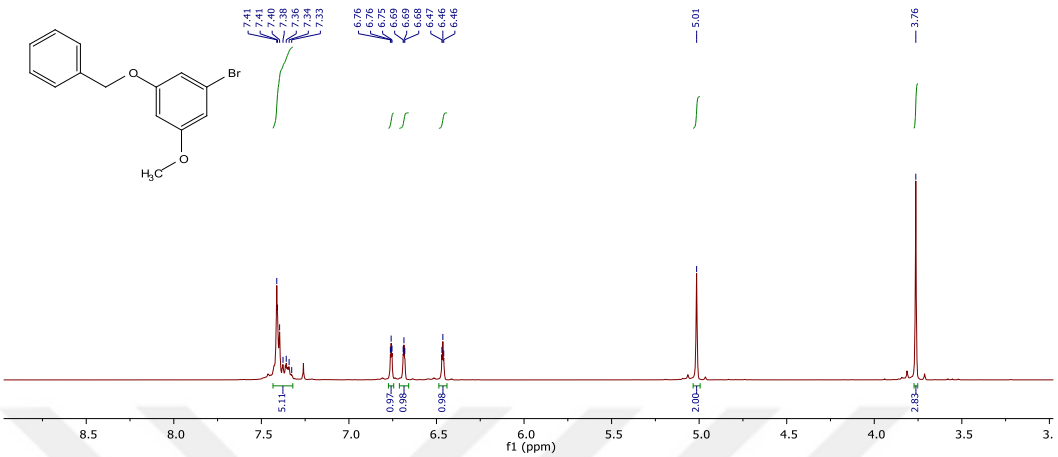

Figure A.7. ^{1H}NMR spectrum of compound **1.4** in $CDCl_3$.

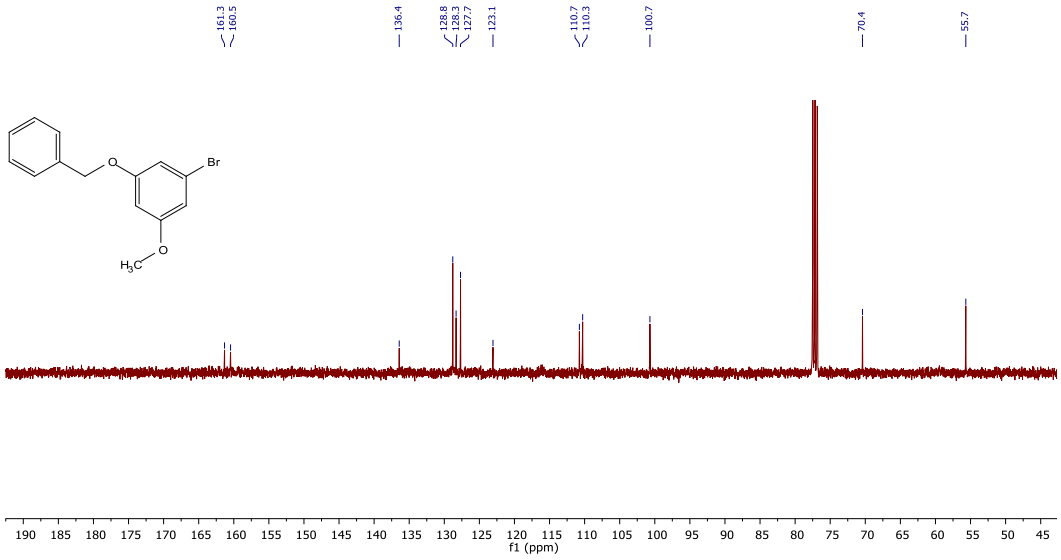

Figure A.8. ^{13C}NMR spectrum of compound **1.4** in $CDCl_3$.

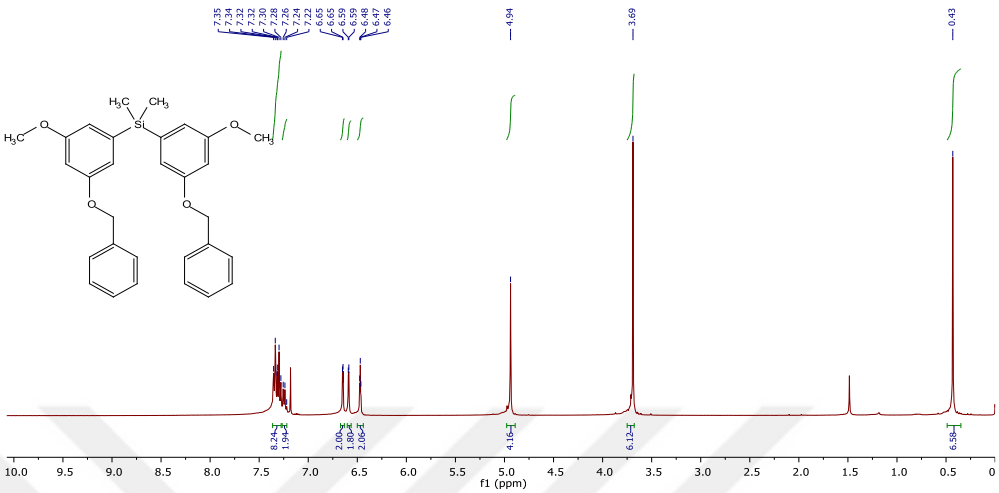

Figure A.9. ^{1H}NMR spectrum of compound **1.5** in $CDCl_3$.

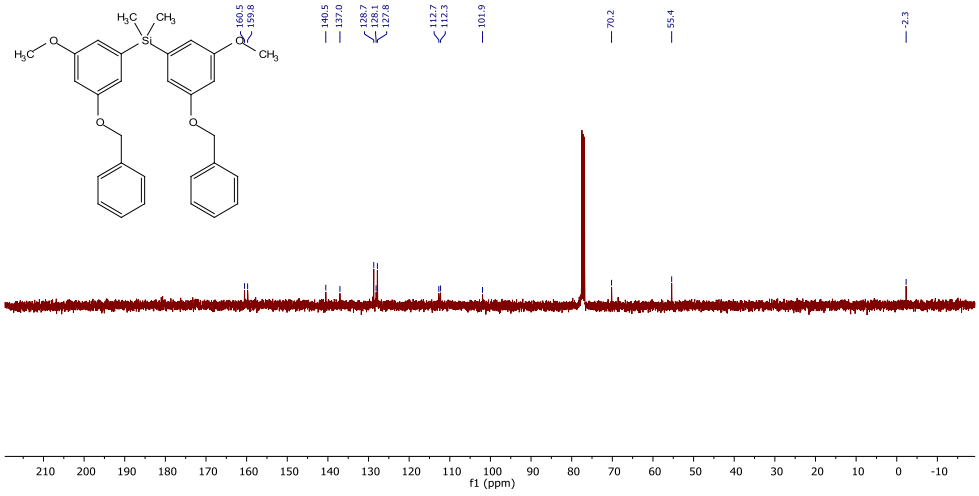

Figure A.10. ^{13C}NMR spectrum of compound **1.5** in $CDCl_3$.

A.2 NMR Spectra of PNO-Morp

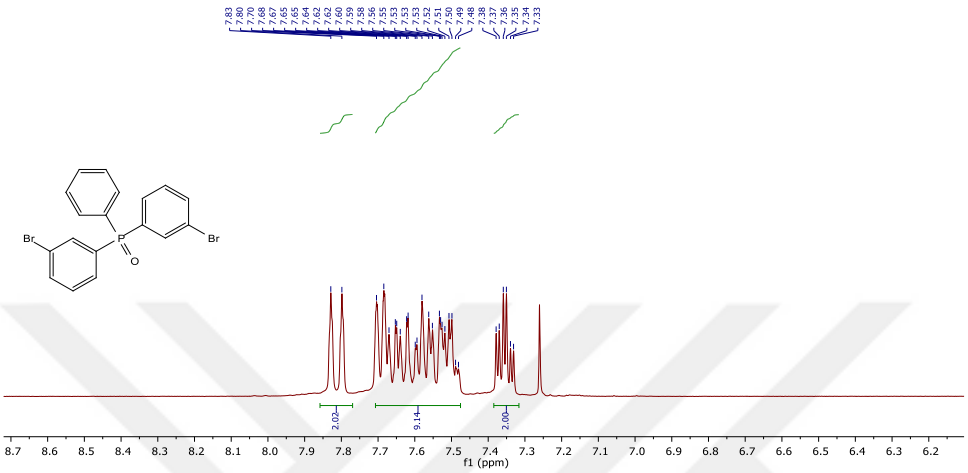

Figure A.11 ^{1H}NMR spectrum of compound **2.1** in $CDCl_3$.

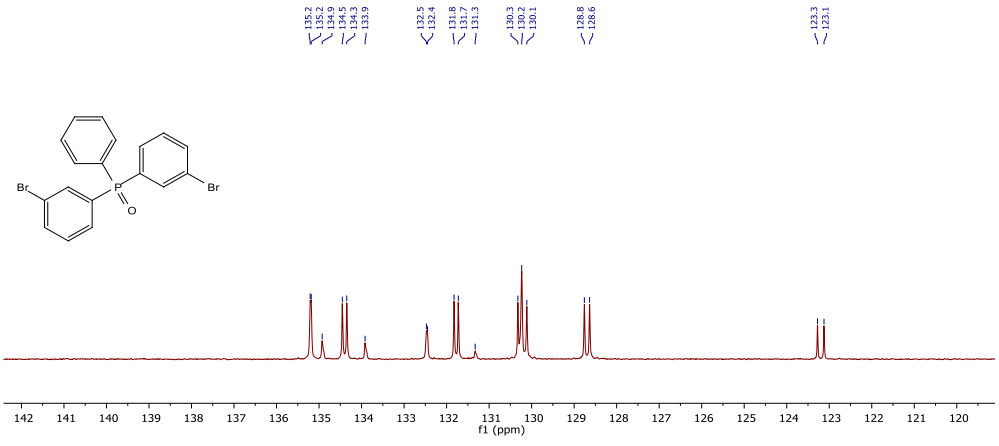

Figure A.12. ^{13C}NMR spectrum of compound **2.1** in $CDCl_3$.

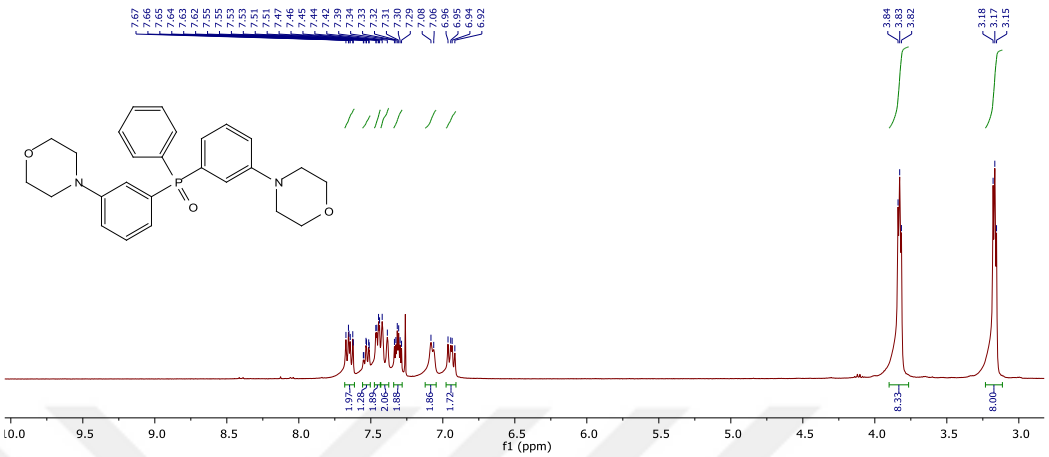

Figure A.13. ^{1H}NMR spectrum of compound **2.2** in $CDCl_3$.

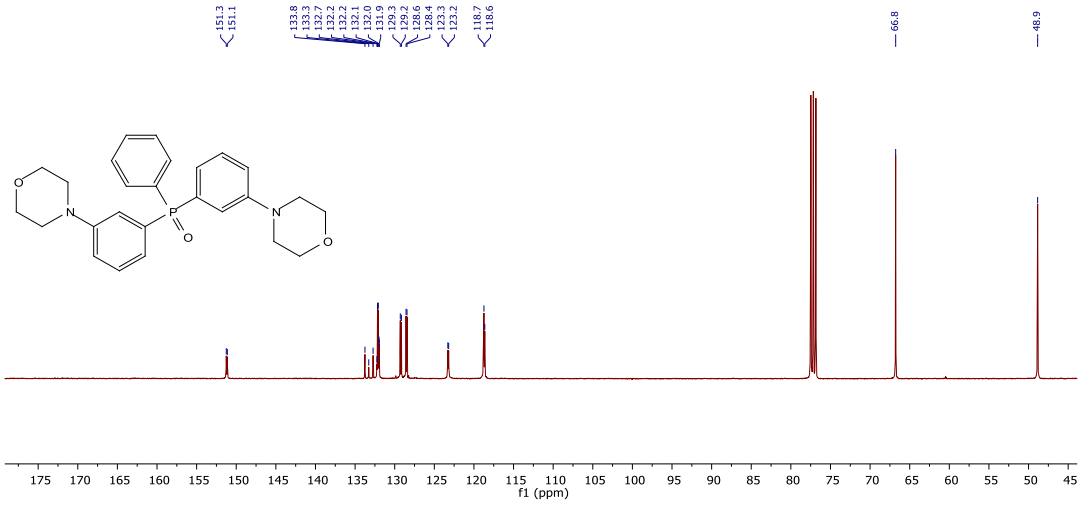

Figure A.14. ^{13C}NMR spectrum of compound **2.2** in $CDCl_3$.

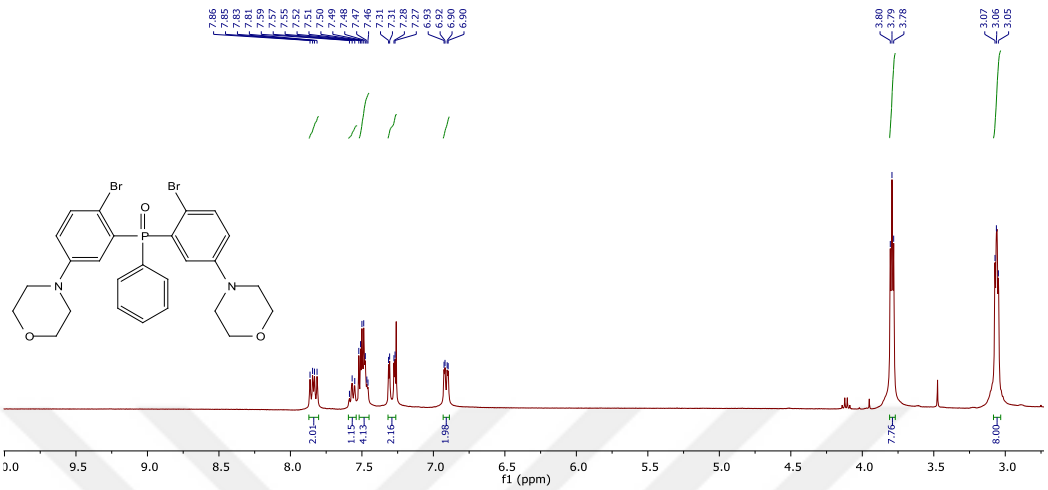

Figure A.15. ^{1H}NMR spectrum of compound **2.3** in $CDCl_3$.

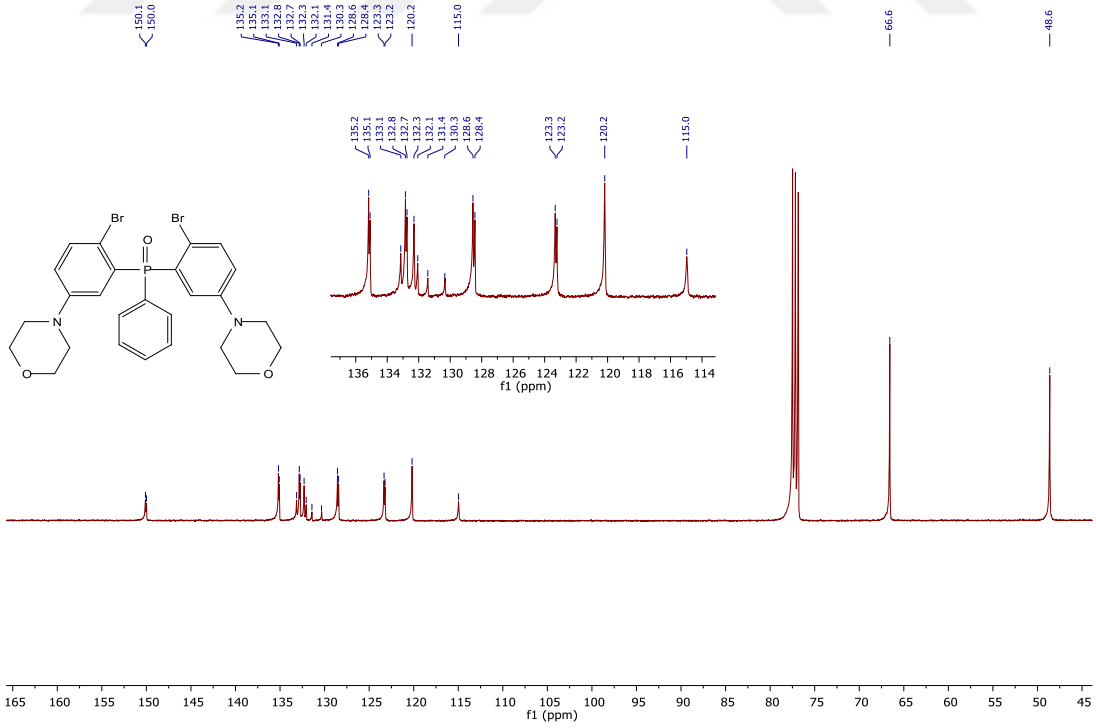

Figure A.16. ^{13C}NMR spectrum of compound **2.3** in $CDCl_3$.

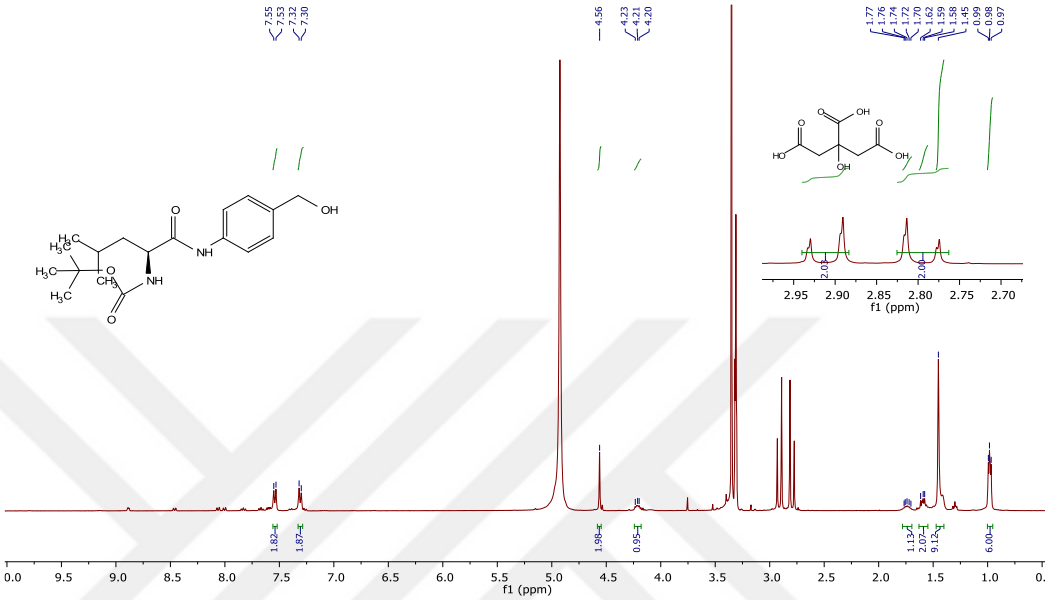

Figure A.17. ^{1H}NMR spectrum of APN handle in CD_3OD.

A.3 NMR Spectra of TPA

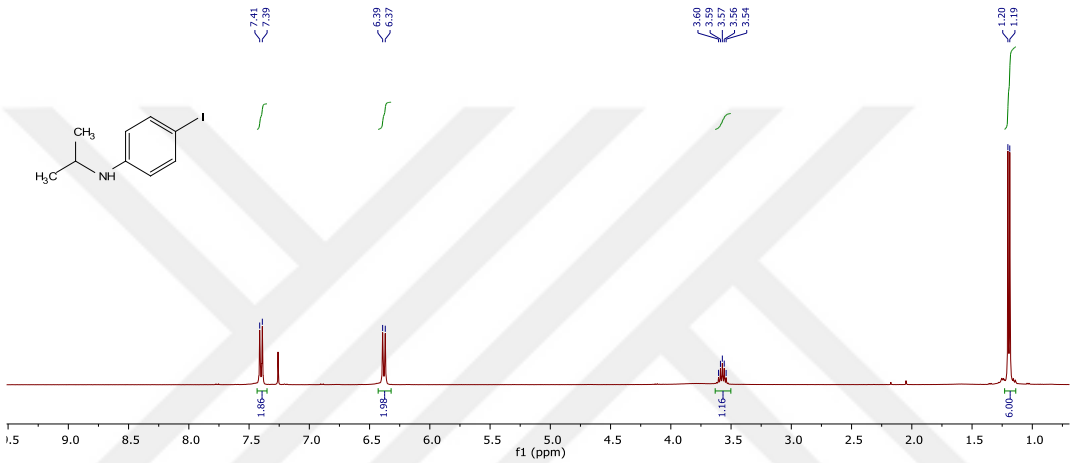

Figure A.18. ^{1H}NMR spectrum of compound **3.1** in $CDCl_3$.

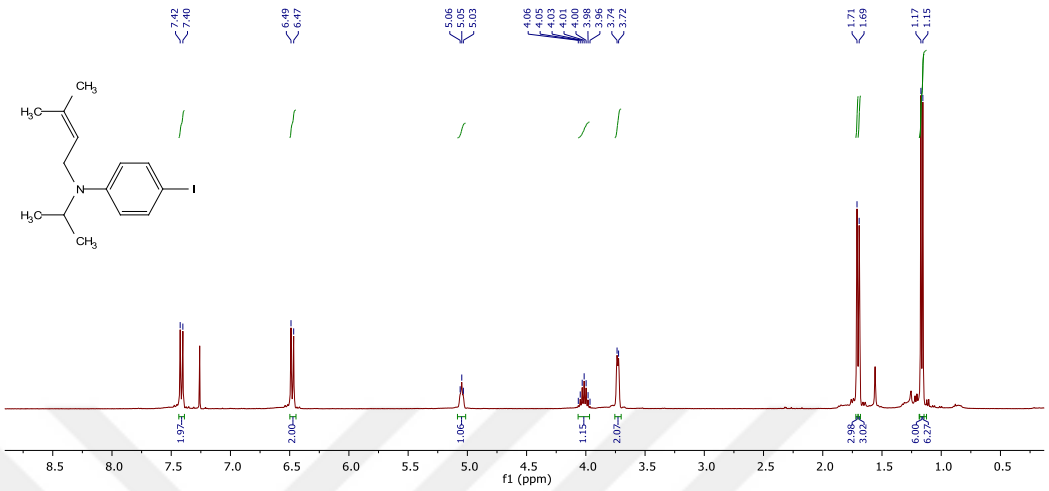

Figure A.19. ^{1H}NMR spectrum of compound **3.2** in $CDCl_3$.

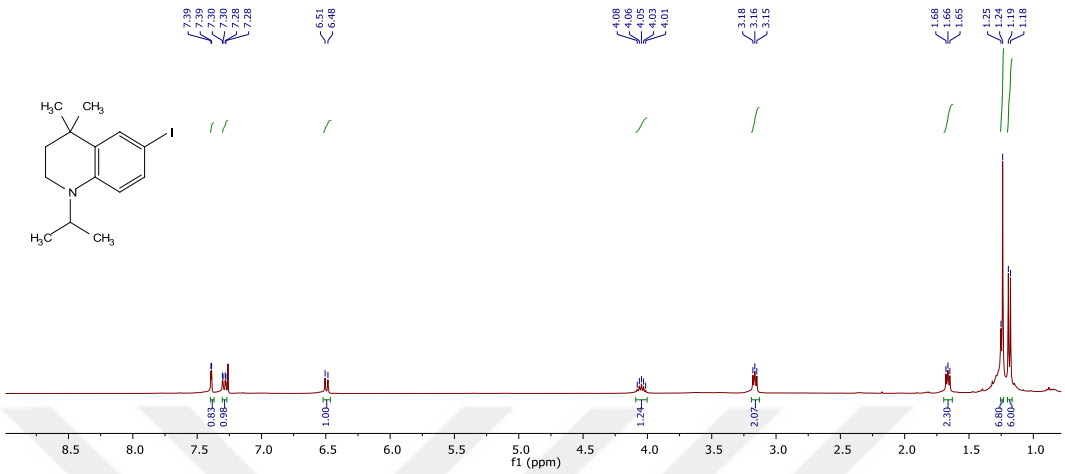

Figure A.20. ^{1H}NMR spectrum of compound **3.3** in $CDCl_3$.

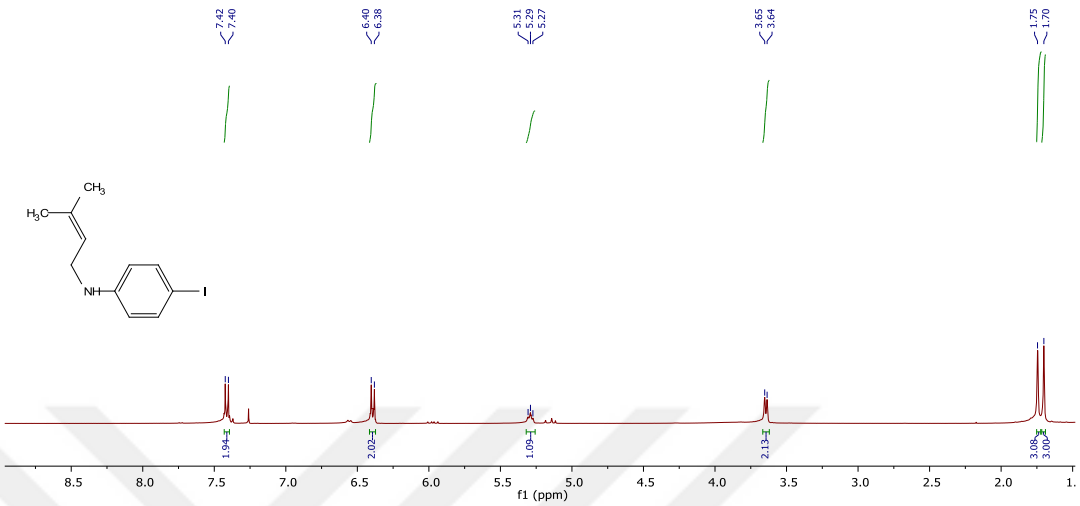

Figure A.21. ^{1H}NMR spectrum of compound **3.4** in $CDCl_3$.

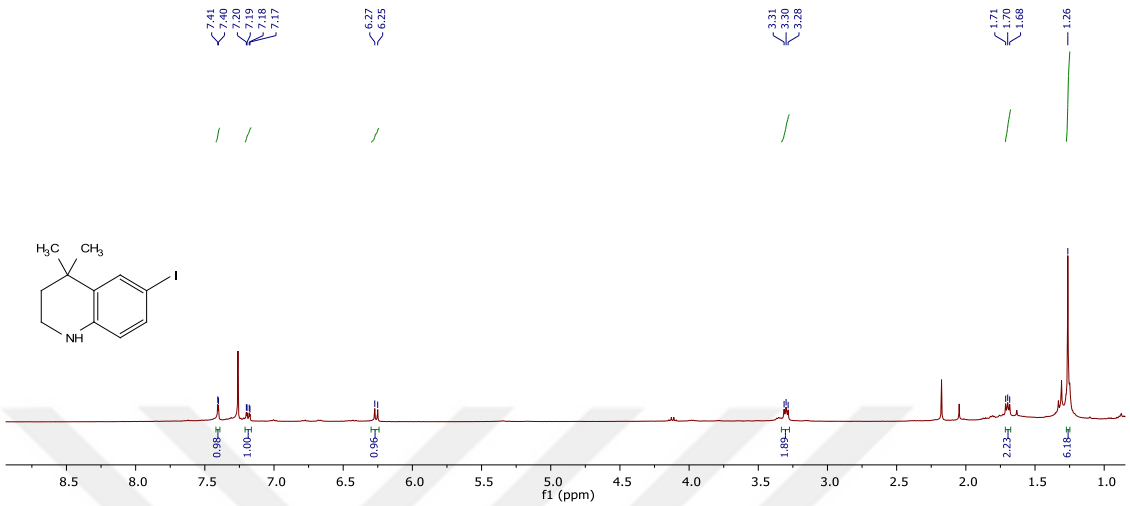

Figure A.22. ^{1H}NMR spectrum of compound **3.5** in $CDCl_3$.

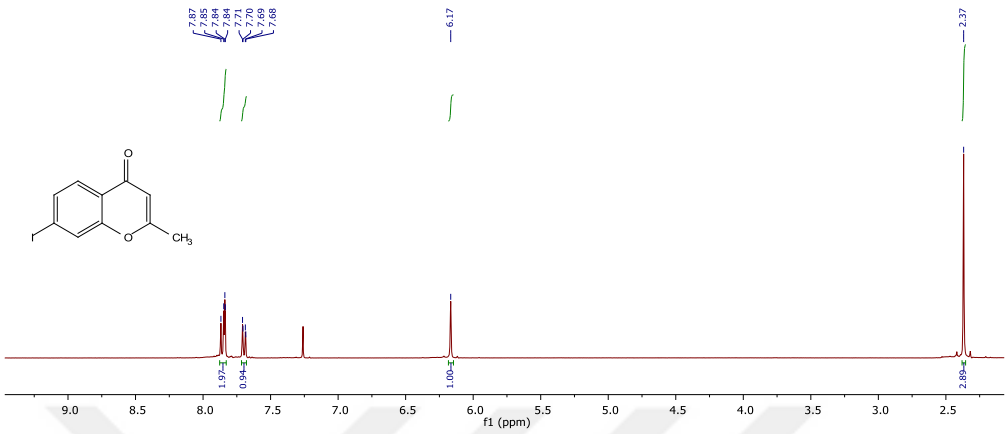

Figure A.23. ^{1H}NMR spectrum of compound **3.6** in $CDCl_3$.

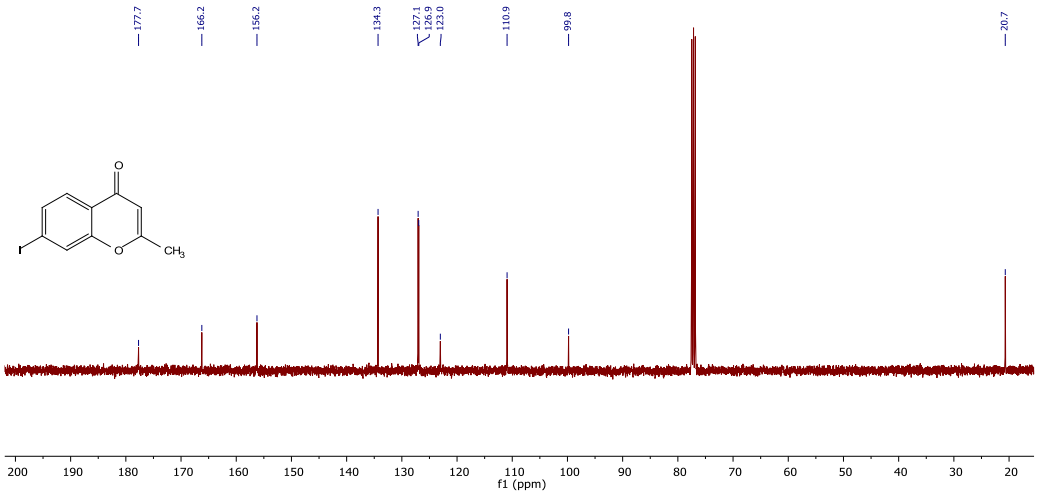

Figure A.24. ^{13C}NMR spectrum of compound **3.6** in $CDCl_3$.

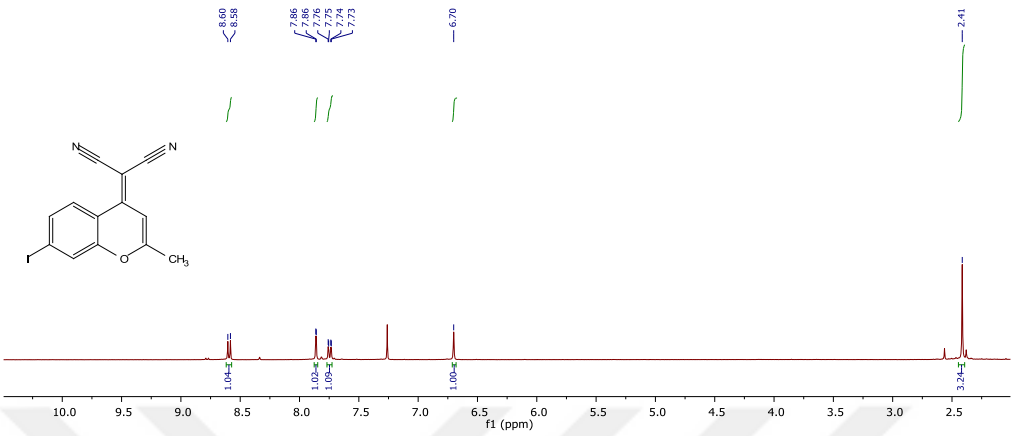

Figure A.25. ^{1H}NMR spectrum of compound **3.7** in $CDCl_3$.

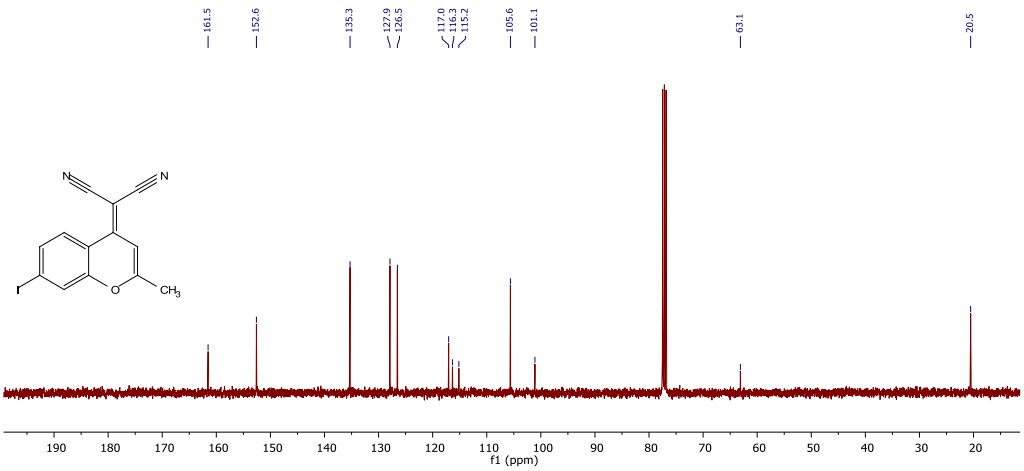

Figure A.26. ^{13C}NMR spectrum of compound **3.7** in $CDCl_3$.

B. HRMS Spectra

Elemental Composition Report

Single Mass Analysis
Tolerance = 1000.0 PPM / DBE: min = -5.5, max = 1000.0 Element prediction: Off
Number of isotope peaks used for i-FIT = 3

Monoisotopic Mass, Even Electron Ions
1 formula(e) evaluated with 1 results within limits (all results (up to 1000) for each mass) Elements Used:
C: 16-16 H: 17-18 N: 1-1 O: 4-4 Si: 1-1

Gizem Atakan Alkan
32590_20210521_05-02 13 (0.518) Cm (1:14)

1: TOF MS ES+
5.51e+004

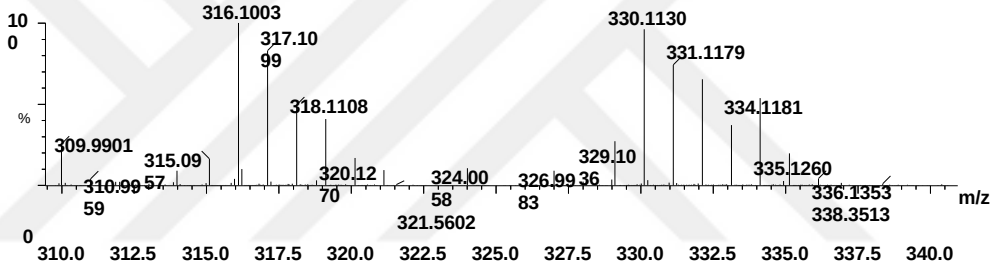

Minimum:				-5.5			
Maximum:		1000.0	1000.0	1000.0			
Mass	Calc. Mass	mDa	PPM	DBE	i-FIT	i-FIT (Norm)	Formula
316.1003	316.1005	-0.2	-0.6	9.5	417.1	0.0	C16 H18 N O4 Si

Figure A.27. HRMS spectrum of **SiNO-OMe** ($NOBF_4$ reaction)

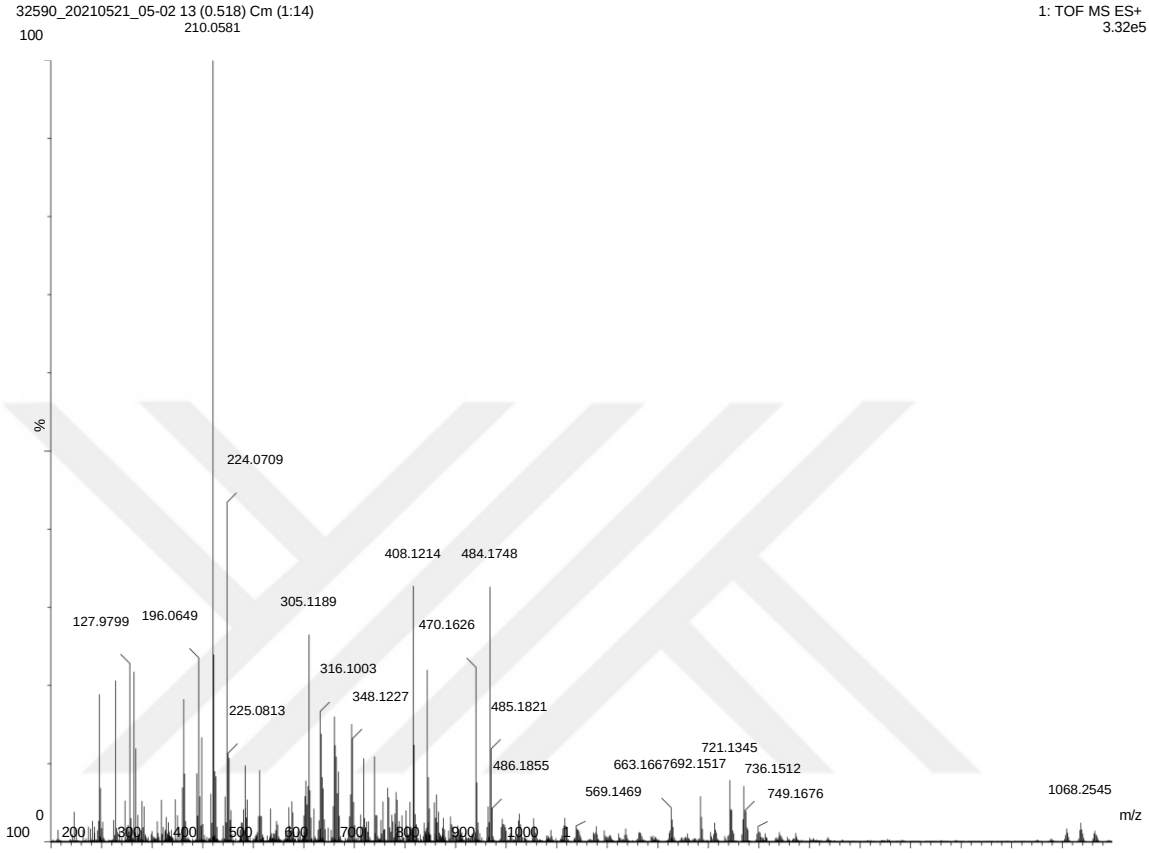

Figure A.28. Whole spectrum of HRMS data of **SiNO-OMe** ($NOBF_4$ reaction)

SiNO-OMe

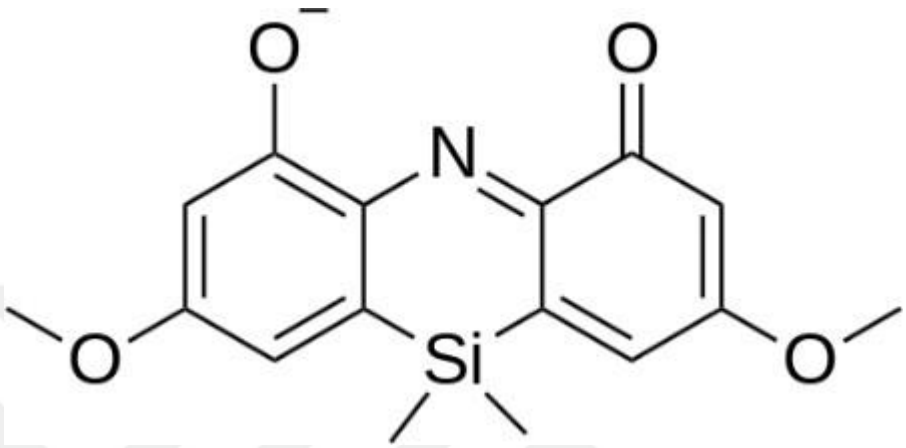

Excited State 1: Singlet-?Sym 1.8816 eV **658.92 nm** f=0.7963
<S**2>=0.000 83 -> 84 0.70741

HOMO (83): -5.214789624
LUMO (84): -2.8261743393

HOMO

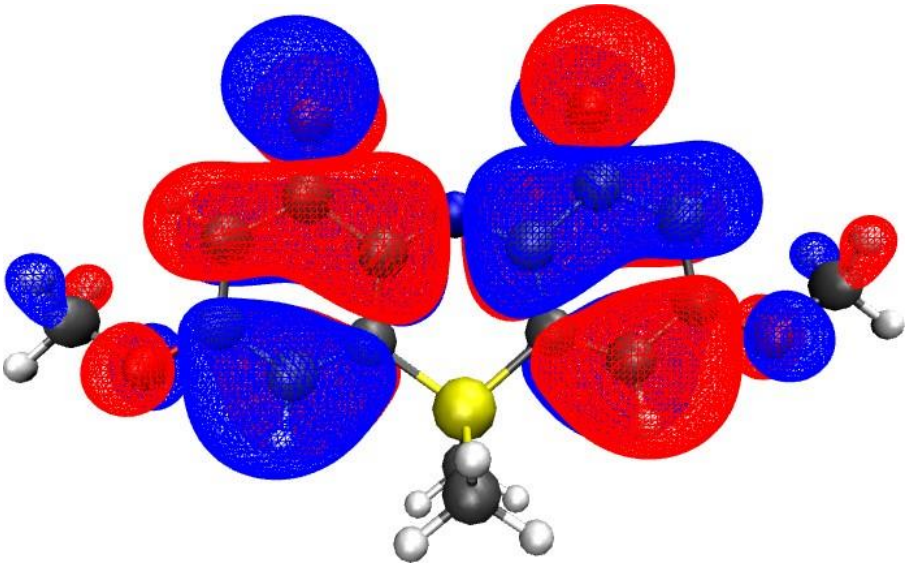

LUMO

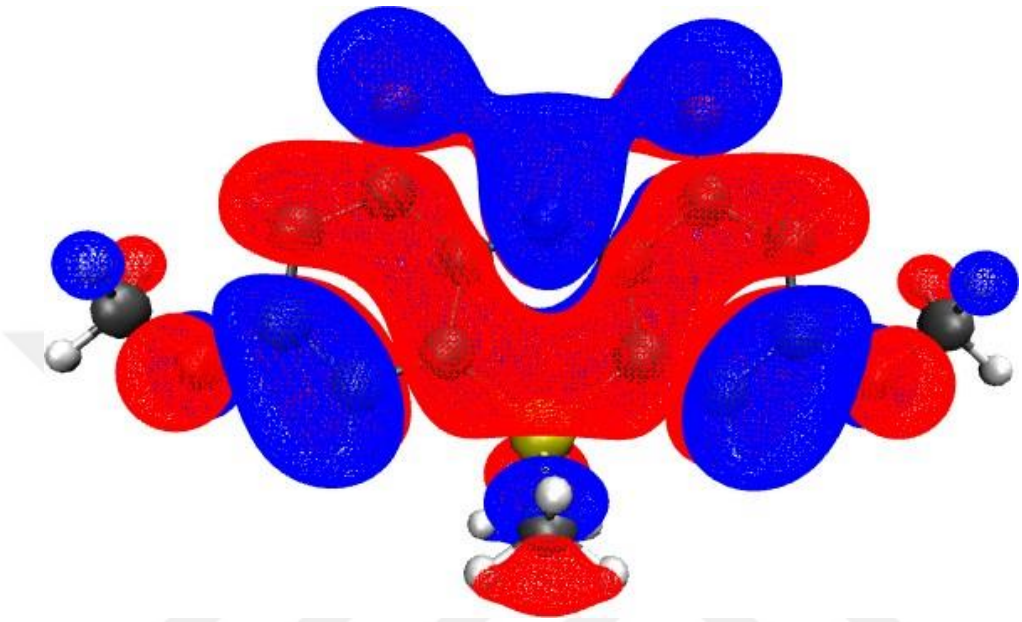

Attachment - Detachment Densities

Integral of detachment density 1.0235

Integral of attachment density 1.0259

Hole/particle overlap (phiS, from PA) 0.7358

Detachment density representation:

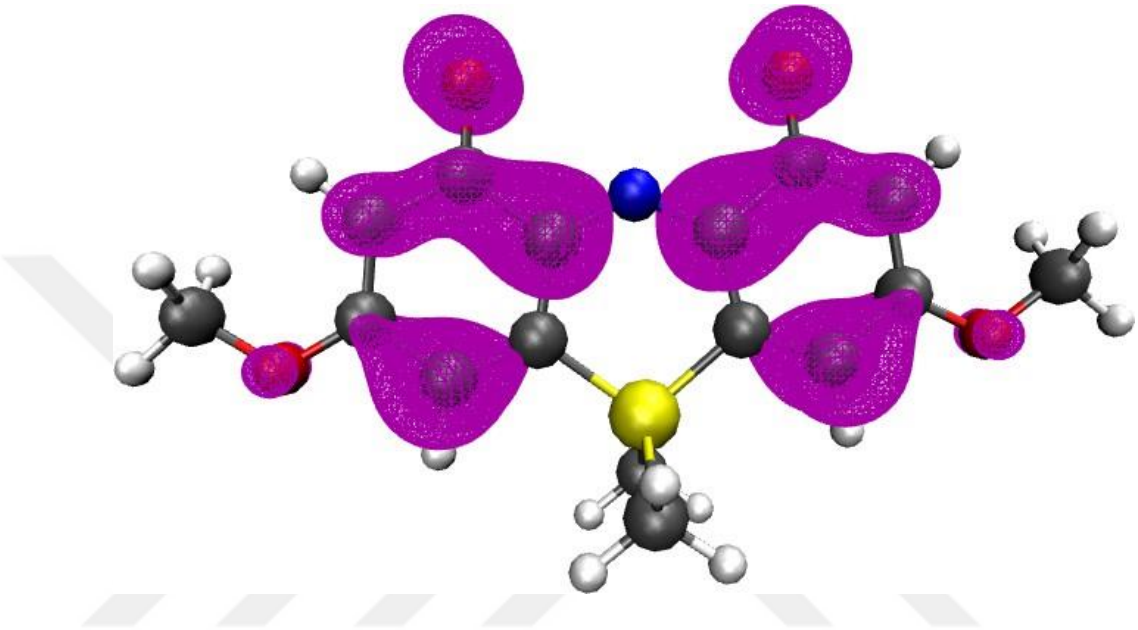

Attachment density representation:

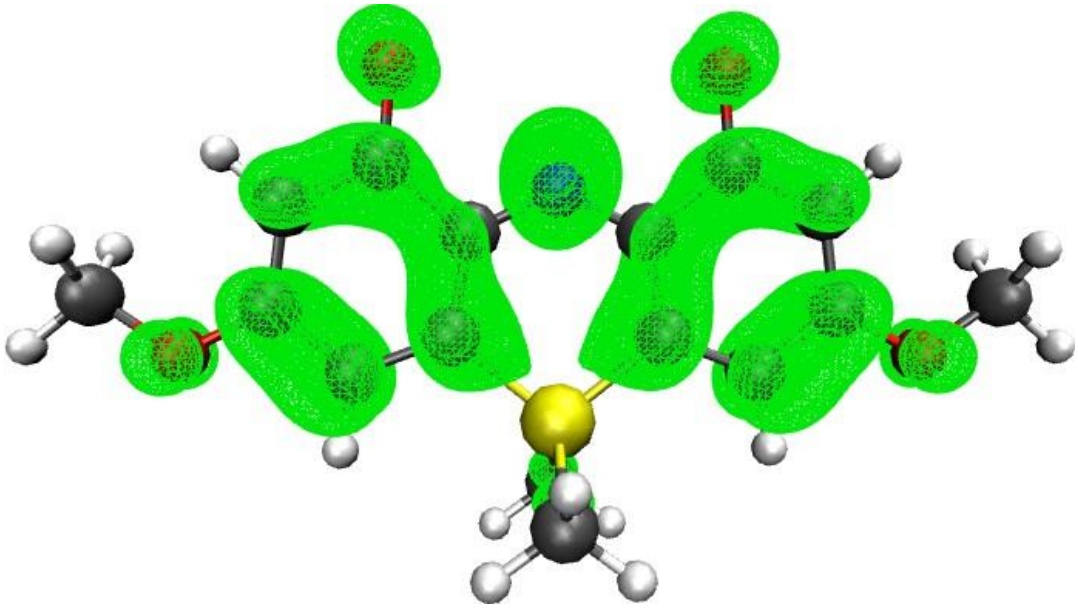

SiNO-OMe 2

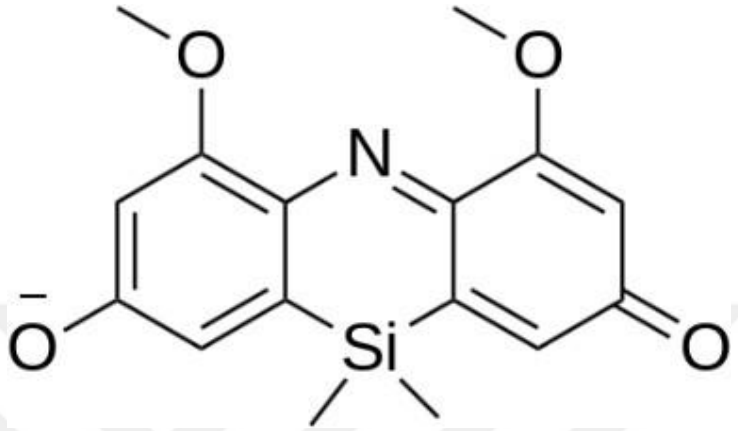

Excited State 1: Singlet-?Sym 1.9416 eV **638.55 nm** f=1.2580
<S**2>=0.000 83 -> 84 0.70710

HOMO (83): -5.232477024
LUMO (84): -2.872161578

HOMO

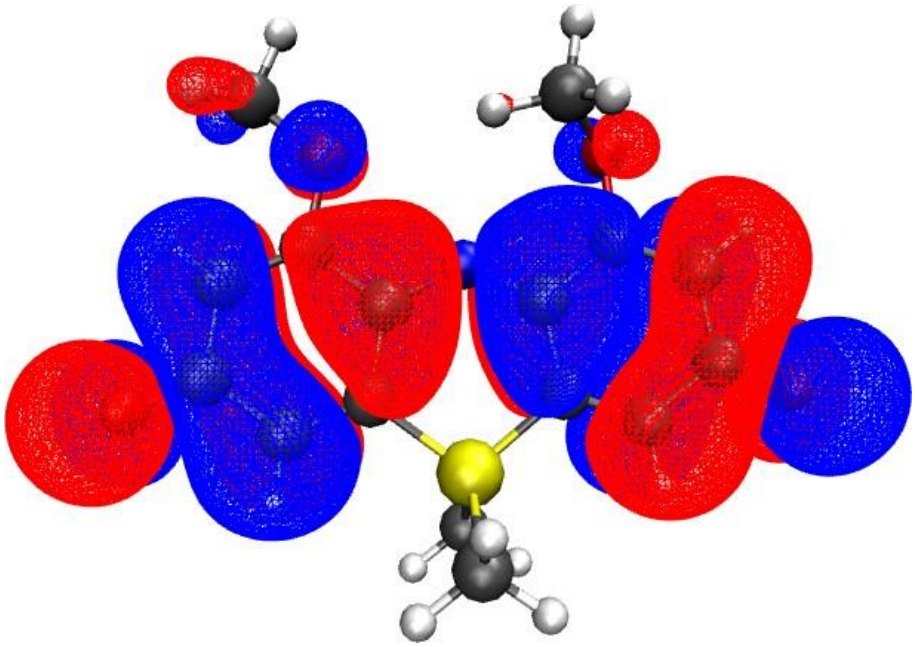

LUMO

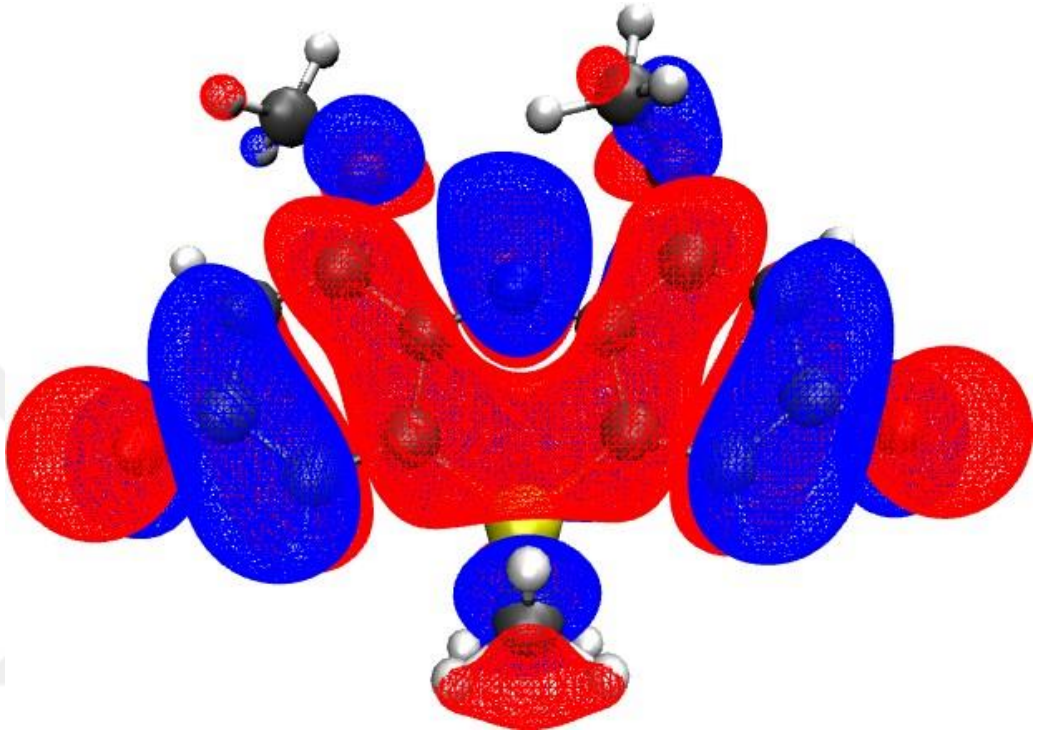

Attachment - Detachment Densities

Integral of detachment density 1.0271

Integral of attachment density 1.0271

Hole/particle overlap (phiS, from PA) 0.7172

Detachment density representation:

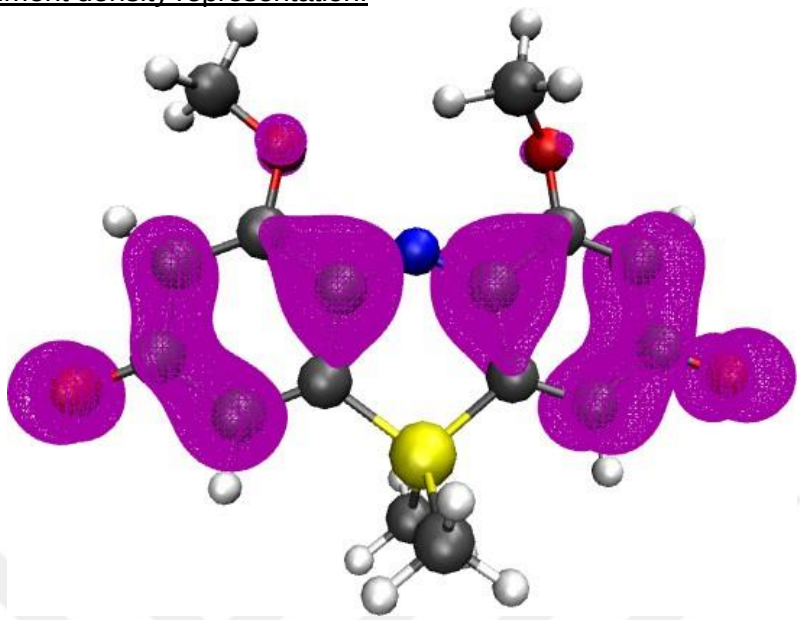

Attachment density representation: